

Graph-Based Simulator for Steam-Assisted Gravity Drainage Reservoir Management

by

Enrique Gallardo Vizcaino

A thesis submitted in partial fulfillment of the requirements for the degree of

Doctor of Philosophy

in

Mining Engineering

Department of Civil and Environmental Engineering  
University of Alberta

© Enrique Gallardo Vizcaino, 2019

## Abstract

Petroleum reservoir managers must make decisions about projects (e.g. infill drilling and/or operational strategies) with uncertain economic results due to imperfect knowledge of the reservoir geometry and properties. Their decision-making workflows should actively manage the geological uncertainty. This requires transferring the geological uncertainty to probability distributions of a response variable suitable for decision-making and use of a decision criterion that considers the reservoir manager's preferences toward the project's return-risk trade-off. This is challenging in petroleum reservoir management because transferring the geological uncertainty is time and computationally expensive. Moreover, common decision-making criteria do not consider preferences toward the geological risk of the projects.

This dissertation improves reservoir management decision-making practices in steam-assisted gravity drainage (SAGD) projects by introducing: 1) A novel graph-based simplified physics simulator, called APDS, that efficiently transfers the geological uncertainty into steam-chamber evolution paths that can directly support SAGD reservoir management or be converted to a monetary response variable, and 2) A decision-making criterion consistent with the utility theory framework that combines Mean-Variance Criterion (MVC) and Stochastic Dominance Rules (SDR) to guide the decision process.

APDS is formulated and implemented using graph theory, simplified porous media flow equations, heat transfer concepts and ideas from discrete simulation. It works on homogeneous and heterogeneous reservoirs and is computationally efficient enough to be applied over multiple geostatistical realizations. A case study performed with a realistic multi-realization geological model validates the predictive capabilities of APDS. Visual

and numerical comparisons with the results obtained from a conventional full physics thermal flow simulation are satisfactory. APDS was 3 orders of magnitude faster than the conventional simulator to model the steam-chamber expansion and to provide predictions of reservoir response. The reduction in the precision of the results is deemed acceptable. Another case study demonstrates that APDS can complement methodologies for assimilation of 4D-seismic dynamic data to improve reservoir characterization.

This thesis also demonstrates that MVC-SDR is a viable criterion for decision making under geological uncertainty. MVC-SDR does not rely on a specific utility function and leads to decisions that are considered rational to risk-averse reservoir managers. The shortcoming is a reduced ability to rank projects with very similar value. Two examples illustrate the use of MVC-SDR, the first one relates to the selection of a SAGD well-pad to be drilled from a set of several possible options, and the second one considers the problem of finding the best vertical location for a SAGD well-pair project in a target volume.

## Preface

Parts of this thesis have been previously published or are in the publication process.

Chapters 2, 3 and 5 are composed in part by Gallardo & Deutsch (2018). Approximate Physics Discrete Simulation of the Steam-Chamber Evolution in SAGD. Published in SPE Journal.

Chapter 4 is composed in part by Gallardo & Deutsch (2019). Decision Making in Presence of Geological Uncertainty with Mean-Variance Criteria and Stochastic Dominance Rules. Submitted to SPE Journal of Reservoir Evaluation & Engineering: Formation Evaluation.

To my wife Sonia and my sons Enrique and Esteban.

Remember my words ten years ago: “my life belongs to all three of you”.

## Acknowledgments

I would like to express my deep gratitude to Dr. Clayton V. Deutsch for being my mentor during my studies at the University of Alberta. His lessons and example have enriched my professional and personal life.

I would also like to thank the members of my supervisory committee, Dr. Jeffery Boisvert and Dr. Yashar Pourrahimian. Their comments and feedback improved the quality of this dissertation.

I acknowledge the financial support provided by members of the Centre for Computational Geostatistics and the Colombian National Oil Company, Ecopetrol.

# Table of Contents

1	Graph-Based Simulator for Steam Assisted Gravity Drainage Reservoir Management.....	1
1.1	Introduction .....	1
1.2	Petroleum Reservoir Management Decision-Making Workflow .....	2
1.3	Problem Setting .....	3
1.4	Proposed Approach.....	4
1.4.1	Graph-Base Steam-Chamber Simulator for Transferring the Geological Uncertainty in SAGD Projects.....	4
1.4.2	Mean-Variance Criteria and Stochastic Dominance Rules to Consider the Geological Risk-Reward trade-off.....	5
1.5	Dissertation Outline .....	6
2	SAGD Steam-Chamber Modeling with APDS: Formulation.....	8
2.1	Introduction .....	8
2.2	Review of Steam-Chamber Modeling Techniques.....	9
2.3	Steam Chamber Evolution Posed as a Shortest Path Problem .....	12
2.4	APDS Formulation .....	13
2.4.1	Graph.....	13
2.4.2	Propagation Algorithm.....	14
2.4.3	Ranking Function .....	16
2.4.4	APDS Outputs.....	19
2.5	APDS Pseudo Code .....	20
2.6	Step-wise Procedure .....	22
2.7	APDS Time Complexity.....	26
2.8	Potential Applications.....	27

2.8.1	SAGD Well-pair Location.....	27
2.8.2	SAGD Operation.....	27
2.8.3	4D-Seismic Integration.....	28
2.8.4	SAGD Geomechanics.....	28
2.9	Discussion.....	28
3	APDS: Implementation and Validation.....	30
3.1	Introduction.....	30
3.2	APDS Assumptions and Simplifications.....	30
3.2.1	Sinks, Parent Sink and Sink Angle ( $\beta$ ).....	31
3.2.2	Transversal Area ( $A_t$ ).....	33
3.2.3	Kinematic Viscosity in the Heated Volume ( $\nu_{hv}$ ).....	33
3.2.4	Permeability.....	35
3.2.5	Steam-chamber Interface Velocity.....	35
3.3	APDS prototype computer program.....	37
3.4	APDS Validation.....	38
3.4.1	Geological Model.....	39
3.4.2	SAGD Project.....	40
3.4.3	Steam-chambers from STARS and APDS.....	41
3.4.4	Metrics from STARS and APDS.....	48
3.4.5	Computational Time.....	58
3.5	Discussion.....	58
3.5.1	APDS Level of Physics.....	58
3.5.2	APDS Validation.....	60
3.5.3	APDS Prototype and Computational Time.....	60
4	Mean-Variance Criterion and Stochastic Dominance Rules for PRM.....	62
4.1	Introduction.....	62

4.2	Decision-Making Model in Presence of Geological Uncertainty.....	63
4.2.1	Set of Feasible Actions or Projects. ....	63
4.2.2	Set of Outcomes .....	64
4.2.3	Preferences and Concept of Rationality .....	65
4.3	Utility Theory in PRM.....	67
4.4	Mean Variance Criterion and Stochastic Dominance Rules.....	68
4.4.1	The Mean-Variance Criterion (MVC).....	69
4.4.2	Stochastic Dominance Rules (SDR) .....	71
4.5	MVC and SDR in PRM.....	77
4.6	Example of MVC-SDR Methodology .....	77
4.7	Discussion.....	81
5	Case-Study: SAGD Vertical Well Placement.....	82
5.1	Introduction .....	82
5.2	SAGD Vertical Placement Well Problem.....	82
5.2.1	Problem Setting.....	82
5.2.2	Set of Feasible Actions.....	83
5.2.3	Geological Model.....	85
5.2.4	Transferring the Geological Uncertainty with APDS .....	85
5.2.5	MVC.....	91
5.2.6	SDR.....	93
5.3	Computational Time.....	95
5.4	Discussion.....	95
6	Case Study: SAGD Reservoir Characterization with APDS .....	97
6.1	Introduction .....	97
6.2	Assessment of Geostatistical Anomaly Enforcement with APDS.....	98
6.2.1	Geological Model.....	98

6.2.2	Assesing SAGD Reservoir Characterization Improvement with APDS	102
6.2.3	APDS Modeling of Steam-Chamber in Point Bar Systems .....	111
6.2.4	Computational Time.....	115
6.3	Discussion.....	115
7	Summary of Contributions and Future Work .....	117
7.1	Summary of Contributions .....	117
7.1.1	APDS Formulation.....	118
7.1.2	APDS Implementation and Validation.....	119
7.1.3	Decision-Making Criterion for Active Management of Geological Uncertainty.....	120
7.1.4	Assisting 4D-Seismic Integration in Reservoir Characterization .....	121
7.2	Limitations and Future Work .....	122
7.2.1	Production Oil Forecast.....	123
7.2.2	Steam-Oil Ratio (SOR) Forecast.....	124
7.2.3	Oil Relative Permeability (Kro).....	125
7.2.4	Cells with High Initial Water Saturation (Swi).....	127
7.2.5	Assisting the Ensemble Kalman Filter (EnKF) Technique with APDS	128
7.2.6	Coupling APDS with a Thermal Wellbore Simulator.....	129
7.2.7	APDS Applications .....	129
7.2.8	APDS Computational Efficiency .....	129
7.2.9	Decision-Maker Position on Geological Risk.....	130
7.2.10	Value of Seismic Information on SAGD projects .....	131
	References.....	132
	Appendix A.....	142
A.1	Dependencies, Requirements and Licenses .....	142
A.1.1	Dependencies and Requirements .....	142

A.1.2 Licenses.....	143
A.2 APDS Workflow.....	149
A.3 APDS Programs.....	157
A.3.1 Graph Generator Module Programs.....	157
A.3.2 Steam-Chamber Module Programs.....	166
A.3.3 Post-processing Module Programs.....	175
Appendix B.....	177

## List of Figures

Figure 1.1: Components of a Petroleum Reservoir Management Decision-Making workflow.....	2
Figure 2.1: Steam-assisted gravity drainage (SAGD) process (obtained from Peacock (2010)).....	8
Figure 2.2: Steam-chamber shapes. a) Original Butler’s analytical model, b) Tandrain model.....	9
Figure 2.3: Steam-chamber with imposed geometry. a) Inverted triangle model, b) Circular model.....	10
Figure 2.4: Steam-chamber from semi-analytical models. a) Butler (1985) semi-analytical model, b) Heidari et al. (2009) semi-analytical model. ....	11
Figure 2.5: Illustration of a 2D-grid geological model represented as a graph. ....	14
Figure 2.6: APDS propagation mechanism. Red shapes are not part of APDS. They were drawn to help visualizing the steam-chamber expansion. Edge labels omitted in this figure are shown in Figure 2.5.....	15
Figure 2.7: Steam-chamber interface and temperature distribution (modified after Butler (1991)).....	18
Figure 2.8: APDS Outputs: a) Ordered sequence of nodes, b) Steam-chamber model, c) Cumulative steam-chamber volume. ....	19
Figure 2.9: APDS stepwise procedure. Top row shows the algorithm initialization and the cell indexes. Well and sinks locations are labeled. Black outlines drawn to help visualizing how the APDS handles barriers. ....	23
Figure 2.10: APDS calculations for the homogeneous reservoir depicted in the left column of Figure 2.9.....	25
Figure 2.11: APDS calculations for the heterogeneous reservoir depicted in the right column of Figure 2.9.....	26
Figure 3.1: Bitumen flowing downward from cell A to the well will pass through one of the sinks (red cells). The angle between cell A and one sink cell is called sink angle. This figure shows two possible sink angles $\beta_1$ and $\beta_2$ . ....	31

Figure 3.2: The bitumen path depends on the relative position between the cell, the well and the barriers. In figures a and b, the steam-chamber approaches cell A from the left-side and the sink 1 is marked as Parent Sink of A. In figure c, the steam-chamber approaches cell A from the right-side and the sink 2 is marked as Parent Sink of A.....	32
Figure 3.3: The transversal side ( <b>St</b> ) concept used in APDS.....	33
Figure 3.4: The advance of the steam-chamber interface at a velocity U is determined by the difference between $q_{in}$ and $q_{out}$ . .....	36
Figure 3.5: The advance of the steam-chamber interface is determined by the difference between the flowing in ( $q_{in}$ ) and flowing out ( $q_{out}$ ) rates. ....	37
Figure 3.6: Structure of the APDS prototype.....	38
Figure 3.7: Illustration of one realization of the geological model.....	39
Figure 3.8: Temperature and compositional dependent relative permeability curves (CMG's SAGD guide (2013))......	41
Figure 3.9: APDS and STARS steam-chamber after 5 years. ....	42
Figure 3.10: Cross-section A and B selected to compare STARS and APDS.....	42
Figure 3.11: Cross-section A comparing APDS and STARS for 5 years.....	44
Figure 3.12: Cross-section B comparing APDS and STARS for 5 years. ....	45
Figure 3.13: Steam-chamber location after 5 years generated by STARS and APDS. ...	46
Figure 3.14: Vertical cross-sections along the axis of the SAGD well-pair. Arrows mark the location of cross-sections plotted in Figure 3.15. ....	47
Figure 3.15: Vertical cross-sections every 300 meters perpendicular to the axis of the SAGD well-pair. ....	47
Figure 3.16: Conformance Index histogram. ....	48
Figure 3.17: COP forecasts from STARS after 5 years for 50 realizations.....	49
Figure 3.18: Histograms of COP from STARS for years 1 to 5 (Y1 to Y5). ....	49
Figure 3.19: Histogram of SCHV from STARS after 5 years. ....	50
Figure 3.20: a) Cumulative SCHV from APDS, b) Histogram of SCHV from APDS after 5 years. ....	51
Figure 3.21: Scatter plots of COP from STARS forecasts from years 1 to 5. ....	52
Figure 3.22: Scatter plots of rank of realizations based on COP from STARS from years 1 to 5. ....	53

Figure 3.23: a) Scatter plot of COP from STARS and APDS from SCHV, b) Scatter plot of COP from STARS ranks and SCHV from APDS ranks. ....	54
Figure 3.24: a) Scatter plot of SCHV from STARS and SCHV from APDS. b) Scatter plot of SCHV ranks from STARS and SCHV ranks from APDS.....	56
Figure 3.25: a) Scatter plot of COP from STARS after 5 years and SCHV from APDS after 7 years. b) Scatter plot SCHV ranks from STARS after 5 years and SCHV ranks from APDS after 7 years.....	57
Figure 3.26: Conceptual level of physics of different transfers functions for SAGD. ....	59
Figure 3.27: Parallelization computing scheme for APDS. Note that the output are cumulative distribution functions (CDF) of the response variables, one per each SAGD project. ....	61
Figure 4.1: Components of a Petroleum Reservoir Management Decision-Making workflow. ....	63
Figure 4.2: Types of utility functions, $u(x)$ .....	67
Figure 4.3: Illustration of Markowitz’s efficient frontier (Modified after Johnstone & Lindley (2013)). ....	69
Figure 4.4: MVC criterion fails to discern which project is preferred between A and B. ....	70
Figure 4.5: Project $F$ dominates project $G$ by FSD because $F(x) \leq G(x), \forall x$ . ....	72
Figure 4.6: a) Since CDFs cross each other, there is not FSD, b) Although CDFs touch each other, $F$ dominates $G$ by FSD. ....	73
Figure 4.7: a) $F$ dominates $G$ by SSD, b) Neither $F$ nor $G$ dominates the other by SSD. ....	74
Figure 4.8: $F$ dominates $G$ by SSD (Modified after Levy (2016)). ....	75
Figure 4.9: Stochastic Dominance Matrix. ....	76
Figure 4.10: SAGD well-pad locations and assumed net present value probability distribution functions. ....	78
Figure 4.11: Red dots are projects on the efficient frontier. Project B dominates D, L and H because it has higher mean and less variance. ....	78
Figure 4.12: PDF (top) and CDF (bottom) of projects on the efficient frontier. After FSD, projects I and F should be discarded. Projects A, B and K remain in the efficient set. ....	79
Figure 4.13: Integral of CDF for projects A, B and K. After SSD, project B should be discarded. Projects A and K remain in the efficient set. ....	80

Figure 4.14: Stochastic Dominance Matrix .....	80
Figure 5.1: Target volume for vertical placement case study. ....	83
Figure 5.2: Description of vertical placement well location challenge. a) Location #1 has ineffective well length, b) Location #2 intersects low-placed barriers, c) Location #3 has a small hydrocarbon column.....	84
Figure 5.3: Cross-section through the target volume on several geostatistical realizations. ....	85
Figure 5.4: Heated hydrocarbon volume forecast for wells in level 5 of target volume. .	88
Figure 5.5: Heated hydrocarbon volume forecast for wells in level 6 of target volume. .	88
Figure 5.6: Box-plots of heated hydrocarbon volume for wells in target zone. ....	89
Figure 5.7: Steam-chamber of well located in second quadrant and level 2. The long ineffective well section has a negative effect on the steam-chamber development. ....	90
Figure 5.8: Steam-chamber of well located in second quadrant and level 7. ....	90
Figure 5.9: Steam-chamber of well located in second quadrant and level 10. Note the large amount of unrecoverable bitumen below the producer well.....	91
Figure 5.10: Efficient frontier and dominated locations after MVC. ....	92
Figure 5.11: Stochastic Dominance Matrix. W33, W34 and W27 dominates by FSD and/or SSD the remaining well locations.....	93
Figure 5.12: Mean-Standard Deviation space. MVC-SDR results on an optimum set with 3 locations. $EF = \{W33, W34, W27\}$ .....	94
Figure 6.1: Reservoir realization of the pre-enforced geological model for the entire drainage area. The figure indicates the well-pair volume extracted for this case study. ..	99
Figure 6.2: Reservoir realization of the pre-enforced geological model for the extracted well-pair volume used in the case study. ....	100
Figure 6.3: a) Vertical cross-section of pre-enforced geological model showing location of well-pair and net-reservoir and non-net reservoir distribution. b) Sketch of the steam-chamber obtained from 4D-seismic. c) The absence of the steam-chamber in net-reservoir sections near the wells represent potential anomalies.....	101
Figure 6.4: Vertical cross-section of: a) Pre-enforced realization showing location of anomalies Type -1. b) Post-enforced realization showing enforced barriers.....	103

Figure 6.5: Vertical cross-section of: a) Pre-enforced realization showing location of anomalies Type -1. b) Post-enforced realization showing enforced barriers..... 104

Figure 6.6: Vertical cross-section of post-enforced realization showing: a) 4D-seismic steam-chamber and anomalies Type -1, b) APDS steam-chamber and anomalies Type -1, and c) Comparison of the steam-chambers. .... 105

Figure 6.7: 3D-steam-chambers modeled with APDS for a 3 year period on six post-enforced geostatistical realizations. .... 107

Figure 6.8: Vertical cross-sections along the axis of the well-pair showing the steam-chamber modeled with APDS for 3 years on 6 post-enforced realizations. .... 108

Figure 6.9: Probability of steam-chamber presence after 3 years..... 109

Figure 6.10: Probability of steam-chamber presence modeled at six different years. .... 110

Figure 6.11: Upward-fining HIS packages with hypothetical gamma ray log (Modified after Labrecque et al. (2011))...... 111

Figure 6.12: Vertical cross-section of one reservoir model used by Yi Su et al. (2017) in the thermal flow simulations. Permeability scale was not presented in original figure. (Modified after Yi Su et al. (2017))...... 112

Figure 6.13: Vertical cross-section of post-enforced realization showing the steam-chamber every 6 months. Years 1 and 2. .... 113

Figure 6.14: Vertical cross-section of post-enforced realization showing the steam-chamber every 6 months. Years 2 to 5..... 114

Figure A.1: Workflow to run APDS..... 149

## List of Tables

Table 2.1: Typical Athabasca oil-sand parameters used in the stepwise procedure (Modified after Cokar et al. (2013)).	24
Table 3.1: Reservoir simulation parameters.	40
Table 3.2: Statistics from APDS and STARS.	53
Table 4.1: Payoff matrix for projects F and G (Modified after Levy and Sarnat (1970)).	70
Table 5.1: Typical design parameters for a 30,000 BPD SAGD project. (Obtained from CERI (2018)).	86
Table 5.2: Supply cost summary for a 30,000 BPD SAGD project. (Obtained from CERI (2018)).	87

## List of Symbols

Symbol	Description
$A_i$	area of the steam-chamber interface, $m^2$
$A_{ob}$	area in contact with the overburden, $m^2$
$A_t$	transversal area in the direction of the sink, $m^2$
$b$	exponent in Cardwell and Parson's equation for relative permeability, dimensionless
$E[\cdot]$	Expected value operator
$g$	gravity constant, $\frac{m}{s^2}$
$k_{abs}$	absolute permeability, $m^2$
$k_o$	effective oil permeability, $m^2$
$k_{ro}$	relative oil permeability, $m^2$
$k_{rw}$	relative water permeability, $m^2$
$K$	thermal conductivity of the reservoir, $\frac{W}{m \cdot ^\circ C}$
$m$	Butler's temperature-viscosity exponent, dimensionless
$M$	volumetric heat capacity of the reservoir, $\frac{J}{kg \cdot ^\circ C}$
$q_o$	oil rate, $\frac{m^3}{s}$
$q_t$	total rate, $\frac{m^3}{s}$
$q_w$	water rate, $\frac{m^3}{s}$
$Q_o$	cumulative recoverable oil, $m^3$
$Q_{ovb}$	heat loss to the overburden, $J$
$Q_{sch}$	heat to expand the steam chamber, $J$
$Q_{stg}$	heat storage ahead of the steam-chamber interface, $J$
$S_{oi}$	initial oil saturation, fraction
$S_{or}$	residual oil saturation, fraction
$S_t$	transversal side, $m$

$S_o$	oil saturation
$S_{wi}$	initial water saturation
$S_{o_{.5y}}$	oil saturation at year 5
$\overline{S_{or}}$	average residual oil saturation, fraction
$S_w$	water saturation, fraction
$S_w^*$	normalized water saturation, fraction
$S_{wirr}$	irreducible water saturation, fraction
$\sin(\beta)$	sine function of the angle $\beta$ , dimensionless
$T$	temperature, $^{\circ}C$
$T_r$	initial reservoir temperature, $^{\circ}C$
$T_{st}$	steam temperature, $^{\circ}C$
$u(x)$	utility function
$U$	steam-chamber velocity in the direction normal to the interface, $\frac{m}{s}$
$V_c$	cell bulk volume, $m^3$
$\alpha$	reservoir thermal diffusivity, $\frac{m^2}{s}$
$\beta$	sink angle, radians
$\delta$	heat-penetration depth, $m$
$\varepsilon$	small random number to break ties in APDS implementation, <i>day</i>
$\Delta S_o$	recoverable oil saturation, fraction
$\mu_R(T)$	viscosity ratio at temperature ( $T$ ), dimensionless
$\mu_{oil}$	dynamic oil viscosity, $mPa\ s$
$\mu_{water}$	dynamic water viscosity, $mPa\ s$
$\nu$	kinematic viscosity, $\frac{m^2}{s}$
$\nu_{hv}$	kinematic viscosity in the heated volume, $\frac{m^2}{s}$
$\nu_{st}$	kinematic viscosity at steam temperature, $\frac{m^2}{s}$
$\nu_{water}$	kinematic water viscosity, $\frac{m^2}{s}$
$\xi$	normal distance to the steam-chamber interface, $m$
$\rho$	Pearson's correlation coefficient

$\rho_o$	oil density, $kg/m^3$
$\rho_s$	Spearman's correlation coefficient
$\emptyset$	porosity, fraction

## List of Abbreviations

Abbreviation	Description
2D	two dimensional
3D	three dimensional
4D	four dimensional
APDS	approximate physics discrete simulator
ART	anomaly recognition tool
bbbl	barrel
BPD	barrel per day
CAD	Canadian dollar
CCG	centre for computational geostatistics
CDF	cumulative distribution function
CERI	Canadian energy research institute
CI	conformance index
CMG	computer modeling group
COP	cumulative oil production
EF	efficient frontier
EnKF	ensemble Kalman filter
FSD	first-degree stochastic dominance
HTPG	hierarchical truncated plurigaussian
IHS	inclined heterolithic strata
MVC	mean-variance criterion
NPV	net present value
PDF	probability density function
PPMT	projection pursuit multivariate transform
PRM	petroleum reservoir management
R	risk tolerance parameter
SAGD	steam-assisted gravity drainage

SCHV	steam-chamber bitumen volume
SDM	stochastic dominance matrix
SDR	stochastic dominance rules
SGS	sequential Gaussian simulation
SOR	steam-oil ratio
SSD	second-degree stochastic dominance
US\$	American dollar
UTF	underground test facility
VOI	value of information
WTI	west Texas intermediate

# 1 Graph-Based Simulator for Steam Assisted Gravity Drainage Reservoir Management

## 1.1 Introduction

Petroleum reservoir managers must make decisions about projects (e.g. infill drilling and/or operational strategies) with uncertain economic results due to imperfect knowledge of the geometry and properties of the reservoir. This geological uncertainty can be characterized by a set of geostatistical realizations that taken all together form a geological model (Pyrzcz & Deutsch, 2014). Geostatistics provides well established methods to generate geological models (Caers, 2011; Chiles & Delfiner, 2012; Deutsch & Journel, 1998; Goovaerts, 1997; Pyrcz & Deutsch, 2014) but the information embedded in them is only partially used.

The substandard practice can be linked to three causes: the high dimensionality of the space of feasible projects that must be searched to find the best project; the time and computational cost of transferring the geological uncertainty into a suitable response variable for decision making; and the lack of a practical decision-making criterion that actively manages the risk that arises from the geological uncertainty.

This research tackles the last two causes in the context of the steam-assisted gravity drainage (SAGD) recovery technology. SAGD is a thermal recovery process in which heat is injected in the reservoir to lower the bitumen viscosity and produce it by gravity. The empty pore-space left behind by the bitumen is replaced by steam creating a steam-chamber in the subsurface. A graph-based simplified physics simulator is developed for efficiently transferring the geological uncertainty into steam-chamber evolution paths that can directly support SAGD reservoir management or be converted to a monetary response variable to input decision-making workflows.

Additionally, a decision-making criterion for active geological risk management is introduced. The criterion is consistent with the utility theory framework and combines Mean-Variance Criterion (MVC) and Stochastic Dominance Rules (SDR) to guide the decision process. Searching the high dimensional space of feasible projects in petroleum reservoir management (PRM) is out of the scope of this thesis.

## 1.2 Petroleum Reservoir Management Decision-Making Workflow

To clarify the jargon of the dissertation and further define the extent of this research, the PRM decision-making workflow is illustrated on Figure 1.1 in the framework of a formal rational decision-making under uncertainty model with four elements: a set of feasible actions, a set of outcomes, a preference ordering of the outcomes and one concept of rationality that governs the decision process (Stirling, 2012).

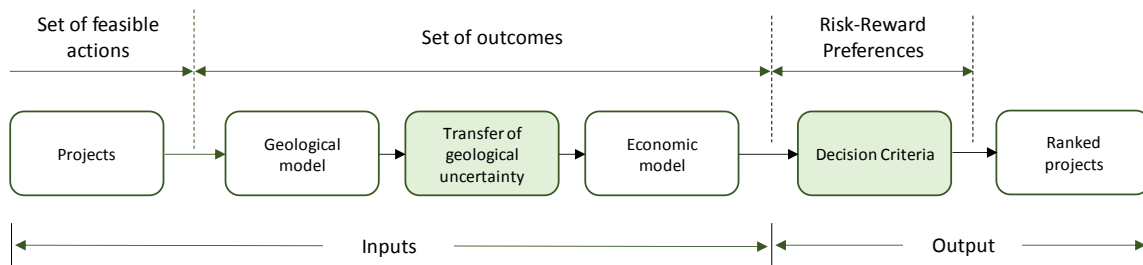


Figure 1.1: Components of a Petroleum Reservoir Management Decision-Making workflow.

The *Set of feasible actions* represents the set of projects from which a choice must be made by the reservoir manager. The type of project that a reservoir manager is concerned with ranges from the selection of type, number and location of wells to the definition of an entire field development plan.

The *Set of outcomes* refers to the consequences of every project under analysis. The results cannot be anticipated with certainty because they depend on unknown reservoir properties. Defining the set of outcomes requires performing two complex and demanding tasks, one is to build a geological model and the other is to process the projects and the geological model through a transfer function (e.g. dynamic flow simulation and cash flow) to obtain a probability distribution of the response variable that will be used to make the decisions.

The *Preferences and the concept of rationality* are required to choose from multiple options with different distributions of value. After transferring the geological uncertainty, selecting a project from the set of feasible actions is equivalent to make a choice between the probability distributions of the response variable (Johnstone & Lindley, 2013). To make that choice, the investor's preferences over the space of outcomes can be encoded in a

utility function (Kochenderfer, 2015) . A decision maker will make a “rational” decision, if he selects a project that maximizes expected utility.

This research focuses on the components of the PRM decision-making workflow highlighted on Figure 1.1, that is, transferring the geological uncertainty in SAGD projects and formulating a decision-making rule that considers the geological risk.

### 1.3 Problem Setting

Reservoir managers of SAGD projects are familiar with a decision-making workflows that does not conform to the managerial principle of considering the risk and reward trade-off, even though the decisions involve significant geological uncertainty. Yet, optimal decision-making is sensitive to the dynamic reservoir response and to geological uncertainty. Decisions that do not consider geological uncertainty may be suboptimal.

One reason for this situation is that reservoir managers often have tight timeframes to make their decisions. For example, projects are constrained by rig contract schedules or must be executed during favorable weather condition windows. Therefore, they cannot wait for the excessive computational time that takes processing projects and all the geostatistical realizations through a full physics flow simulator to feed their decision-making workflows. Moreover, being SAGD a thermal recovery process, the complex combination of heat and flow transport phenomena makes the numerical simulation even more time-demanding than for conventional displacement techniques (Majdi Yazdi & Jensen, 2014) exacerbating the problem of timely transferring of the geological uncertainty for decision making purposes.

When the set of realizations is processed through a reasonable transfer function, the projects are customarily selected based on the maximum expected monetary value criterion, not on the maximum expected utility criterion. The maximum monetary expected value rule is a special case in the utility theory framework that assigns a risk neutral linear utility function to the decision maker. As a consequence, the approach considers that the reservoir manager is only concerned about the returns of the projects and not the associated risks (Levy 2016). In this situation, the effort of using many geostatistical realizations may not be completely compensated by the quality of the decision.

The following example of deficiencies found in the technical literature support the research undertaken in this thesis: (1) despite having a geological model, only one scenario is chosen to be further processed through the dynamic flow simulator (e.g. Alusta et al. 2012), (2) clustering or ranking techniques are applied to select a small set of realizations that are then post-processed (e.g. Sarma et al. 2013). The propagation of the geological through the whole workflow is not undertaken; and, (3) after geological uncertainty transferring the projects are selected based on the maximum expected monetary value criterion, not on the maximum expected utility criterion (e.g. Shirangi and Durlofsky 2015).

## 1.4 Proposed Approach

### 1.4.1 Graph-Base Steam-Chamber Simulator for Transferring the Geological Uncertainty in SAGD Projects

SAGD is a thermal recovery technique that uses gravity as the driving force to produce heavy oil. Steam is injected in the reservoir through a horizontal injector well to heat the bitumen and decrease its viscosity. The heated bitumen becomes mobile and drains by gravity to a producer well completed below the injector well. As the bitumen moves down, the steam moves up to occupy the pore space creating an expanding steam-chamber (Butler, 1991).

SAGD performance in terms of oil production and steam consumption is intrinsically coupled with the expansion rate and the geometry of the steam-chamber. For that reason, since the conception of SAGD in the 1980's, understanding and modeling the evolution of the steam-chamber has been an important research topic.

Notwithstanding the extensive research, current techniques for modeling the steam-chamber have shortcomings that limit their practical implementation, especially when many possible SAGD projects need to be evaluated. Analytical and semi-analytical SAGD models (Butler, 1985; Butler, McNab, & Lo, 1981; Butler & Stephens, 1981) predict the movement of the steam-chamber but only for idealized homogeneous reservoirs. Others authors modified the Butler's model by imposing specific steam-chamber shapes; for

example, triangular (Reis, 1992) and circular (Azad & Chalaturnyk, 2012). 4D-seismic images provide reliable information about the steam-chamber location but is not by itself a predictive method. Full physics thermal flow simulation is perhaps the best method to predict the expansion of the steam-chamber but is too computationally demanding and time consuming to assess SAGD projects that requires evaluating a large number of alternatives. For instance, thermal flow simulation is impractical to evaluate the response of a SAGD well-pair location over a set of geostatistical realizations or for considering many possible SAGD well-pair locations over large areas.

A novel graph-based algorithm named Approximate Physics Discrete Simulator (hereafter APDS) is proposed in this dissertation for SAGD geological uncertainty transferring. APDS efficiently integrates Darcy's Law, material balance and heat transfer concepts to represent the reservoir and emulate the flow of the bitumen and the steam in SAGD. APDS models the steam-chamber evolution as a shortest-path problem where the objective is to find the minimum travel time for the steam to move from the well to the remaining connected nodes in the graph. The problem is solved using a propagation mechanism inspired in the algorithm proposed by Dijkstra (1959) to find the one-to-all shortest-paths in a graph. The output is a model of the steam-chamber expansion through time. APDS works with heterogeneous reservoirs and is computationally efficient.

Additionally, working on the hypothesis that the performance of SAGD projects is strongly linked to the size, shape and rate of growing of the steam-chamber, this research demonstrates that a response variable obtained from APDS on a multi-realization geological model, is a suitable input for a decision-making workflow. The goodness of the chosen variable is measured through its degree of correlation to a pair of metrics calculated from a full physics thermal flow simulator.

#### 1.4.2 Mean-Variance Criteria and Stochastic Dominance Rules to Consider the Geological Risk-Reward trade-off

At the heart of petroleum reservoir management (PRM) resides the challenge of selecting the best project from a group of feasible candidates in the presence of geological uncertainty. The challenge is particularly relevant in low oil price investment environments

where many upstream projects are economically marginal and must be optimized. Companies are now more cautious. Investors are aware that they should consider not only the rewards of the projects, but also their risks. For these reasons, the selection of the projects to be implemented in the field should consider the geological risk and the capacity of the companies to tolerate it. The decision-making criterion adopted ultimately determines which project is selected and implemented.

A decision-making criterion for active geological risk management is formulated and implemented. The criterion is consistent with the utility theory framework and combines Mean-Variance Criterion (MVC) and Stochastic Dominance Rules (SDR) to guide the decision process. It differs from other researches that applied the utility framework to PRM (Güyagüler & Horne, 2004; Ozdogan & Horne, 2006) because a specific utility function is not required. Projects selected using MVC-SDR are reasonable to all risk-averse reservoir managers. The shortcoming is a reduced ability to rank projects with very similar cumulative distribution function response variables. The thesis demonstrates that MVC-SDR is a viable criterion for SAGD decision-making under geological uncertainty.

## 1.5 Dissertation Outline

**Chapter 2** presents the APDS formulation and its components: the graph, the propagation algorithm and the ranking function. This chapter also discusses the relationship between the SAGD steam-chamber expansion and the shortest path problem found in the study of transportation networks (Deo & Pang, 1984). It also describes a pseudocode to implement APDS and a stepwise execution example for a homogeneous and a heterogeneous reservoir.

**Chapter 3** is devoted to the APDS implementation and validation. The chapter first describes the assumptions made to implement an APDS prototype in the Python programming language. After that, it presents a case-study performed with a realistic multi-realization geological model demonstrating that the APDS steam-chamber and metrics calculated from it compares satisfactorily with results obtained from full physics thermal flow simulation.

**Chapter 4** introduces the MVC-SDR decision-making criterion for PRM problems. First, PRM problems are stated in terms of a formal decision-making model under uncertainty. Then, concepts of projects, geological uncertainty characterization, transfer of geological uncertainty, preferences over the outcomes and utility theory are discussed. After that, the theory of MVC and SDR are introduced to PRM. The chapter ends with one conceptual example explaining how these two criteria works together.

**Chapter 5** presents a case-study where the reservoir manager must decide the location of a SAGD horizontal well-pair inside a target volume. It is a representative problem commonly found in the exploitation of oil sands in Western Canada. The case-study uses APDS to transfer the geological uncertainty and then uses MVC-SDR as decision-making criterion.

**Chapter 6** presents a case-study that illustrates how APDS efficiently assists a geostatistical-anomaly enforcement methodology (Hadavand & Deutsch, 2017) to integrate 4D-seismic information to SAGD reservoir characterization.

**Chapter 7** discusses the merits and shortcomings of APDS and MVC-SDR to support SAGD decision-making workflows. It also presents research avenues for future works and concludes the thesis.

The thesis includes several appendices with the Python code implementing APDS.

## 2 SAGD Steam-Chamber Modeling with APDS: Formulation

### 2.1 Introduction

SAGD is a thermal recovery technique that uses gravity as the driving force to produce heavy oil as illustrated in Figure 2.1. Steam is injected in the reservoir through a horizontal injector well to heat the bitumen and decrease its viscosity. The heated bitumen becomes mobile and drains by gravity to a producer well completed 5 to 10 meters below the injector well. As the bitumen moves down, the steam moves up to occupy the pore space creating an expanding steam-chamber (Butler, 1991).

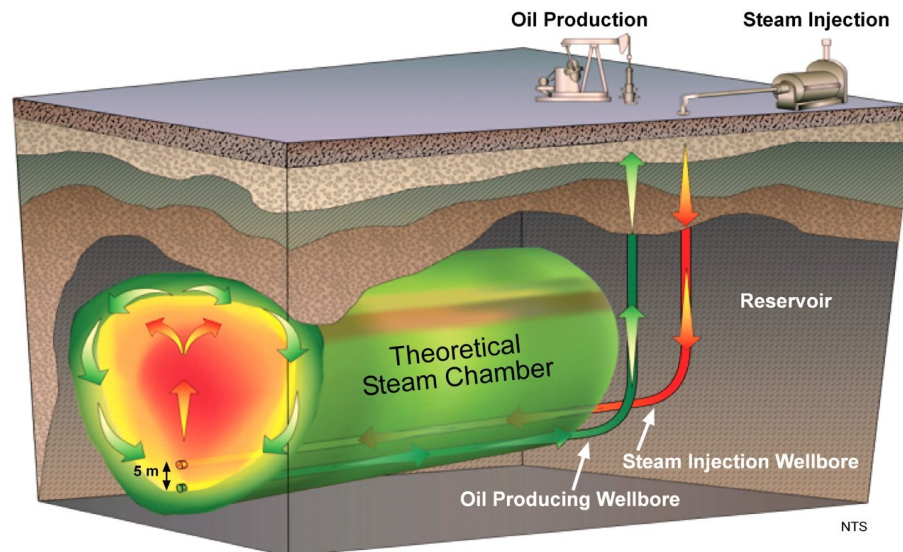


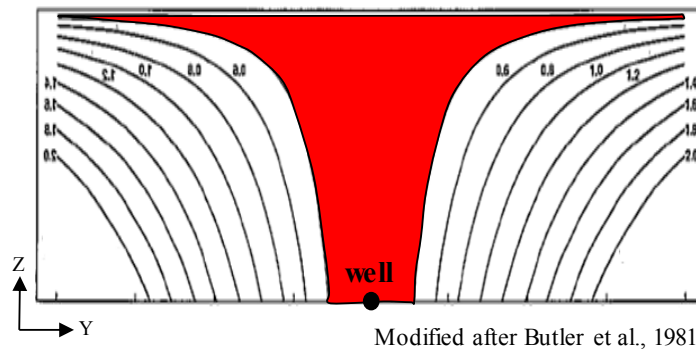
Figure 2.1: Steam-assisted gravity drainage (SAGD) process (obtained from Peacock (2010)).

SAGD performance in terms of oil production and steam consumption is intrinsically coupled with the expansion rate and the geometry of the steam-chamber. For that reason, since the conception of SAGD in the 1980's, understanding the evolution of the steam-chamber has been an important research topic.

## 2.2 Review of Steam-Chamber Modeling Techniques

Contrary to APDS that first models the steam-chamber geometry and then calculates metrics from it to support decisions, current techniques focus on forecasting the bitumen production and the location of the steam-chamber is calculated as a by-product. The first analytical model for SAGD production forecasting in homogeneous reservoirs was proposed by Butler and his colleagues (Butler et al., 1981). They obtain the steam-chamber shown in Figure 2.2.a. The chamber has the issue that the lower part of the interface moves away from the production well (Butler et al., 1981). Afterwards, Butler & Stephens (1981) assumed that the steam-chamber interface remains straight in the lower part and that is tangent to the curves of the original model. This model was called Tandrain and is illustrated in Figure 2.2.b.

**a) BUTLER et al, 1981**



**b) TANDRAIN MODEL**

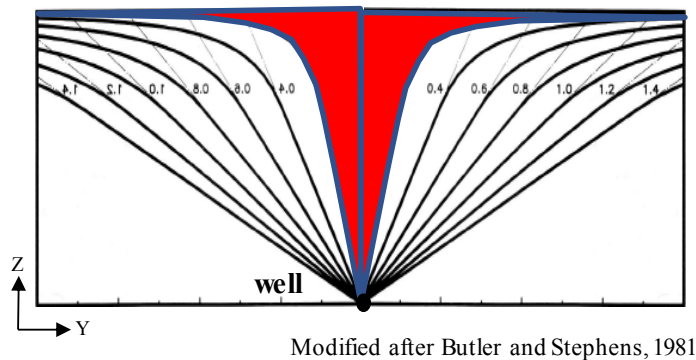


Figure 2.2: Steam-chamber shapes. a) Original Butler's analytical model, b) Tandrain model.

Other authors modified Butler's analytical model by imposing specific steam-chamber shapes; for example, triangular (Reis, 1992) and circular (Azad & Chalaturnyk, 2012) as depicted in Figure 2.3.

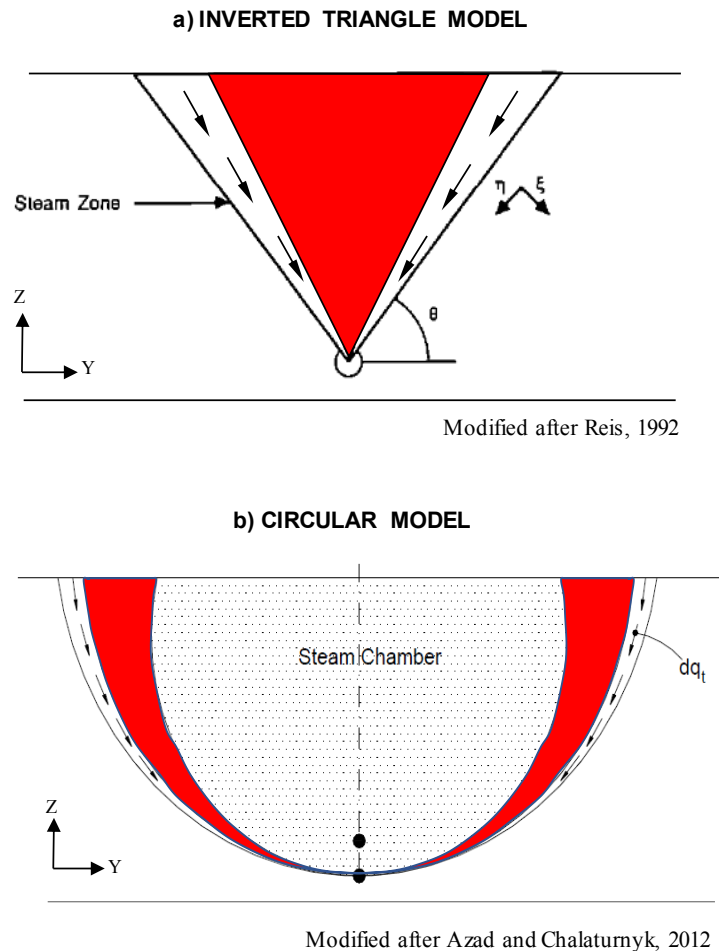
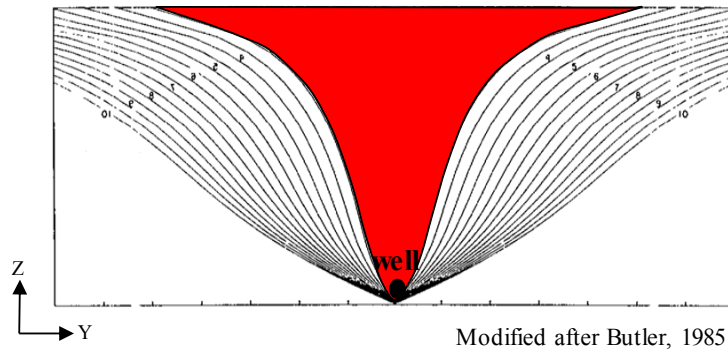


Figure 2.3: Steam-chamber with imposed geometry. a) Inverted triangle model, b) Circular model.

Butler (1985) proposed a semi-analytical model to predict the SAGD production rate and the movement of the interface obtaining the steam-chamber illustrated on Figure 2.4.a. The model was re-visited by Heidari, Pooladi-Darvish, Azaiez, & Maini (2009) to analyze the effect of drainage height in the SAGD performance obtaining the steam-chamber shown in Figure 2.4.b.

**a) BUTLER SEMI-ANALYTICAL, 1985**



**b) HEIDARI et. al SEMI-ANALYTICAL, 2009**

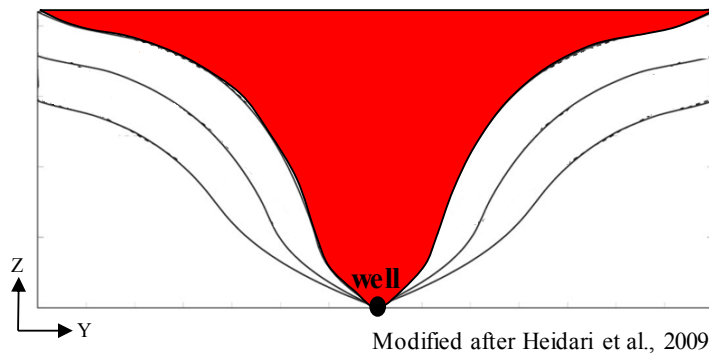


Figure 2.4: Steam-chamber from semi-analytical models. a) Butler (1985) semi-analytical model, b) Heidari et al. (2009) semi-analytical model.

Note that the aforementioned analytical and semi-analytical models predict the movement of the steam-chamber for idealized homogeneous reservoirs. Yet, reservoirs are heterogeneous and the steam-shape can take any irregular shape.

Dehdari (2014) developed a semi-analytical approximate thermal simulator and proposed an empirical method based on connected hydrocarbon volume (Wilde & Deutsch, 2012) to forecast the location of the steam-chamber in heterogeneous reservoirs.

4D-seismic images provide reliable information about the steam-chamber location but is not by itself a predictive method. Full physics thermal flow simulation is perhaps the best method to predict the expansion of the steam-chamber; however, this approach is too

computationally demanding and time consuming to be used in SAGD projects that require evaluating a large number of alternatives in a timely manner.

### 2.3 Steam Chamber Evolution Posed as a Shortest Path Problem

APDS uses graph theory to model the reservoir and the steam-chamber evolution through time. Since the work of Fatt (1956) pore-scale networks models have been extensively used to study the flow of fluids in porous media with the goal of predicting macroscopic transport properties from pore-scale parameters (Oren, Bakke, & Arntzen, 1998). However, the use of graphs proposed in this dissertation at the macroscopic scale of the cells of the numerical model to predict a mega-scale reservoir response such as the steam-chamber in SAGD is novel in the technical literature.

Modeling the evolution of the steam-chamber has similarities with the shortest-path problem found in the study of transportation networks (Deo and Pang, 1984). In transportation, the objective is to find the minimum distance from one given location to another destination or to all other destinations in a network. Usually the distances between vertices are known before hand and the path-length is the sum of the length of intermediate edges or arcs. However, the notion of distance can be generalized to represent other properties of the path being traversed, such as minimum travel time (Deo and Pang, 1984). In steam-chamber SAGD modeling, the objective is to find the path with the minimum travel time for the steam to move from the well to all connected nodes in the graph. This is also the path with the least resistance for the heated bitumen to flow toward the producer well. Different to the transportation network case, how fast or slow the bitumen can move between two nodes in the graph is not known beforehand. This has to be calculated during the steam-chamber growth. APDS solves this problem using a propagation mechanism inspired in the algorithm proposed by Dijkstra (1959) to find the one-to-all shortest-paths in a graph. The output is a model of the steam-chamber expansion through time. The next section presents how APDS uses graph theory, Darcy's Law, material balance and heat transfer concepts to represent the reservoir and efficiently emulate the flow of the bitumen and the steam in SAGD. APDS works in homogeneous and heterogeneous reservoirs.

## 2.4 APDS Formulation

APDS has three main components: a graph, a propagation algorithm and a ranking function. They are integrated to obtain the steam-chamber evolution. These components are described below.

### 2.4.1 Graph

Graphs are convenient mathematical tools to model the SAGD recovery process. They consist of nodes and edges. The nodes can store petrophysical and fluid information, and the edges can be assigned with direction and weights related to porous media flow concepts. Figure 2.5 shows a reservoir cross-section represented as a graph. It has  $n = 9$  vertices and  $m = 20$  directed edges. The set of vertices is  $V = \{x_1, x_2, x_3, \dots, x_9\}$  and the set of edges or arcs is  $E = \{e_{1-2}, e_{2-1}, \dots, a_{5-9}\}$ . Each edge is an ordered tuple representing the connection between two vertices. For example,  $e_{1-4} = (x_1, x_4)$  where  $x_1$  is the initial vertex and  $x_4$  is the terminal vertex. Note that the vertex  $e_{4-1} = (x_4, x_1)$  where  $x_4$  is the initial vertex and  $x_1$  is the terminal vertex is not present in the graph. In APDS, the cells in the geological model with permeable rocks (i.e. sands) are connected vertices in the graph  $\{x_1, x_2, x_3, x_4, x_5, x_7, x_8, x_9\}$ . Non-permeable rocks (i.e. shales) are isolated vertices in the graph, vertex  $\{x_6\}$ . Two vertices connected by an edge are neighbors, and all the neighbors of a given vertex  $x$  are called the neighborhood of  $x$  (Voloshin, 2009). For example, the neighborhood of  $x_1$  is  $N(x_1) = \{x_2, x_5, x_4\}$ . A path is a sequence of edges connecting vertices. In Figure 2.5 a path from the vertex  $x_1$  to  $x_9$  denoted as  $(x_1, x_9) - path = \{x_1, x_5, x_9\}$ . Vertices store petrophysical information and a real-valued function  $w$  generates the edges weights. Since the graph represents a geological model in APDS, the terms cells, nodes and vertices are used interchangeably.

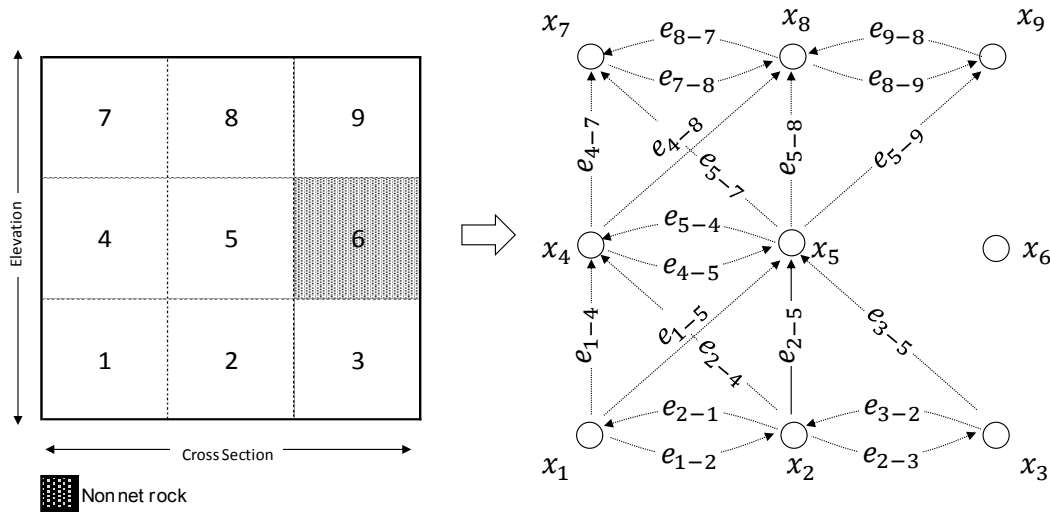


Figure 2.5: Illustration of a 2D-grid geological model represented as a graph.

## 2.4.2 Propagation Algorithm

APDS models the steam-chamber evolution as a shortest-path problem where the objective is to find the minimum travel time for the steam to move from the well to the remaining connected nodes in the graph. A technique for solving the shortest-path problem is the Dijkstra algorithm (Dijkstra, 1959) that finds the one-to-one and one-to-all shortest-paths in a graph. It works with non-negative arc values that must be known beforehand. The algorithm is efficient, easy to understand, implement and customize. Interested readers can find the description of Dijkstra's algorithm in books devoted to graph algorithms (e.g. Even 2011; Ortega-Arranz et al. 2015).

Although the direct application of Dijkstra's algorithm does not model the evolution of the steam-chamber in SAGD, its structure was the base to formulate the propagation algorithm in APDS. It works one cell at the time, that is called the active cell, and while the computation progresses the cells are classified as being part of the steam-chamber or the heated volume. Figure 2.6 illustrates the propagation algorithm:

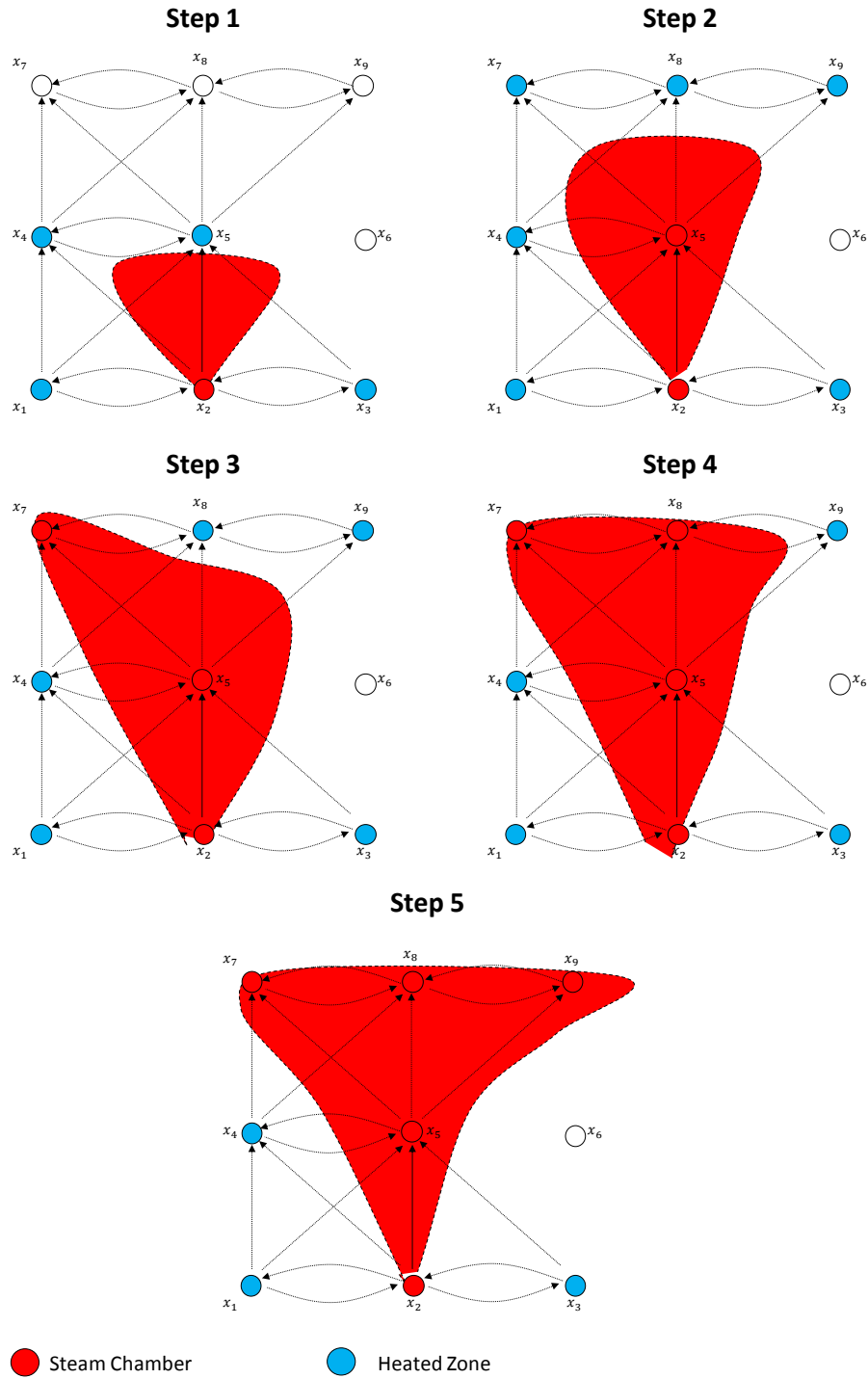


Figure 2.6: APDS propagation mechanism. Red shapes are not part of APDS. They were drawn to help visualizing the steam-chamber expansion. Edge labels omitted in this figure are shown in Figure 2.5.

- To initialize the algorithm, the producer well location is provided, vertex  $x_2$  in this example. At step 1, heated bitumen drains through the vertex  $x_2$  and steam concurrently fill-up the empty pore-space expanding the steam-chamber. Vertex  $x_2$  becomes part of the red colored steam-chamber. Now, bitumen can drain from the neighborhood  $N(x_2) = \{x_1, x_3, x_4, x_5\}$  that becomes part of the blue colored heated volume. The travel time for the edges  $\{e_{2-1}, e_{2-3}, e_{2-4}, e_{2-5}\}$  connecting  $x_2$  with its neighborhood is calculated with the ranking function explained in section 2.2.3.
- At step 2, bitumen drains from the vertex in the heated volume through the edge with the lowest travel time, edge  $e_{2-5}$  in this case, and the vertex  $x_5$  is added to the steam-chamber. Now, bitumen can also drain from the neighborhood  $N(x_5) = \{x_4, x_7, x_8, x_9\}$  that is added to the heated volume.
- The algorithm progresses until all vertices connected to  $x_2$  are processed. Note that the isolated vertex  $x_6$  will not be part of the steam-chamber. Figure 2.6 shows three additional steps. The red filled shape was added to highlight the steam-chamber generated by the propagation algorithm.

Observe that the order in which the cells are added to the steam-chamber is intended to reflect the evolution of the steam-chamber in the subsurface.

### 2.4.3 Ranking Function

The ranking function to calculate the travel time plays a key role in the propagation algorithm. It maps the petrophysical properties, the fluid properties and the local geometrical features of the reservoir model into ranking values - edge weights in graph terminology - that governs the development of the steam chamber.

The ranking function is the sum of two components, the cell time and the model time. It has the units of time.

### 2.4.3.1 Cell Travel Time

Cell travel time measures how long it takes to drain movable bitumen from one cell to an adjacent cell in the direction of a sink. Cell travel times are computed independently for every edge without a reference time; however, because these values are based on Darcy's Law, material balance and heat transfer concepts, they are comparable across different locations in the reservoir. In other words, no matter their location in the reservoir model, two cells with the same petrophysical, fluid and geometrical properties will have the same cell travel time.

Darcy's Law (Equation 2.1) and material balance at the cell scale (Equation 2.2) are used for the cell travel time. The formulation assumes that gravity is the only driving force (Butler et al., 1981). Chapter 3 demonstrates that the current APDS implementation is consistent with a heat transfer mechanism by conduction with a steady state temperature ( $T$ ) distribution ahead of the advancing steam-chamber interface given by Equation 2.3.

$$q_o = \frac{A_t k_o g \sin \beta}{\nu_{hv}} \quad (2.1)$$

Where,  $q_o$  is the oil rate,  $A_t$  is the transversal area for the flow in the direction of the angle ( $\beta$ ),  $k_o$  is the effective oil permeability,  $g$  is the gravity constant,  $\beta$  is the sink angle and  $\nu_{hv}$  is the kinematic oil viscosity in the heated volume.

$$Cell\ Travel\ Time = \frac{V_c \phi \Delta S_o}{q_o} \quad (2.2)$$

Where,  $V_c$  is bulk cell volume,  $\phi$  is porosity and  $\Delta S_o$  is recoverable oil saturation.

$$\frac{T - T_r}{T_{st} - T_r} = e^{-U\xi/\alpha} \quad (2.3)$$

Where,  $T_r$  is the initial reservoir temperature,  $T_{st}$  is the steam temperature,  $U$  is the steam-chamber velocity in the direction normal to the interface,  $\xi$  is the distance measure normal to the steam-chamber interface and  $\alpha$  is the reservoir thermal diffusivity. Figure 2.7 illustrates most terms of previous equations.

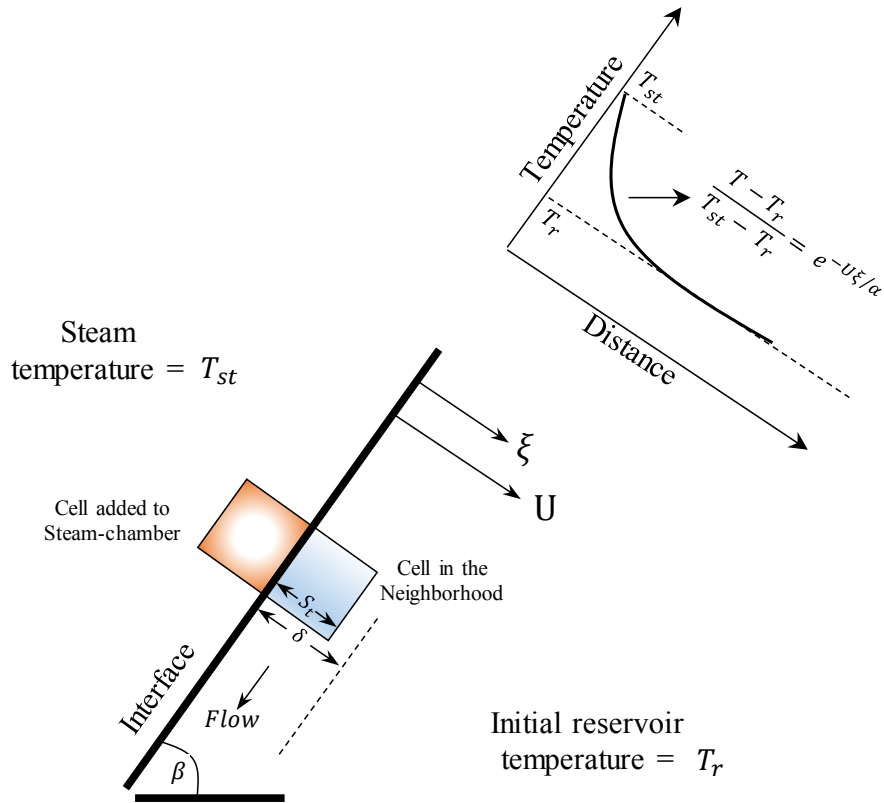


Figure 2.7: Steam-chamber interface and temperature distribution (modified after Butler (1991)).

The concepts of sink angle ( $\beta$ ), transversal area ( $A_t$ ) and kinematic oil viscosity in the heated volume ( $v_{hv}$ ) in the context of the APDS are further explained in Chapter 3 devoted to the implementation and validation of APDS.

#### 2.4.3.2 Model Time

The model time tracks the time elapsed from the beginning of the steam-chamber. It provides the reference starting point to every cell time. Model time is defined as the ranking value of the latest cell added to the steam-chamber; and therefore, it is continuously being updated as the steam-chamber grows. When a cell becomes part of the steam-chamber, its ranking value is saved and added to the cell time in its neighborhood.

## 2.4.4 APDS Outputs

APDS generates a sequence of graph nodes ordered by time as depicted in Figure 2.8.a. for the example presented in section 2.2.2. The nodes do not appear at regular time intervals because the algorithm only captures the time when the event of one cell moving from the heated volume to the steam-chamber occurs. In this sense APDS is a discrete event simulator. If the geological model has a large number of cells, the small time interval between events creates an output that is almost continuous in time ; this is clearer during the early stages - rising and spreading- of the steam-chamber (Butler, 1991). The sequence of ordered nodes reflects the evolution of the steam-chamber in the subsurface (Figure 2.8.b). It can also be assembled and combined with the volumetric information of the nodes to generate the steam-chamber volume variable that is a proxy of the cumulative oil forecast (Figure 2.8.c).

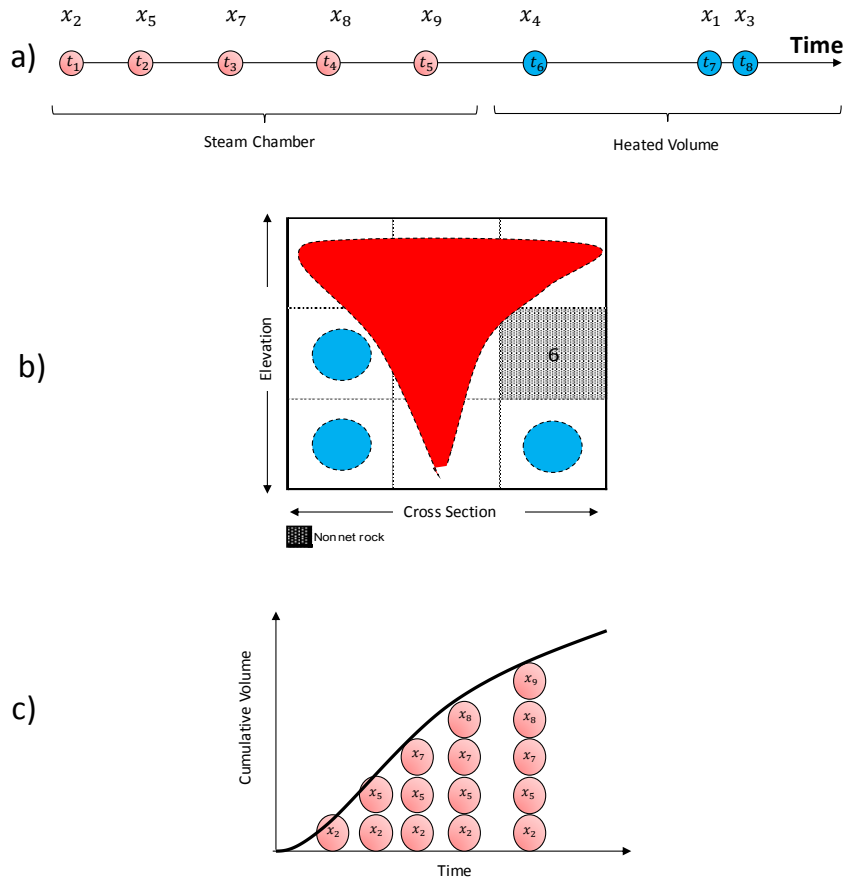


Figure 2.8: APDS Outputs: a) Ordered sequence of nodes, b) Steam-chamber model, c) Cumulative steam-chamber volume.

The following sections present pseudocode for APDS and a stepwise execution example for a homogeneous and a heterogeneous reservoir.

## 2.5 APDS Pseudo Code

The following pseudocode implements APDS. A line-by-line explanation is given below.

```
1  APDS (Graph, Source, Sink):
2  Create containers. Steam Chamber (SCH), Heated Zone (HZ) and Parent Sink (PS)
3      for each node  $x$  in Source:
4          HZ [ $x$ ]  $\leftarrow$  0 ranking value
5          PS [ $x$ ]  $\leftarrow x$ 
6          add  $x$  to Sink
7      while HZ is not empty:
8          active-cell  $\leftarrow$  node in HZ with minimum ranking value
9          remove active-cell from HZ
10         SCH [active-cell]  $\leftarrow$  ranking value
11         Model Time  $\leftarrow$  ranking value of active-cell plus delay
12
13         if active-cell in Sink:
14             temp-PS  $\leftarrow$  active-cell
15         else:
16             temp-PS  $\leftarrow$  PS [active-cell]
17
18         for each neighbor  $x$  of the active-cell and not in SCH:
19              $\beta$   $\leftarrow$  Sink angle between temp-PS and neighbor  $x$ 
20
21             if  $\beta$  equals zero (0):
22                 temp-ranking value  $\leftarrow$  arbitrary large ranking value
23             else:
```

```

24             temp-ranking value = Model Time + Cell Time +  $\epsilon$ 
25
26         if  $x$  not in HZ:
27             HZ [ $x$ ]  $\leftarrow$  temp-ranking value
28             PS [ $x$ ]  $\leftarrow$  temp-PS
29
30         if  $x$  in HZ and temp-ranking value < HZ [ $x$ ]:
31             HZ [ $x$ ]  $\leftarrow$  temp-ranking value
32             PS [ $x$ ]  $\leftarrow$  temp-PS
33
34     return SCH [ ]

```

Pseudocode description:

*Line 1.* APDS inputs are: (1) a Graph, the reservoir mathematical model, (2) the Source, a list of indexes of the cells intersected by the production wells. The source is not limited to one set of adjacent cells, for that reason, APDS can handle multiple well locations, and (3) the Sink, a list of indexes pointing all the cells that could behave like sinks in the reservoir.

*Line 2.* APDS maintains three containers: (1) the Steam Chamber (SCH), for preserving the order in which the cells are added to the steam chamber and their ranking values, (2) the Heated Zone (HZ), a priority queue with cells ordered according to the ranking values, and (3) the Parent Sink (PS), for tracking the parent sink history of every node in the graph.

*Lines 3 to 6:* APDS initialization. All nodes in Source are assigned to HZ with an initial ranking value of zero (0). Note that any other convenient ranking value can be used to initialize APDS. Moreover, every cell in the Source can have its own initialization value. This property is useful to model SAGD well-pairs that enter in production at different times. All nodes in Source are also defined with their own PS and added to the Sink.

*Line 7.* The main loop of the algorithm. APDS will run until exhausting all nodes in the HZ.

*Lines 8 to 10.* The node with the minimum ranking value is extracted from the HZ, labeled as the active-cell and added to SCH.

*Line 11.* Model time is updated to be the active-cell ranking value plus a delay.

*Line 13 to 16.* If the active-cell is a sink, it is assigned temporarily as the neighborhood parent sink. If the active-cell is not a sink, the neighborhood temporarily inherits the active-cell parent sink.

*Line 17.* Loop through the neighborhood of the active-cell

*Line 19.* Calculate the sink angle.

*Line 22.* If the sink angle is zero (0), the time to mobilize bitumen from a cell to its PS tends to infinite. For that reason, the implementation assigns an arbitrary large ranking value, so the cell will be placed at the end of the priority queue HZ.

*Line 24.* If the sink angle is not zero (0), the ranking value plus  $\epsilon$  is calculated.  $\epsilon$  is a very small random number introduced in the APDS implementation to break ties between cells having the same raking value.

*Lines 26 to 28.* If the cell is visited for the first time, it is added to HZ with its raking value and PS.

*Lines 30 to 32.* If the cell is already in HZ and the newer calculated ranking value is smaller to the previously stored value, the raking value and the PS are updated. Consequently, the cell will jump positions in the priority queue HZ.

*Line 34.* APDS exits when the HZ is exhausted and returns SCH.

## 2.6 Step-wise Procedure

The application for a cross-section in a homogeneous and a heterogeneous reservoir shown in Figure 2.9 is intended to further explain the pseudocode and how it deals with the presence of barriers. The example uses typical Athabasca oil-sand parameters (Cokar, Kallos, & Gates, 2013) listed in Table 2.1. The cell size is 1m x 1m x 1m in x, y and z directions, respectively. Figure 2.10 and Figure 2.11 show detailed calculations.

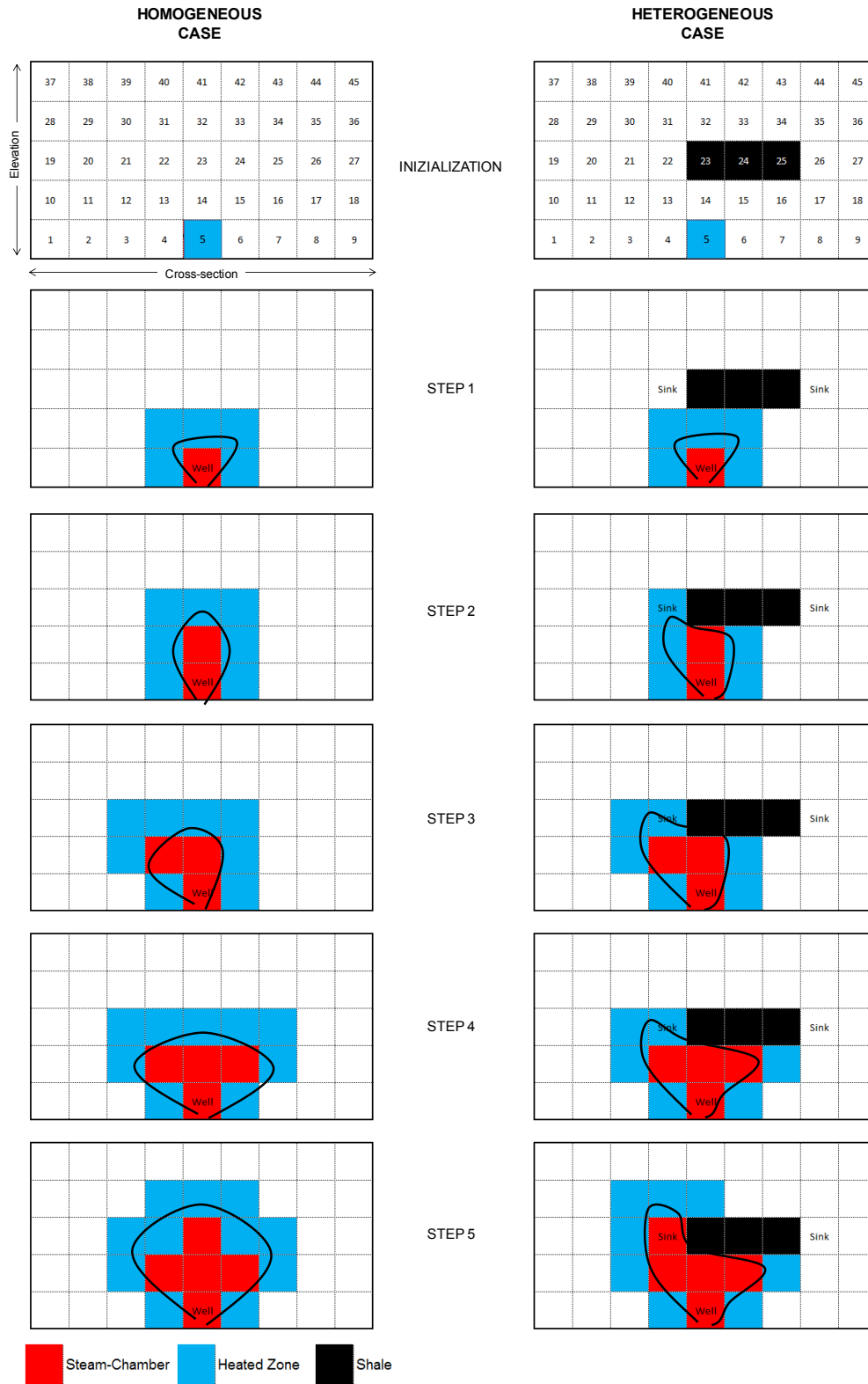


Figure 2.9: APDS stepwise procedure. Top row shows the algorithm initialization and the cell indexes. Well and sinks locations are labeled. Black outlines drawn to help visualizing how the APDS handles barriers.

The first row in Figure 2.9 is the initialization of the algorithm. The well is located in cell 5 that is added to the heated zone (Priority queue). Cell 5 is also considered a sink. Note that if any other cell is selected for the well, the algorithm will generate a very different steam-chamber shape, especially in the heterogeneous case.

At step 1, cell 5 is extracted from the heated zone. It becomes the first cell in the steam-chamber in both cases. Neighbors of cell 5 are added to the heated zone with their ranking values. Note that cells 4 and 6 have a sink angle of zero (0) that results in an infinite ranking value. Then APDS assigns an arbitrary ranking value of 10950 days (30 years) to ensure that these cells will occupy the end of the priority queue. At step 2, cell 14 is extracted from the heated zone and added to the steam-chamber in both cases. Note that in the heterogeneous reservoir some neighbors of cell 14 are shales, then the barrier begins to affect the steam-chamber growing. Figure 2.9 shows 3 additional steps. At step 5, the shape of the heated zone is very different for the two cases and the order in which the cells are added to the steam-chamber starts to change.

Table 2.1: Typical Athabasca oil-sand parameters used in the stepwise procedure (Modified after Cokar et al. (2013)).

<b>Property</b>	<b>Value</b>
$T_r$ ( $^{\circ}C$ )	10
$T_{st}$ ( $^{\circ}C$ )	260
$\rho_o$ ( $kg/m^3$ )	998
$\emptyset$	0.35
$k_{abs}$ ( $m^2$ )	$3.05 \times 10^{-12}$
$k_{ro}$ ( $m^2$ )	0.2
$S_{io}$	0.84
$S_{or}$	0.14
$v_{st}$ ( $m^2/s$ )	$4.28 \times 10^{-6}$
m	3

Step	Initial Heated Zone (Priority Queue)	Steam-chamber (List)	Active Cell (Index)	Nbors. Cells (Index)	Parent Sink (Index)	Sink Angle (deg.)	Cell Time (day)	Model Time (days)	$\epsilon$ (days)	Current Ranking Value (day)	Previous Ranking Value (day)	Comment	Final Heated Zone (Priority Queue)
1	{5}	{5}	5	4	5	0.0	10950	0.000	0.004	10950		Ranking value set to 30 years	{14,13,15,4,6}
				13	5	45.0	6.210	0.000	0.023	6.210			
				14	5	90.0	3.121	0.000	0.028	3.121			
				15	5	45.0	6.215	0.000	0.028	6.215			
				6	5	0.0	10950	0.000	0.011	10950		Ranking value set to 30 years	
2	{14,13,15,4,6}	{5,14}	14	13	5	45.0	6.210	3.121	0.023	9.330	6.210	Ranking value from step 1 is smaller	{13,15,23,22,24,4,6}
				22	5	63.4	3.868	3.121	0.001	6.988			
				23	5	90.0	3.119	3.121	0.026	6.240			
				24	5	63.4	3.874	3.121	0.007	6.994			
				15	5	45.0	6.215	3.121	0.028	9.335	6.215	Ranking value from step 1 is smaller	
3	{13,15,23,22,24,4,6}	{5,14,13}	13	12	5	26.6	7.740	6.210	0.007	13.950			{15,23,22,24,21,12,4,6}
				21	5	45.0	6.225	6.210	0.039	12.435			
				22	5	63.4	3.868	6.210	0.001	10.078	6.988	Ranking value from step 2 is smaller	
				23	5	90.0	3.119	6.210	0.026	9.329	6.240	Ranking value from step 2 is smaller	
				14	5	90.0						Cell in Steam-Chamber	
4	{15,23,22,24,21,12,4,6}	{5,14,13,15}	15	14	5	90.0						Cell in Steam-Chamber	{23,22,24,25,21,12,16,4,6}
				23	5	90.0	3.119	6.215	0.026	9.334	6.240	Ranking value from step 2	
				24	5	63.4	3.874	6.215	0.007	10.088	6.994	Ranking value from step 2	
				25	5	45.0	6.199	6.215	0.013	12.413			
				16	5	26.6	7.770	6.215	0.037	13.984			
5	{23,22,24,25,21,12,16,4,6}	{5,14,13,15,23}	23	22	5	63.4	3.868	6.240	0.001	10.107	6.988	Ranking value from step 2	{22,24,32,33,31,25,21,12,16,4,6}
				31	5	71.6	3.471	6.240	0.034	9.711			
				32	5	90.0	3.124	6.240	0.031	9.364			
				33	5	71.6	3.468	6.240	0.031	9.708			
				24	5	63.4	3.874	6.240	0.007	10.113	6.994	Ranking value from step 2	

Figure 2.10: APDS calculations for the homogeneous reservoir depicted in the left column of Figure 2.9.

Step	Initial Heated Zone (Priority Queue)	Steam-chamber (List)	Active Cell (Index)	Nbors. Cells (Index)	Parent Sink (Index)	Sink Angle (deg.)	Cell Time (day)	Model Time (days)	$\epsilon$ (days)	Current Ranking Value (day)	Previous Ranking Value (day)	Comment	Final Heated Zone (Priority Queue)
1	{5}	{5}	5	4	5	0.0	10950	0.000	0.004	10950		Ranking value set to 30 years	{14,13,15,4,6}
				13	5	45.0	6.210	0.000	0.023	6.210			
				14	5	90.0	3.121	0.000	0.028	3.121			
				15	5	45.0	6.215	0.000	0.028	6.215			
				6	5	0.0	10950	0.000	0.011	10950		Ranking value set to 30 years	
2	{14,13,15,4,6}	{5,14}	14	13	5	45.0	6	3.121	0.023	9.330	6.210	Ranking value from step 1 is smaller	{13,15,22,4,6}
				22	5	63.4	3.868	3.121	0.001	6.988			
				23	5	90.0						Shale	
				24	5	63.4						Shale	
				15	5	45.0	6	3.121	0.028	9.335	6.215	Raking value from step 1 is smaller	
3	{13,15,22,4,6}	{5,14,13}	13	12	5	26.6	8	6.210	0.007	13.950			{15,22,21,12,4,6}
				21	5	45.0	6.225	6.210	0.039	12.435			
				22	5	63.4	3.868	6.210	0.001	10.078	6.988	Ranking value from step 2 is smaller	
				23	5	90.0						Shale	
				14	5	90.0						Cell in Steam-Chamber	
4	{15,22,21,12,4,6}	{5,14,13,15}	15	14	5	90.0						Cell in Steam-chamber	{22,21,12,16,4,6}
				23	5	90.0						Shale	
				24	5	63.4						Shale	
				25	5	45.0						Shale	
				16	5	26.6	8	6.215	0.037	13.984			
5	{22,21,12,16,4,6}	{5,14,13,15,23}	22	21	22	0.0	10950	6.988	0.001	10957	12.435	Ranking value from step 3 is smaller	{31,21,32,30,12,16,4,6}
				30	22	45.0	6.221	6.988	0.034	13.209			
				31	22	90.0	3.124	6.988	0.031	10.112			
				32	22	45.0	6.217	6.988	0.031	13.206			
				23	22	0.0						Shale	

Figure 2.11: APDS calculations for the heterogeneous reservoir depicted in the right column of Figure 2.9.

## 2.7 APDS Time Complexity

The time complexity of APDS is associated to Dijkstra's algorithm (Dijkstra, 1959) and its implementation. The current APDS version uses a priority queue that leads to a complexity of  $O = (m \log(n))$ , where  $n$  is the number of cells and  $m$  is the number of edges (Ortega-Arranz et al., 2015).

## 2.8 Potential Applications

APDS has a straightforward mathematical formulation to secure an efficient computational implementation; it is not intended as a replacement for a full physics thermal simulator. APDS is mainly envisioned to be a cost-effective transfer function to support decision making models that considers geological uncertainty. APDS is especially suitable for guiding decisions in SAGD that can be made based on the geometry and growth rate of the steam-chamber. In this context, some potential applications are described below.

### 2.8.1 SAGD Well-pair Location.

The oil production and steam consumption in SAGD depend on the steam-chamber evolution that is a consequence of the relative position between the well-pairs and the barriers in the reservoir. While the location of the well-pairs is an engineering decision, the location of the barriers is uncertain. APDS allows to test every candidate well-pair location through the geostatistical realizations to obtain a cumulative distribution function (CDF) of the steam-chamber size at a time of interest. These CDFs are used to decide about the well-pair location.

### 2.8.2 SAGD Operation.

SAGD performance can be affected by reservoir layers with high permeability and low oil saturation that might increase heat losses and affect the steam-chamber growth (C. Wang & Leung, 2015). These layers are called lean zones and their analysis is often addressed using numerical simulation (e.g. Xu et al. 2014; Wang and Leung 2015) with the limitations imposed by the computational cost of this technique. APDS applied on geostatistical realizations allows to identify areas where the steam-chamber has higher probability of contacting lean zones. An estimation of the time in which the contact might occur is also readily available. This information helps to anticipate operational pressure strategies to control heat losses, and to consider using flow control devices.

### 2.8.3 4D-Seismic Integration.

4D-seismic provides reliable images of the steam-chamber. These images might reveal anomalies by the absence or unexpected location of the steam-chamber that can be enforced into geostatistical realizations to improve reservoir characterization (Hadavand & Deutsch, 2017). Analyzing the effect of the geostatistical-anomaly enforcement methodology requires comparing the estimation of the steam-chamber before and after applying the enforcement through all the geostatistical realizations (Hadavand & Deutsch, 2017). APDS is efficient enough to perform this task and serve as a tool for assisting 4D-seismic integration in SAGD reservoir characterization.

### 2.8.4 SAGD Geomechanics.

The geomechanical response of a reservoir to SAGD processes is influenced by steam-chamber growth that impact the stress and strain field in situ (Chalaturnyk & Li, 2004). Deformations of the reservoir and caprock can yield to failure of both, affecting the safety of SAGD operations (Pathak, Tran, & Kumar, 2014). Assessing caprock integrity requires considering the steam-chamber dimensions, the pay thickness (Collins, 2007) and the reservoir heterogeneity, among other factors. The uncertainty associated with caprock integrity due to reservoir heterogeneity has been study using coupled geomechanics thermal reservoir simulation (e.g. Pathak et al. 2014), but computational time is even longer than in conventional thermal simulation. APDS provides continuous measures of steam-chamber dimensions, such as volume, height and width, that can enrich analysis of the uncertainty associated with caprock integrity.

## 2.9 Discussion

The APDS was conceived to support workflows that requires the assessment of many SAGD projects. For example, quantification of the impact on a SAGD performance of the geological uncertainty represented in a set of geostatistical realizations, or scanning vast areas in the early development of SAGD fields. For this reason, APDS is intended to be

mathematically simple and yet to have reasonably good predictive capabilities. The predictive capabilities of APDS are bounded by the simplifications imposed in its algorithmic structure and equations. For example, APDS does not model any physics beyond the heated zone and it cannot predict complex physical phenomena that might occur inside the heated zone but that the ranking function does not describe.

The ranking function can be expanded to more closely reproduce the STARS results, but this improvement may decrease computational efficiency. APDS is not designed to replace robust full physics thermal simulator. APDS with a complex ranking function will not match the sophistication and complexity of a thermal simulator, but it might lose its efficiency advantage.

APDS has optional by-products that can support the design and operation of SAGD projects. Some examples are the path of the steam from the producer well to each cell, an approximate value of the steam chamber's interface dimension, the number of non-producing cells –overburden and shales – contacted, and the number and locations of the sinks.

The next chapter describes the assumptions made to implement APDS.

## 3 APDS: Implementation and Validation

### 3.1 Introduction

The APDS formulation is based on well-established engineering principles of flow in porous media, material balance and heat-transfer. However, a successful implementation of the algorithm in a graph framework requires assumptions and practical simplifications that are presented in the first part of this chapter. The structure of the APDS prototyped in the Python programming language is discussed. In the second part of the chapter, a case-study performed with a realistic multi-realization geological model is compared to a commercial simulator to validate the predictive capability and computational efficiency of APDS. The results strongly favor the use of APDS as a fast way to use multiple realizations to support SAGD decision making workflows in the presence of geological uncertainty.

### 3.2 APDS Assumptions and Simplifications

As discussed in Section 2.4.3.1, the steam-chamber expansion is controlled by Equations 3.1 (Darcy's Law) and 3.2 (Material balance). This section describes their variables and explains the assumptions and simplifications applied.

$$q_o = \frac{A_t k_o g \sin \beta}{\nu_{hv}} \quad (3.1)$$

Here,  $q_o$  is the oil rate,  $A_t$  is the transversal area for the flow in the direction of the parent sink,  $k_o$  is the effective oil permeability,  $g$  is the gravity constant,  $\beta$  is the sink angle and  $\nu_{hv}$  is the kinematic oil viscosity in the heated volume.

$$\text{Cell Travel Time} = \frac{V_c \phi \Delta S_o}{q_o} \quad (3.2)$$

Here,  $V_c$  is bulk cell volume,  $\phi$  is porosity and  $\Delta S_o$  is recoverable oil saturation.

### 3.2.1 Sinks, Parent Sink and Sink Angle ( $\beta$ )

During the steam-chamber growth, the heated bitumen flowing downward will go around the barriers (shales). The cells at the edges of the barriers act like sinks for the bitumen on its way down to the producer well. The angle between one cell and one sink is called sink angle ( $\beta$ ), it reflects the initial direction of the flow. Figure 3.1 shows the sink angle between cell A and two out of 13 available sinks, red cells in layer 3.

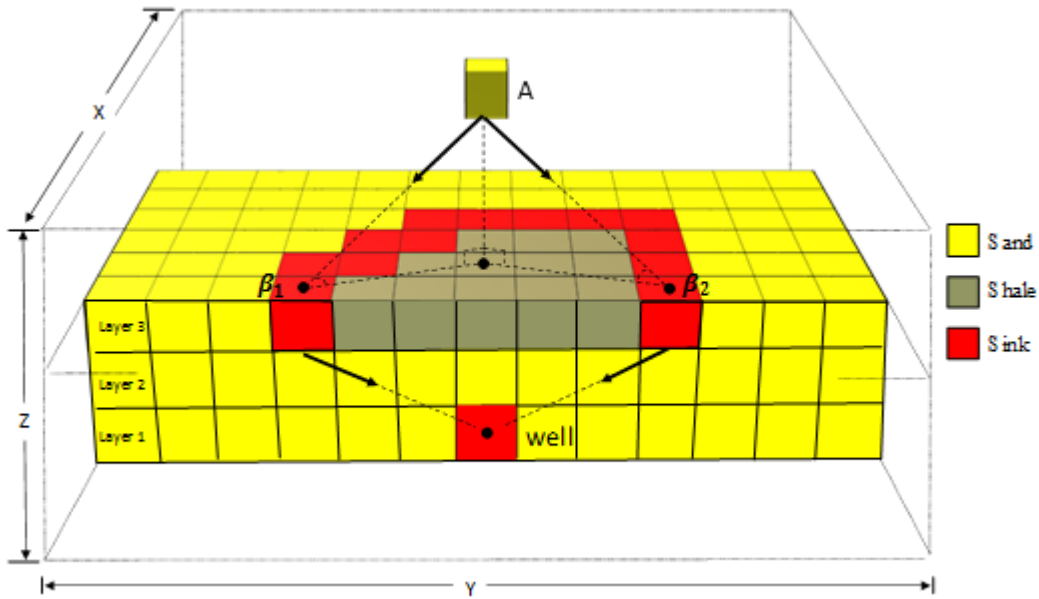


Figure 3.1: Bitumen flowing downward from cell A to the well will pass through one of the sinks (red cells). The angle between cell A and one sink cell is called sink angle. This figure shows two possible sink angles  $\beta_1$  and  $\beta_2$ .

During the expansion of the steam-chamber, APDS uses the ranking value to assign a unique sink to cell A that is called the parent sink of A. The parent sink is the sink that minimizes the travel time. It depends on the relative position between the cell, the barriers and the producer well. Figure 3.2 illustrates the concept. The top image sketches a vertical cross-section of a reservoir with one horizontal barrier. It has 2 potential sinks located at the edges of the barrier. There are 3 producer-well locations, named W1, W2 and W3. The figures below (a, b, c) describe the bitumen path from an arbitrary chosen cell A to each well location.

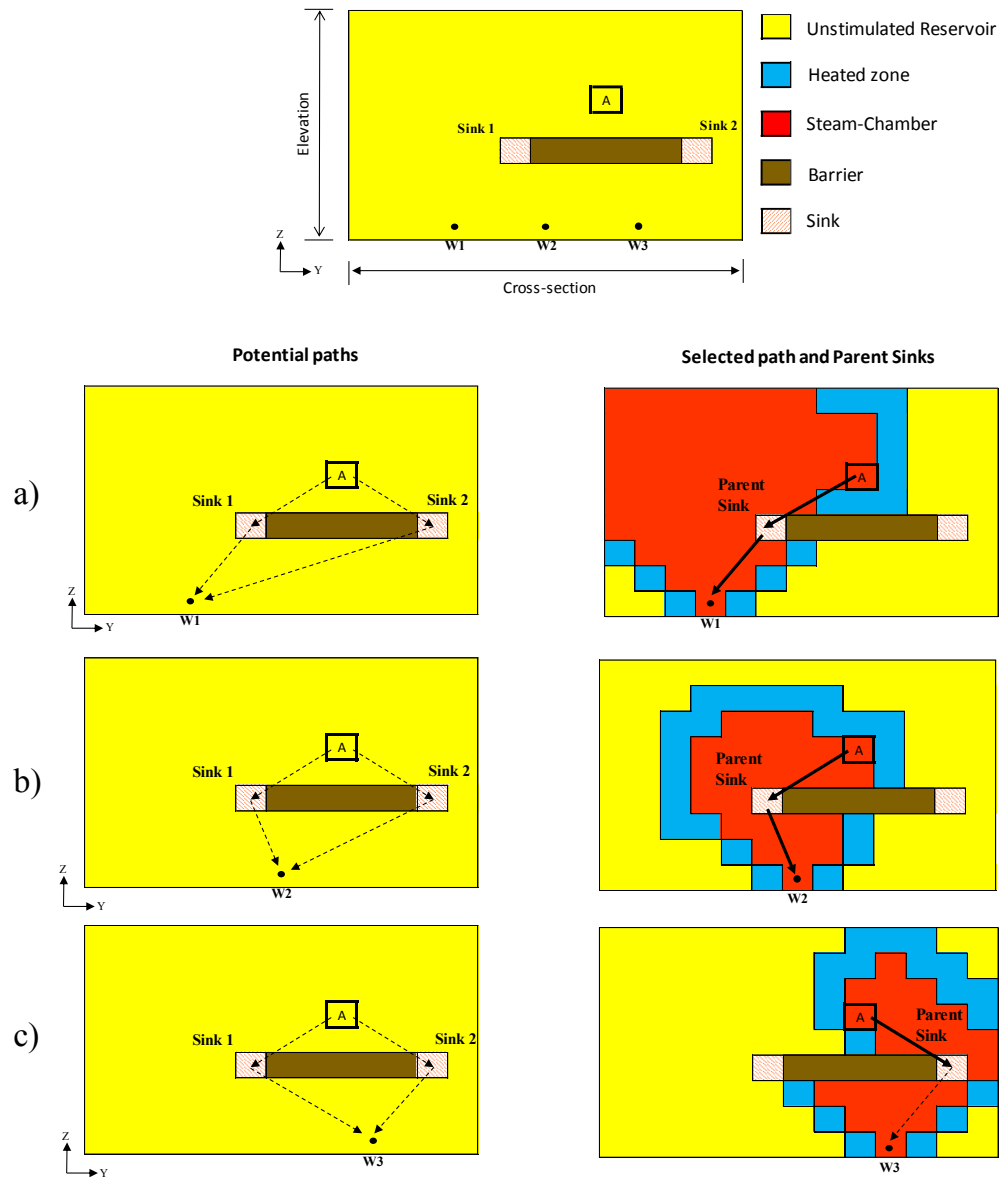


Figure 3.2: The bitumen path depends on the relative position between the cell, the well and the barriers. In figures a and b, the steam-chamber approaches cell A from the left-side and the sink 1 is marked as Parent Sink of A. In figure c, the steam-chamber approaches cell A from the right-side and the sink 2 is marked as Parent Sink of A

Figure 3.2.a. (left column) shows two potential paths for the bitumen in cell A to circumvent the barrier and reach well-1. In this case, the steam-chamber is approaching cell A from the left-side. Therefore, bitumen will drain to the well through the sink-1 that is marked as the Parent Sink of cell A. Figure 3.2.b. shows a different well location (W2) that also results in sink-1 being marked as the Parent Sink of cell A. On the contrary, Figure 3.2.c. presents a case where due to the location of the well-3, the steam-chamber is

approaching the cell A from the right side. Here, the bitumen will drain through sink-2 that becomes the Parent Sink of cell A. Note how even in these simple examples, there are very different steam-chamber shapes.

### 3.2.2 Transversal Area ( $A_t$ )

The bitumen flows from a heated cell toward an adjacent cell in the direction defined by its parent sink angle ( $\beta$ ).  $A_t$  is calculated perpendicular to the direction of the flow. For a cell of unit thickness measured into the paper  $A_t = S_t \times 1$ , where  $S_t$  is the transversal side as shown in Figure 3.3. If  $\beta$  is greater than  $45^\circ$ ,  $S_t$  is calculated with the length of the cell. If  $\beta$  is smaller than  $45^\circ$ ,  $S_t$  uses the height of the cell.

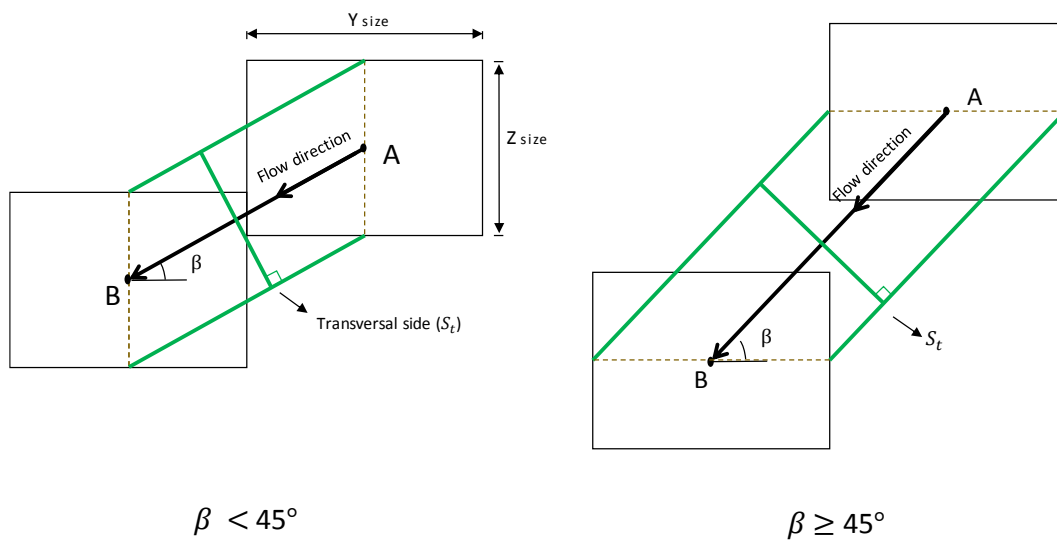


Figure 3.3: The transversal side ( $S_t$ ) concept used in APDS.

### 3.2.3 Kinematic Viscosity in the Heated Volume ( $\nu_{hv}$ )

The kinematic viscosity depends on the temperature distribution in the heated volume. The temperature distribution in its turn depends on the petrophysical and thermal rock properties, the fluids in the reservoir and the front velocity of the expanding steam-chamber (Butler, 1991; Irani & Cokar, 2016). Based on the work of Butler and his colleagues

(Butler, 1985; Butler et al., 1981) APDS assumes a steady state temperature ( $T$ ) distribution ahead of the advancing steam-chamber interface given by Equation 3.3. The temperature-dependent kinematic viscosity ( $\nu$ ) relationship is given by Equation 3.4.

$$\frac{T - T_r}{T_{st} - T_r} = e^{-U\xi/\alpha} \quad (3.3)$$

Here,  $T_r$  is the initial reservoir temperature,  $T_{st}$  is the steam-chamber temperature,  $U$  is the steam-chamber velocity in the direction normal to the interface,  $\xi$  is the distance measure normal to the steam-chamber interface and  $\alpha$  is the reservoir thermal diffusivity.

$$\frac{\nu_{st}}{\nu} = \left( \frac{T - T_r}{T_{st} - T_r} \right)^m \quad (3.4)$$

Here,  $\nu_{st}$  is the kinematic viscosity at steam temperature and the parameter  $m$  captures the effect of temperature on viscosity.  $m$  can be calculated from Equation 3.5. and its value is typically in the range 3 to 5 (Butler & Stephens, 1981).

$$m = \left[ \int_{T_r}^{T_{st}} \left( \frac{1}{\nu} - \frac{1}{\nu_r} \right) \frac{dT}{T - T_r} \right]^{-1} \quad (3.5)$$

From Equations 3.3 and 3.4, Butler (1985) demonstrated for a section of unit thickness measured into the paper, that the flow parallel to the steam-chamber interface is given by Equation 3.6. This equation implies that the heat transfer is by conduction only and at a constant velocity  $U$ .

$$q_0 = \frac{\delta k_o g \sin \beta}{m \nu_{st}} \quad (3.6)$$

Here,  $\delta = \alpha/U$  is the heat-penetration depth. APDS assumes that when a cell is added to the steam-chamber its neighborhood is already heated, therefore, by comparing Equation 3.1 to Equation 3.6 it follows that if  $S_t = \delta$  then  $\nu_{hv} = m \nu_{st}$ .

### 3.2.4 Permeability

Permeability anisotropy impacts the steam-chamber expansion and hence the SAGD project performance (Azom & Srinivasan, 2013; Sharma, Khataniar, Patil, Kamath, & Dandekar, 2002). During the SAGD process, the interface angle of the steam-chamber continuously changes, and because the bitumen flows parallel to it, it is reasonable to conclude that the relative influence of the vertical permeability ( $K_v$ ) and horizontal permeability ( $K_h$ ) on the bitumen flow is also continuously changing. This is a local phenomenon. At any given time, there are sectors of the steam-chamber's edge where  $K_v$  dominates over  $K_h$ , and others where the contrary occurs. To account for this phenomenon, APDS implements the permeability model given by Equation 3.7.

$$K_\beta = K_v \sin^2 \beta + K_h \cos^2 \beta \quad (3.7)$$

Here,  $K_v$  and  $K_h$  are the permeability in the vertical and the horizontal direction, respectively.  $K_\beta$  is the permeability in the direction of the angle  $\beta$ .

Azom & Srinivasan (2011) derived this permeability model by resolving the SAGD flow in the direction of the resultant gravity head. They concluded that Equation 3.7 is mathematically in agreement with Butler's analytical model.

### 3.2.5 Steam-chamber Interface Velocity

APDS works one cell at a time, and once a grid-cell has been classified as part of the steam-chamber it is not processed again. This mechanism is myopic about the future evolution of the steam-chamber and overestimates the interface velocity. A deceleration exponent applied to the model time variable introduced in Section 2.4.3.2 corrects this overestimation.

Figure 3.4 illustrates the cause of the overestimation. It shows the rate of bitumen flowing in ( $q_{in}$ ) and flowing out ( $q_{out}$ ) of a cell in the heated zone. Note that the advance of the steam-chamber interface at a velocity  $U$  is only possible if  $q_{out} > q_{in}$ . In other words, the advance of the interface is determined by the difference in the rates, and not

only by the output rate (Butler, 1991). Because APDS considers  $q_{in} = 0$ , the cell travel time calculated with the Equations 3.1 and 3.2 is less than a value calculated with  $q_{in} > 0$ . Consequently, the interface velocity  $U$  and the steam-chamber expansion rate increases.

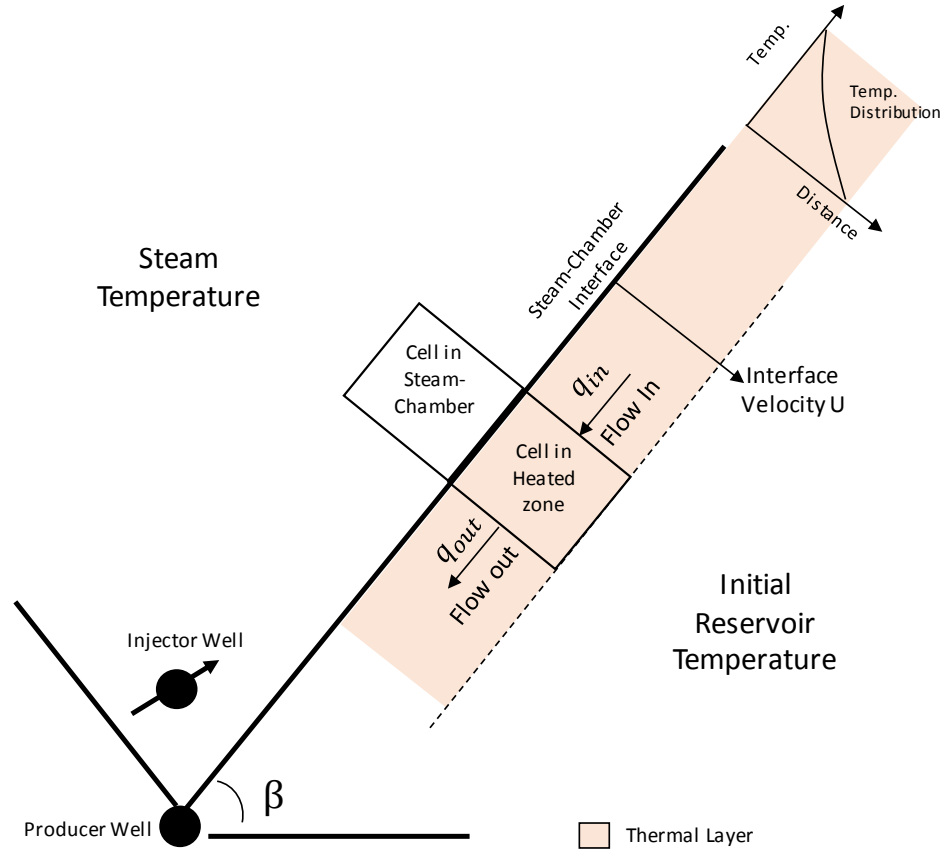


Figure 3.4: The advance of the steam-chamber interface at a velocity  $U$  is determined by the difference between  $q_{in}$  and  $q_{out}$ .

Figure 3.5 shows that assuming  $q_{in} = 0$  is reasonable for cells located on the top edge of the steam-chamber (e.g. top-cell A), but questionable for cells located on the lateral edge of it (e.g. lateral-cell B). At the beginning of the steam-chamber, there are more top-cells than lateral-cells; therefore, the estimated interface velocity is acceptable. However, as the steam-chamber grows, the number of lateral-cells increases at a faster rate than the number of top-cells, resulting in the overestimation of the interface velocity.

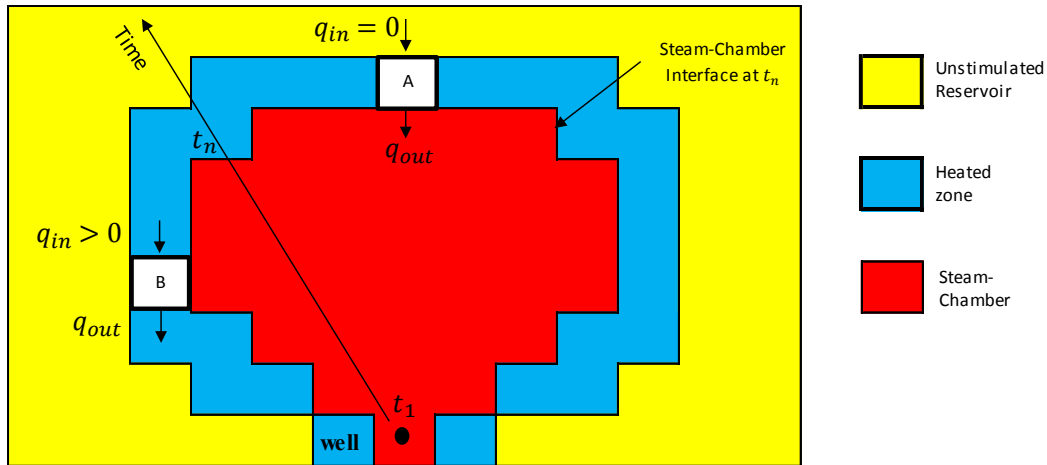


Figure 3.5: The advance of the steam-chamber interface is determined by the difference between the flowing in ( $q_{in}$ ) and flowing out ( $q_{out}$ ) rates.

Because the surface of the steam-chamber increases exponentially with time, it is expected that the interface velocity also accelerates exponentially. For that reason, APDS controls the inflation of the steam-chamber interface velocity with a deceleration exponent. It is applied directly to the model time variable (Sections 2.4.3.2 and 2.5) acting as a delay to the ranking value time of every cell.

### 3.3 APDS prototype computer program

APDS was prototyped in the Python programming language. The code is presented in Appendix A. The program has 3 modules: the graph generator, the steam-chamber generator and the post-processing module. They interact according to the diagram shown in the Figure 3.6.

The graph generator module takes the numerical reservoir model in GSLIB format (Deutsch & Journel, 1998) and outputs the graph and a list with all the cell-sinks. The input must contain the porosity, vertical and horizontal permeability, fluid saturation and rock-type data to be stored at the graph nodes. The module not only transforms the mathematical representation of the reservoir, but also enriches it by adding flow path information particular to the SAGD recovery process, through the number and direction of the graph edges.

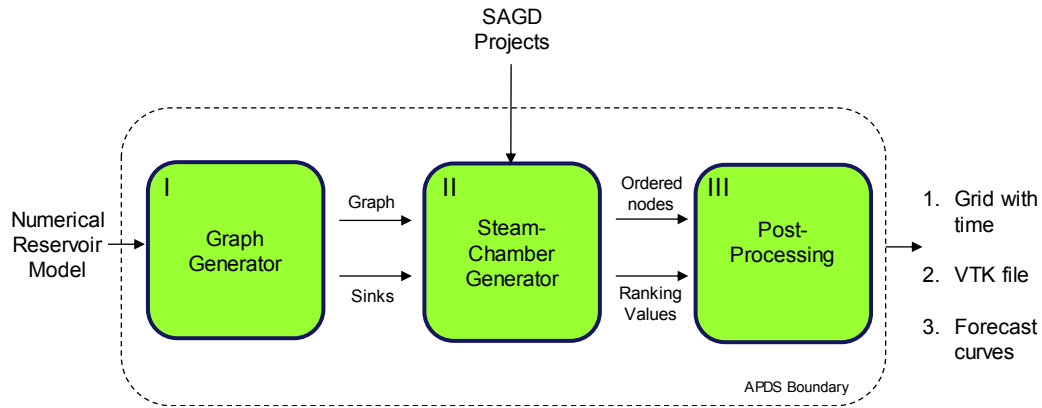


Figure 3.6: Structure of the APDS prototype.

The steam-chamber generator module takes the graph, the sinks and the SAGD project. The definition of the SAGD project must include the trajectories of the producer and the injector wells in GSLIB format, the bitumen kinematic viscosity at steam temperature, the Butler’s temperature-viscosity exponent,  $m$ . This module outputs the sequence of graph nodes ordered by ranking values or time.

The post-processing module transforms the ordered sequence of nodes to GSLIB format. The outputs include a grid with the time (ranking values) that each-cell was added to the steam-chamber, and a file in VTK format (Schroeder, Martin, & Lorensen, 2006) to visualize their evolution in a third-party software. A forecast of the cumulative steam-chamber volume is also generated.

### 3.4 APDS Validation

APDS is mainly envisioned to be a cost-effective transfer function to support decision making models that considers geological uncertainty. To evaluate its suitability for the task, a case-study was prepared to compare results from the Computer Modeling Group (CMG) thermal flow simulator STARS (CMG, 2010) and APDS over a set of 100 geostatistical realizations. STARS is widely used in industry operations and academic research to flow simulate SAGD projects, and hence, it is a reasonable benchmark to validate APDS.

APDS would be considered a suitable transfer function for SAGD projects if 1) there is a good visual and quantitative agreement between the steam-chambers obtained from

STARS and APDS over the entire set of realizations, 2) metrics calculated from STARS and APDS exhibit good/strong positive correlation, and 3) the ranking of the reservoir realizations using a STARS's metric is similar to that with a APDS's metric.

This section presents the geological model and the engineering assumptions for flow simulating the SAGD project. Steam-chambers and metrics extracted from APDS and STARS are compared visually and numerically, and the results discussed. The computational time to run both methods is reported.

### 3.4.1 Geological Model

The geological model consists of 100 geostatistical realizations. Each realization has 200,000 cells: 40 x 50 x 100 cells in the x, y and z directions, respectively. The grid blocks are 25 m x 1 m x 1 m in the x, y and z directions, respectively. The interested reader is referred to Hadavand & Deutsch (2017) for a detailed description of the numerical reservoir model and the geostatistical workflow used to generate it. Figure 3.7 depicts some of the main characteristics of the reservoir model. The images have a data aspect ratio between the x-axis to y-axis and x-axis to z-axis of 5 in both cases.

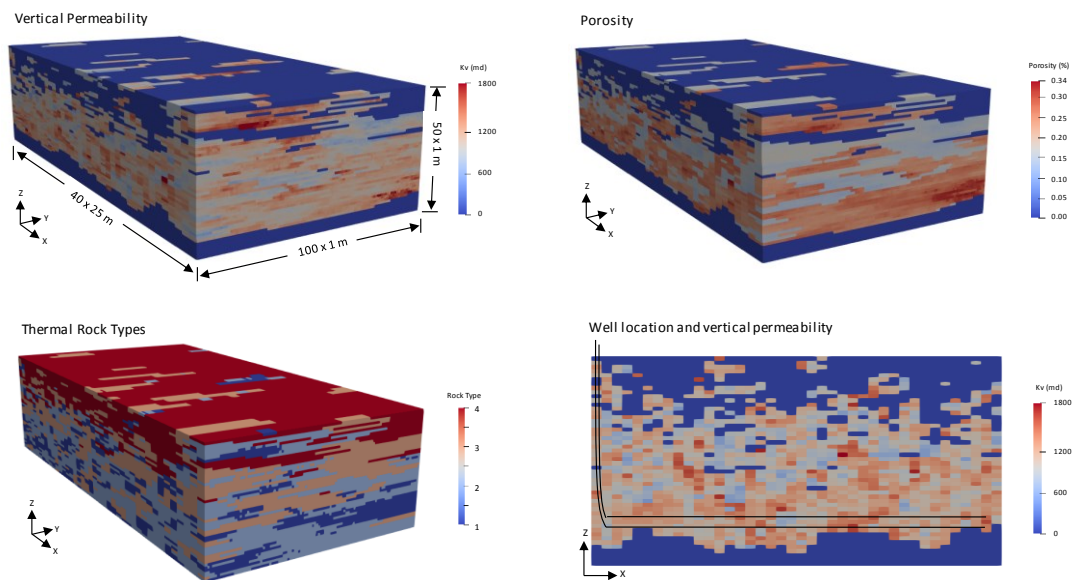


Figure 3.7: Illustration of one realization of the geological model.

Hadavand (2017) reports that the construction of the geological model used spatial bootstrap to account for parameter uncertainty related to the well data (porosity, permeability and water saturation), but not related to the categorical variable. It is worthy to highlight that the decision-making workflow will benefit from incorporating parameter uncertainty in the geostatistical simulation (Khan & Deutsch, 2016). However, the APDS validation discussed in this chapter is not affected by the workflow implemented to construct the geological model.

### 3.4.2 SAGD Project

In the reservoir-simulation model, the well-pair length is 1000 m and the vertical inter-well distance is 5 m. The steam-injection pressure is constrained to a maximum value of 3,500 KPa and the maximum steam injection rate is set to  $400 \text{ m}^3/d$  with 90% steam-quality. The production well is constrained to a maximum steam rate of  $5 \text{ m}^3/d$  to mimic steam-trap control. A circulation period of 4 months was modeled with heater wells. Table 3.1 summarizes other parameters used in the reservoir simulation. Temperature and compositional dependent relative permeability curves taken from the CMG SAGD guide (CMG, 2013) are depicted in Figure 3.8. APDS uses the same well-pair geometry, the viscosity at steam-temperature is  $\nu_{st} = 7.11 \times 10^{-6} \text{ m}^2/s$ , the Butler's temperature-viscosity exponent  $m = 4.1$  and the oil relative permeability is  $K_{r_o} = 0.25$ .

Table 3.1: Reservoir simulation parameters.

<b>Parameter</b>	<b>Value</b>
Well length ( $m$ )	1000
Inter-well distance ( $m$ )	5
Reservoir thickness ( $m$ )	35-40
Initial reservoir temperature $T_r$ ( $^{\circ}C$ )	12
Initial reservoir pressure at top of the model ( $kPa$ )	2500
Depth at top of the model ( $m$ )	500
Dead bitumen viscosity at $15 \text{ }^{\circ}C$ ( $mPa \cdot s$ )	3,260,000
Bitumen density at $T_r$ ( $kg/m^3$ )	1012
Bitumen molecular mass ( $g/gmol$ )	600
Initial methane molar fraction (%)	5

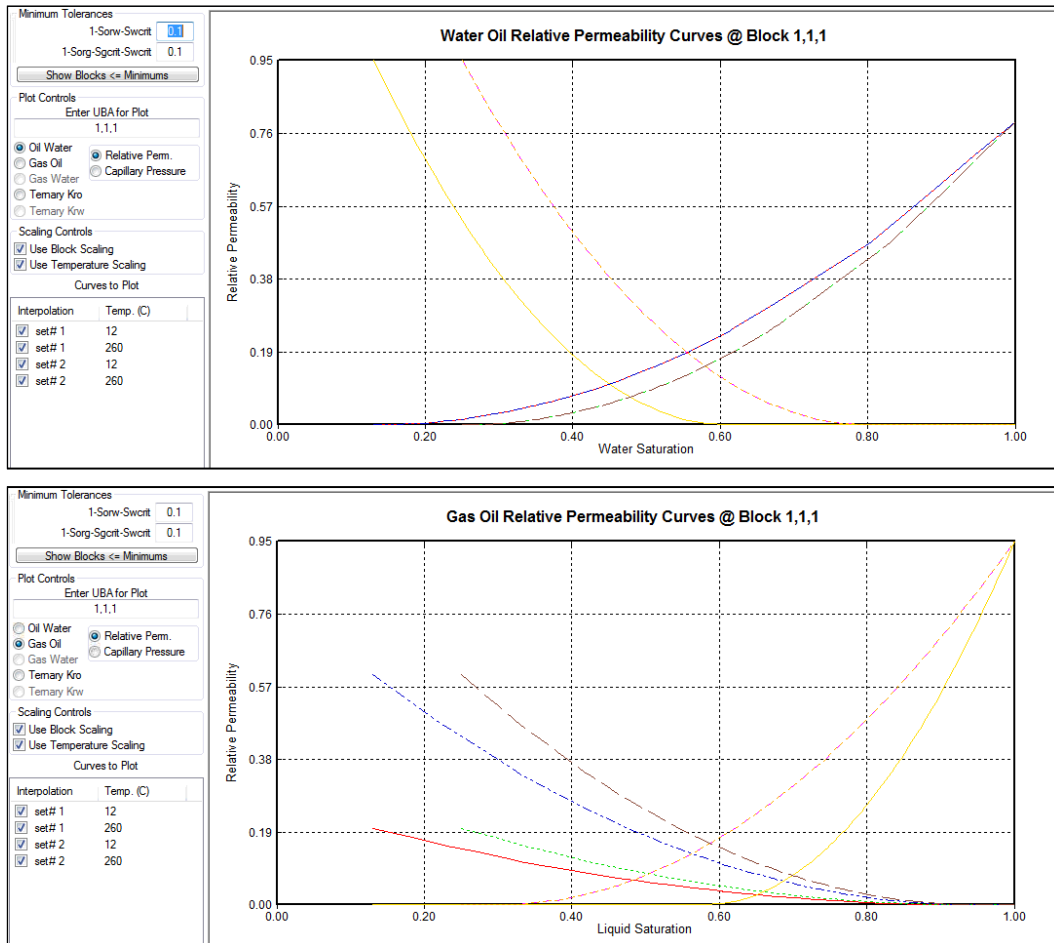


Figure 3.8: Temperature and compositional dependent relative permeability curves (CMG's SAGD guide (2013)).

### 3.4.3 Steam-chambers from STARS and APDS

A visual comparison between APDS and STARS for two geostatistical realizations confirms the ability of APDS to model the steam-chamber expansion in SAGD. They also serve to illustrate how this novel algorithm handles complex reservoir heterogeneities. A Conformance Index calculated over the 100 geostatistical realizations validates the good predictive capabilities of APDS.

### 3.4.3.1 Visual Comparison #1.

The location of the steam-chamber from STARS was calculated every year using the oil saturation ( $S_o$ ). It was assumed that a difference of 10% between the initial oil saturation ( $S_{oi}$ ) and the oil saturation at a time of interest (e.g. oil saturation after 5-years,  $S_{o_{5y}}$ ) indicates the presence of the steam-chamber at that time. Similarly, the APDS output originally in time units, was transformed to an indicator variable showing the location of the steam-chamber – years 1 to 5 - for comparison purposes.

Figure 3.9 shows the steam-chamber from APDS and STARS after 5 years. The match between the two results appears satisfactory. A detailed comparison was performed in two vertical cross-sections separated by 250 m along the x-axis as depicted in Figure 3.10. Cross-section A is located in the middle of the horizontal well-pair and cross-section B toward the toe.

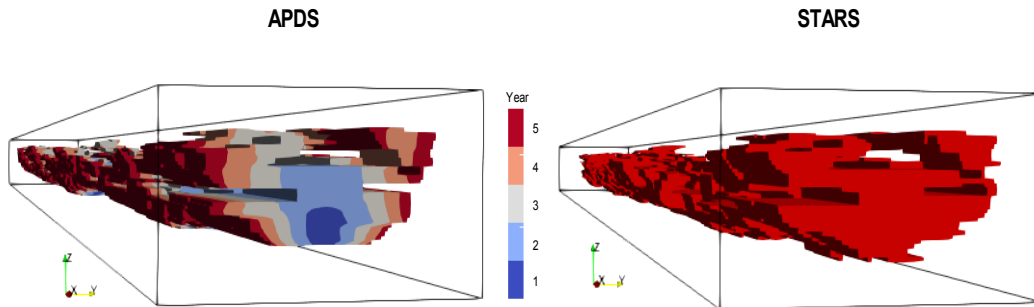


Figure 3.9: APDS and STARS steam-chamber after 5 years.

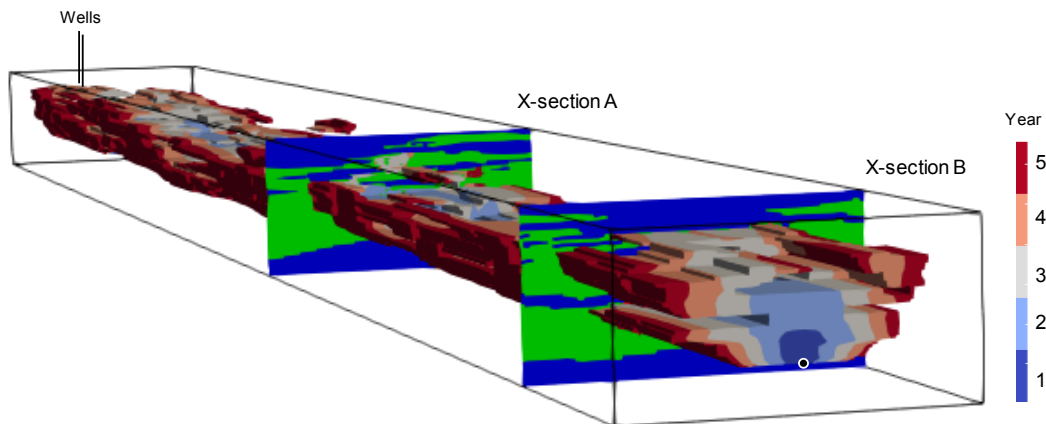


Figure 3.10: Cross-section A and B selected to compare STARS and APDS.

Cross-section A in Figure 3.11 shows from the bottom to the top the steam-chamber evolution for 5 years. The left and right columns show the results from STARS and APDS, respectively.

A visual comparison demonstrates a close agreement between the STARS and the APDS results in this cross-section. At the beginning, the APDS steam-chamber does not rise as quickly, but soon it reaches a similar growth rate to the STARS's steam-chamber. The APDS steam-chamber evolves honoring the reservoir heterogeneity. For example, a long barrier located at the right-side of the cross-section reduces the vertical growth of the chamber between years 2 and 3 causing it to rise asymmetrically to the left of the cross-section. The STARS results confirm this complex behavior. Figure 3.11 shows that the good agreement in shape and size is maintained through the studied time horizon.

Figure 3.12 shows cross-section B; again, there is a good agreement between the STARS and APDS results. Note that cross-section B has a different geometric pattern than cross-section A. In this case, two long stair-stepped barriers located at the left of the cross-section inhibit the movement of the steam. Figure 3.12 illustrates how APDS predicts the impact of these obstacles in a similar way to STARS. Once more, the good agreement in the shape and size is maintained through the studied time horizon.

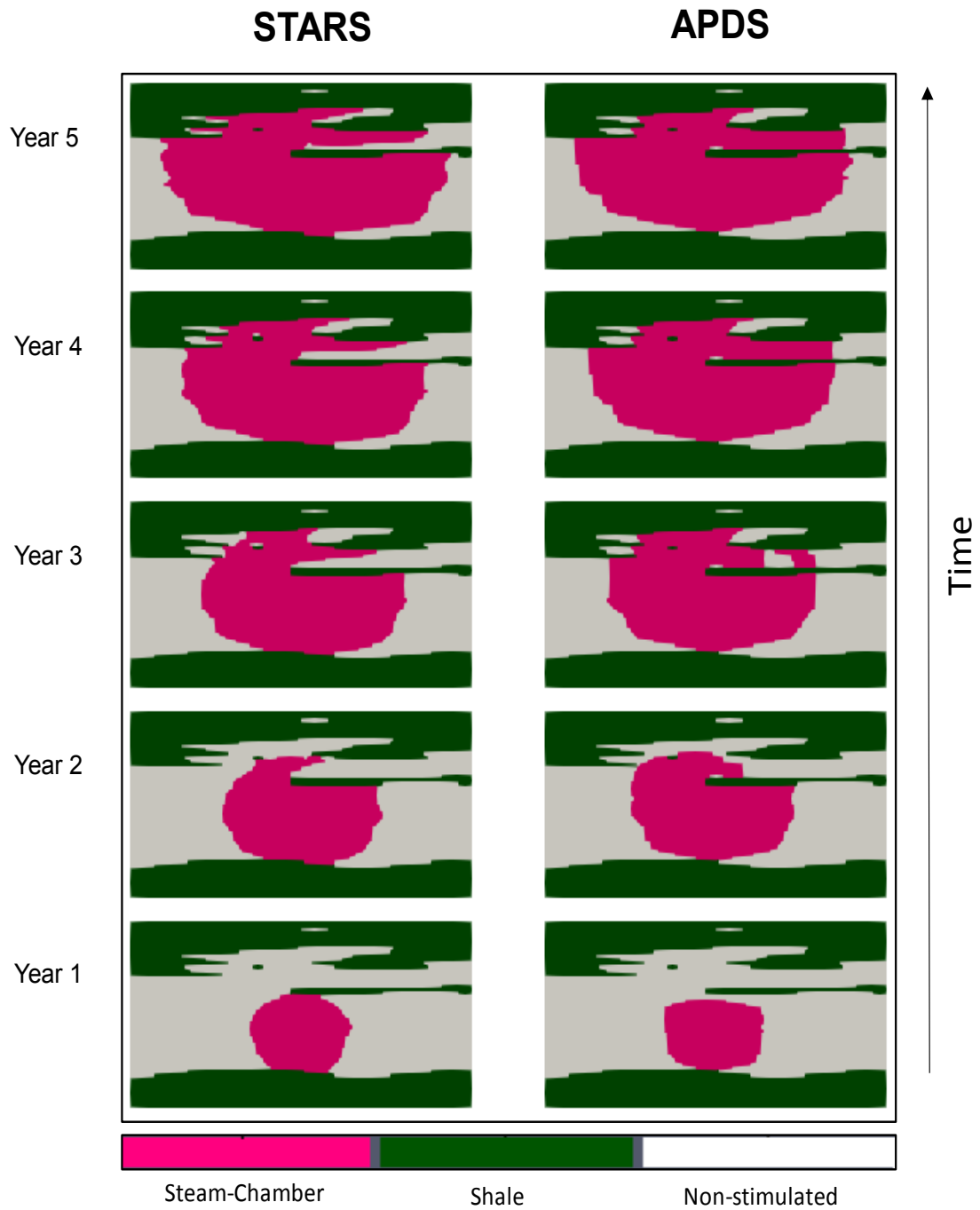


Figure 3.11: Cross-section A comparing APDS and STARS for 5 years.

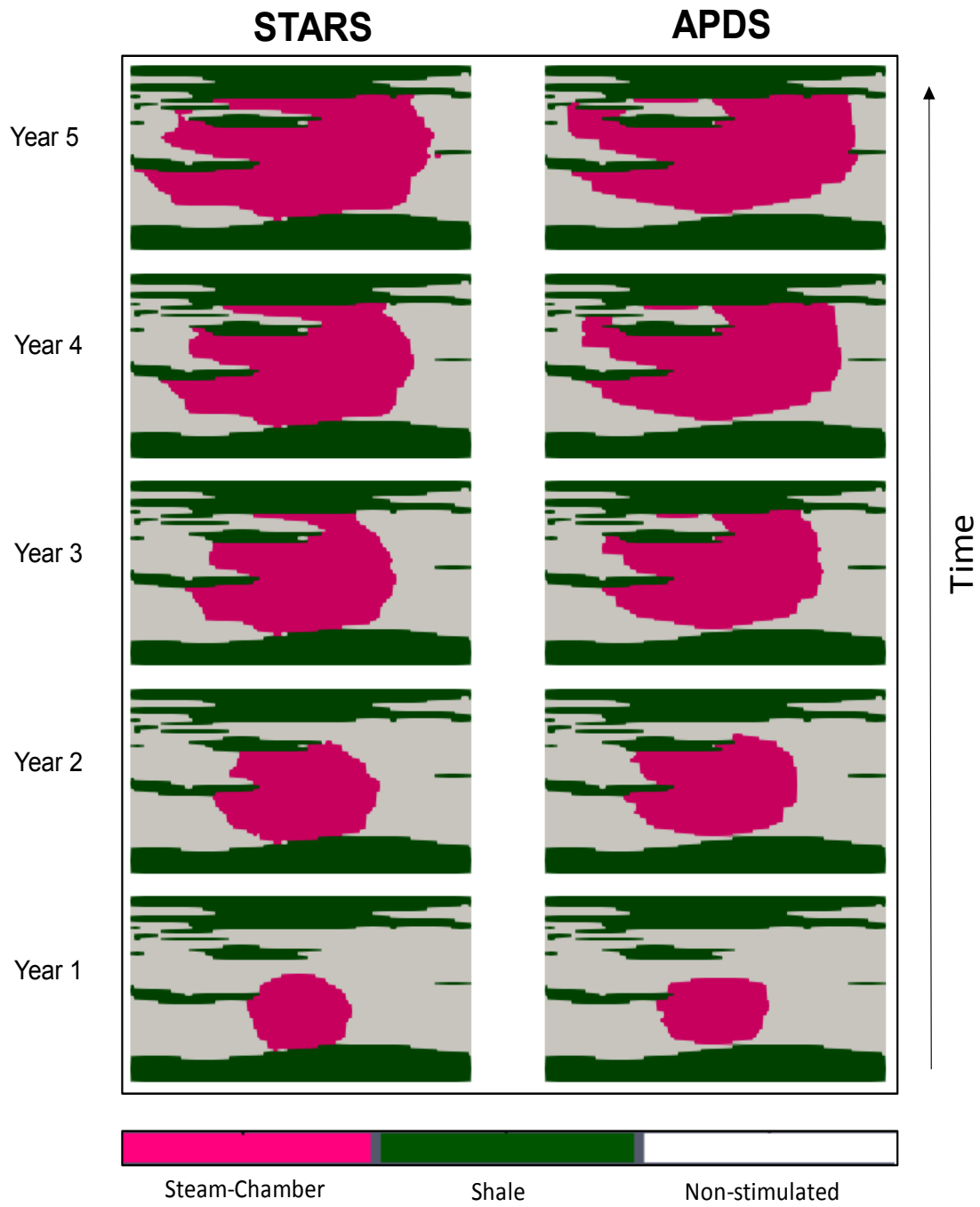


Figure 3.12: Cross-section B comparing APDS and STARS for 5 years.

### 3.4.3.2 Visual Comparison #2.

In this comparison, the location of the steam-chamber from STARS was calculated after 5 years using the oil saturation ( $S_o$ ). Likewise, the APDS output was transformed to an indicator variable showing the location of the steam-chamber at year 5.

Figure 3.13 shows a satisfactory match between the STARS and APDS steam-chambers once more. The top image shows the location of permeable and not-permeable rocks. Note how the barriers in the well-pair proximities hamper the expansion of the steam-chamber leading to unstimulated planes. The negative effect of the reservoir heterogeneity in the SAGD performance is captured correctly by APDS.

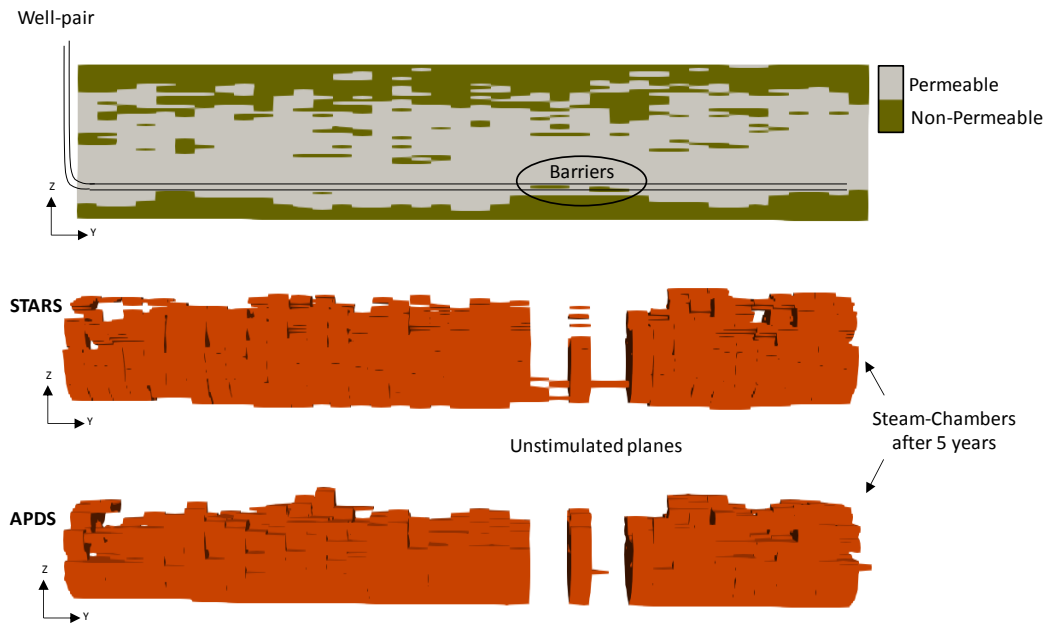


Figure 3.13: Steam-chamber location after 5 years generated by STARS and APDS.

Figure 3.14 and Figure 3.15 present a detailed comparison of vertical cross-sections along the axis of the well-pair, and perpendicular to the axis the well-pair every 300 meters. In all the cases, the visual comparison demonstrates a close agreement between APDS and STARS results. Note how APDS deals with the complex reservoir heterogeneity.

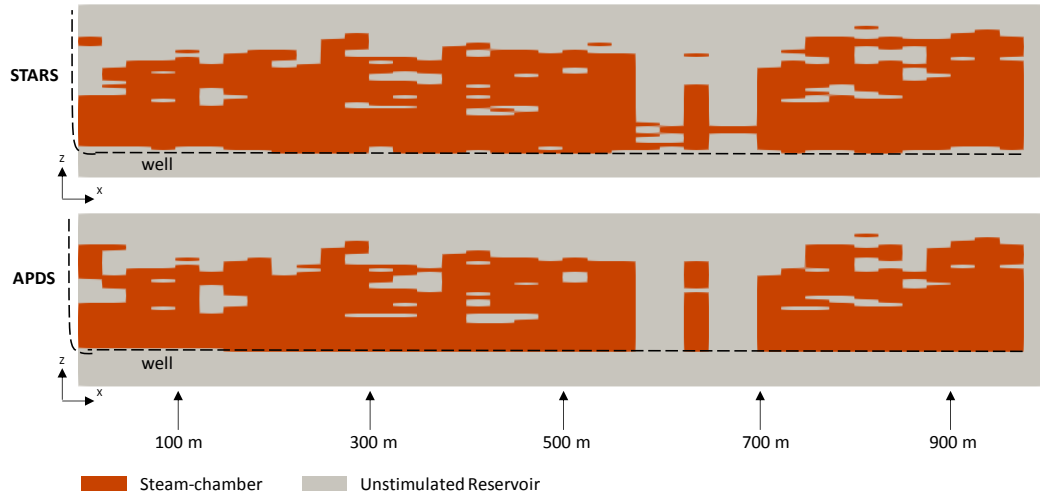


Figure 3.14: Vertical cross-sections along the axis of the SAGD well-pair. Arrows mark the location of cross-sections plotted in Figure 3.15.

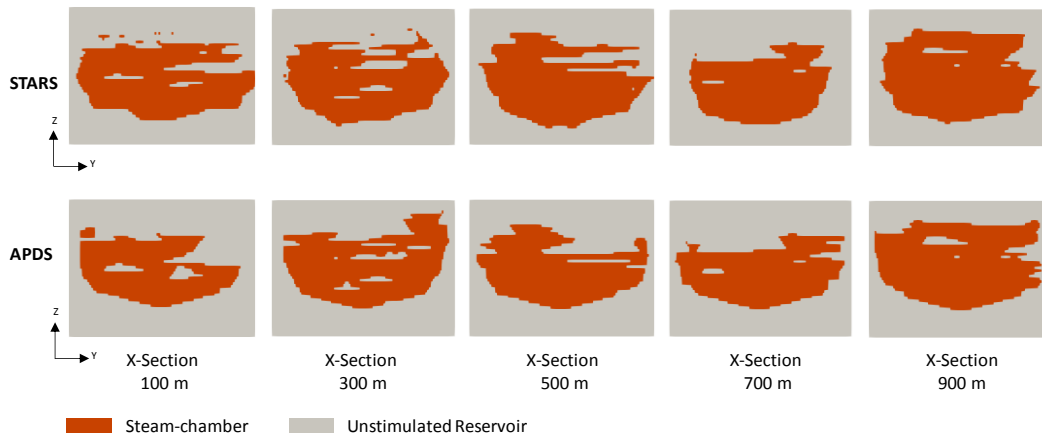


Figure 3.15: Vertical cross-sections every 300 meters perpendicular to the axis of the SAGD well-pair.

### 3.4.3.3 Conformance Index

Since it is not practical to perform a one-to-one visual comparison of the 3D steam-chambers over the entire set of geostatistical realizations, a Conformance Index (CI) defined as the percentage of cells in the STARS steam-chamber correctly predicted by APDS was calculated for all of them. The histogram in Figure 3.16 shows that in average 87% of STARS steam-chamber cells are correctly predicted by ADPS. It also reveals that for 75%

of the realizations, the CI is at least 86%. This result confirms the good predictive capabilities of APDS.

The CI changes with time. At early stages CI tends to have relatively low values due to instabilities in both methods, APDS and STARS, associated to modeling the process of establishing the initial thermo-hydraulic communication between the producer and the injector well. At later stages, CI tends to have artificially high values because the steam-chambers reach the limits of the reservoir. Gallardo & Deutsch (2018) showed an example describing how CI changes with time.

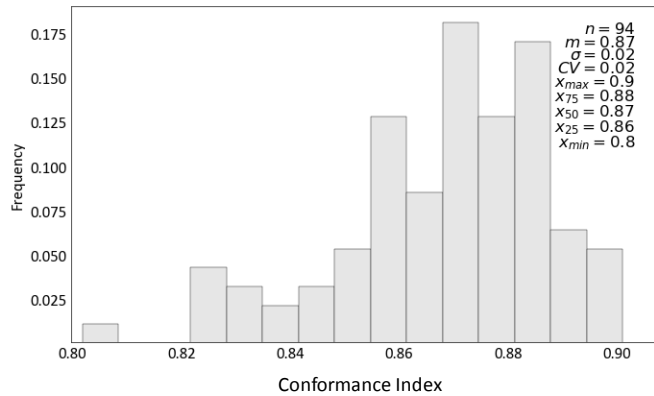


Figure 3.16: Conformance Index histogram.

### 3.4.4 Metrics from STARS and APDS

The metrics to numerically compare APDS to STARS are the Cumulative Oil Production (COP) and the Steam-Chamber Bitumen Volume (SCHV) as described below.

#### 3.4.4.1 STARS Cumulative Oil Production

Figure 3.17 shows the COP forecasts for a subset of 50 realizations and Figure 3.18 shows COP histograms at every year. Only 94 values are reported because 6 flow simulations failed to reach 5 years of production. CPO at every year will help to understand the stability through time of this variable to rank the geostatistical realizations for SAGD.

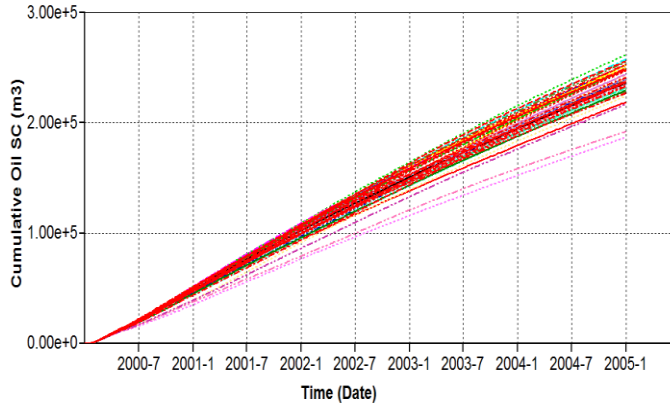


Figure 3.17: COP forecasts from STARS after 5 years for 50 realizations.

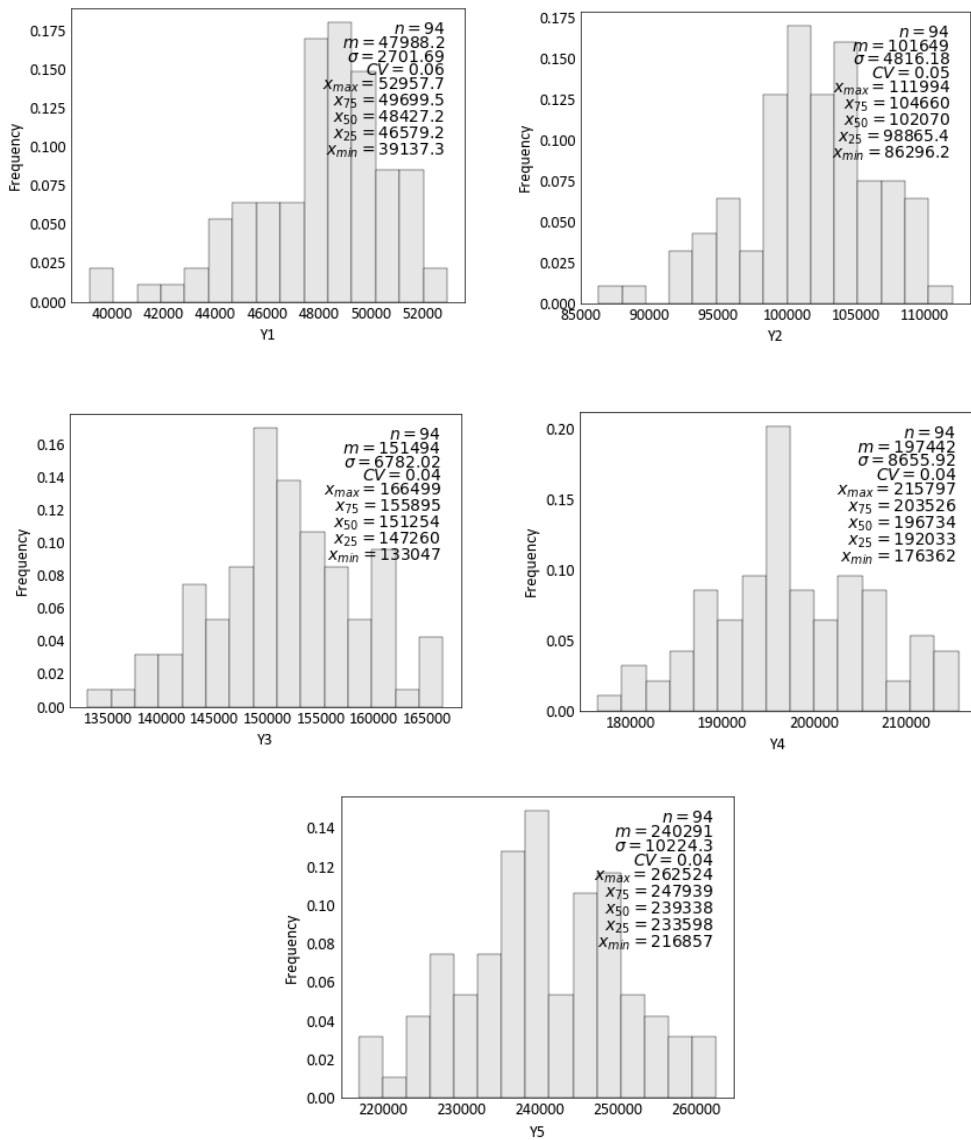


Figure 3.18: Histograms of COP from STARS for years 1 to 5 (Y1 to Y5).

### 3.4.4.2 STARS Steam-Chamber Bitumen Volume

SCHV from STARS was calculated using the porosity and recoverable oil saturation of the cells inside the steam-chambers calculated in section 3.4.3. Figure 3.19 shows the histogram.

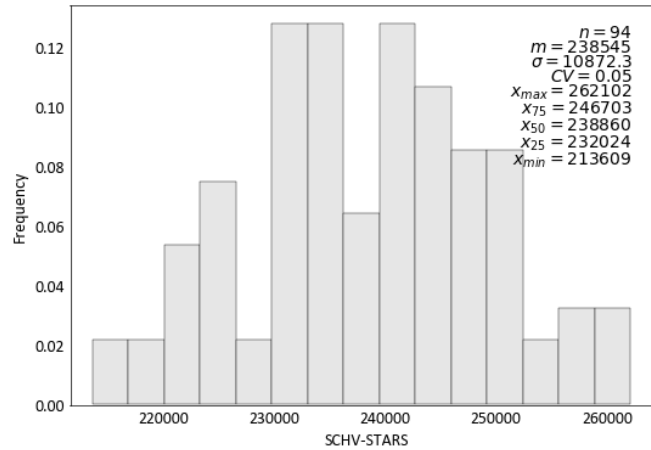


Figure 3.19: Histogram of SCHV from STARS after 5 years.

### 3.4.4.3 APDS Steam-Chamber Bitumen Volume

SCHV from APDS was calculated by accumulating the oil volume of the ordered cells until year 5, as shown in Figure 3.20a. These curves resemble the COP from STARS forecasts depicted on Figure 3.17. They are somehow different because there is a time lag between them that depends on the rock-fluid interaction properties and on the size and shape of the steam-chamber. Figure 3.20b shows the SCHV from APDS histogram after 5 years.

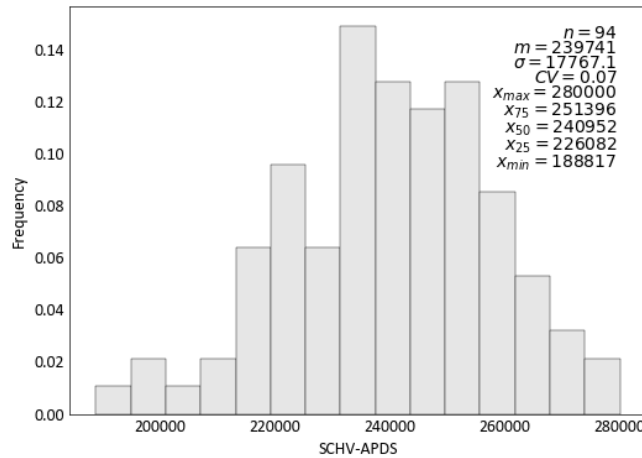
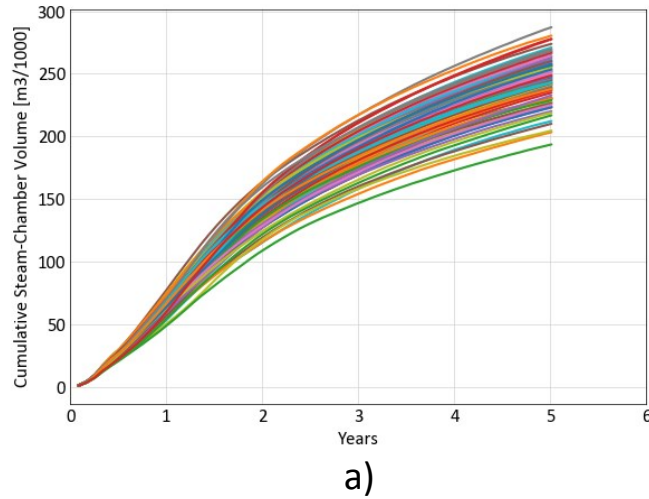


Figure 3.20: a) Cumulative SCHV from APDS, b) Histogram of SCHV from APDS after 5 years.

#### 3.4.4.4 Analysis

A good visual agreement between the steam-chambers obtained from STARS and APDS over the entire set of realizations was already established in Section 3.4.3. Now, a good/strong positive correlation coefficient between STARS's COP versus APDS's SCHV and between STARS's SCHV versus APDS's SCHV will also support the use of APDS as a tool for decision making workflows.

Since the COP curves cross each other, the rank of the realizations using this variable changes from one year to another. Then, a first step of the analysis is to determine a time

horizon in which the comparison between STARS and APDS will produce stable results. Figure 3.21 shows the scatter plots of STARS's COP forecast from year 1 to 5. Note that the correlation coefficient between two consecutive years increases with time only until year 4. For instance, the correlation coefficient between years 1 and 2 (Y1 and Y2) is  $\rho=0.91$ , between years 2 and 3 (Y2 and Y3) is  $\rho=0.96$  and between years 3 and 4 (Y3 and Y4) is  $\rho=0.98$ . This tendency demonstrates that ranking this set of geostatistical realizations based on COP is stable after 4 years of production.

Figure 3.22 shows scatter plots of the rank of geostatistical realizations based on STARS's COP from year 1 to 5. In this case study, ranking with COP is stable after 4 years of production. Ranking based on 1 or 2 years of COP is not recommended, since by year 5 the result could be significantly different. On the other hand, ranking with 4 or 5 years of COP provides similar results. The Spearman rank correlation coefficient between years 4 and 5 (Y4 vs Y5) is  $\rho_s = 0.98$ .

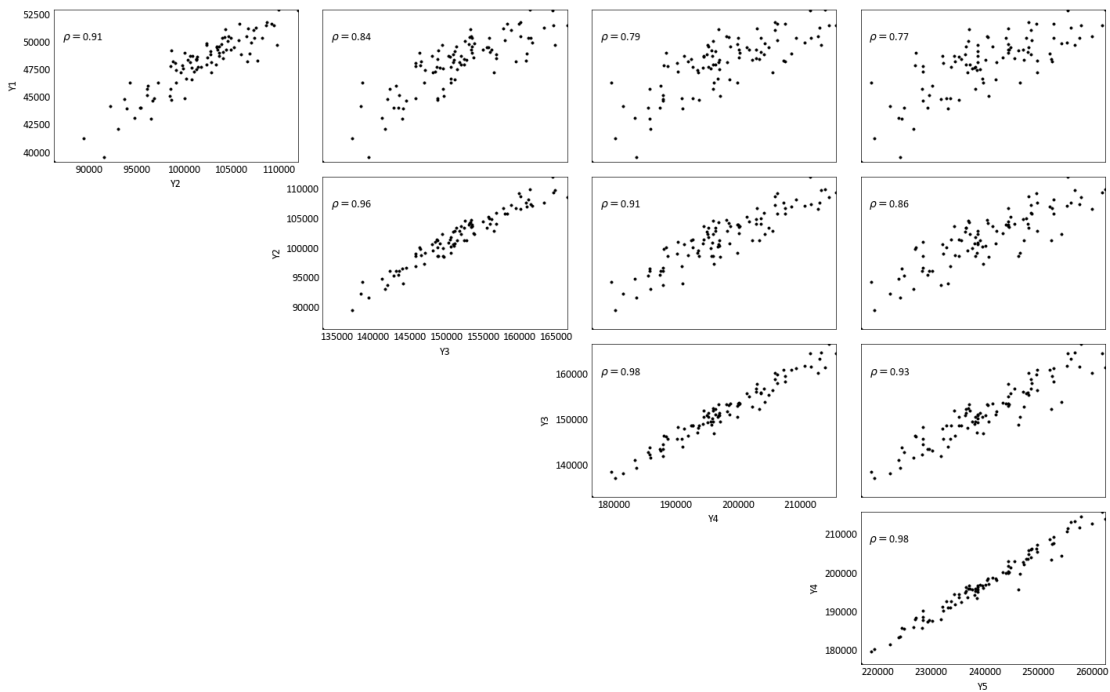


Figure 3.21: Scatter plots of COP from STARS forecasts from years 1 to 5.

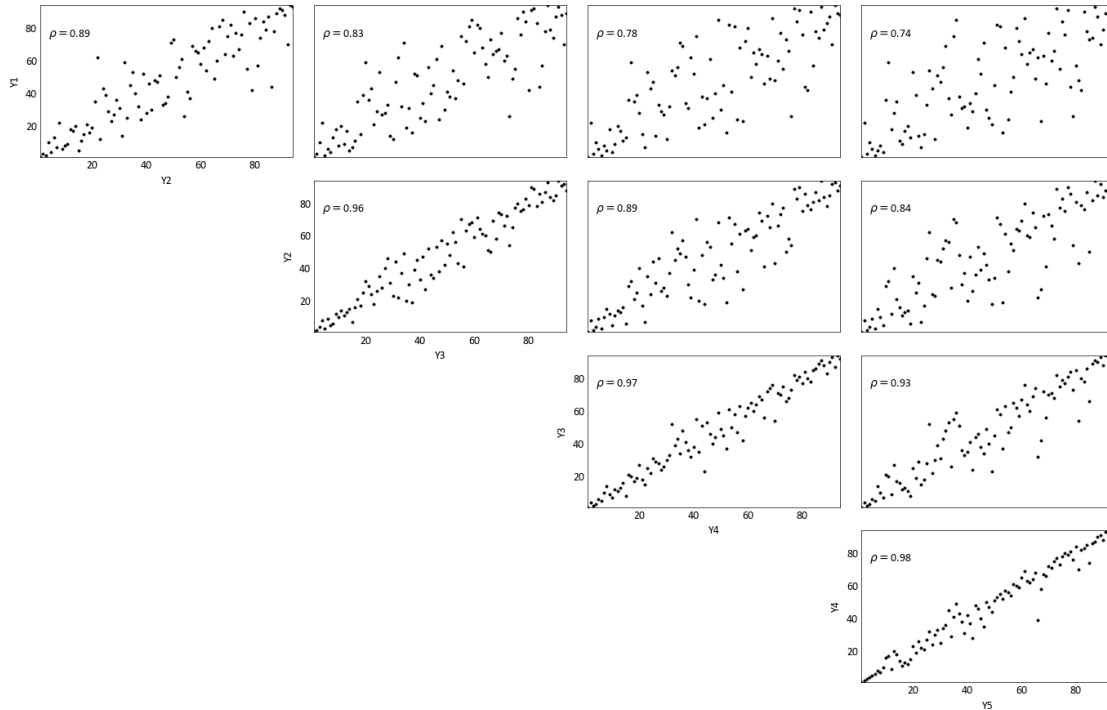


Figure 3.22: Scatter plots of rank of realizations based on COP from STARS from years 1 to 5.

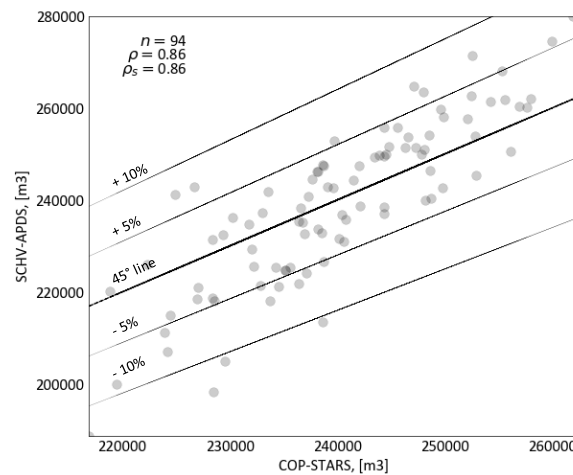
Table 3.2: Statistics from APDS and STARS.

	<b>COP-STARS</b> <b>(m3/1000)</b>	<b>SCHV-</b> <b>STARS</b> <b>(m3/1000)</b>	<b>SCHV-APDS</b> <b>(m3/1000)</b>
<b>Mean</b>	240.2	238.5	239.7
<b>p75</b>	247.9	246.7	251.4
<b>p50</b>	239.3	238.8	240.9
<b>p25</b>	233.6	232.0	226.1
<b>Min</b>	262.5	262.1	280.0
<b>Max</b>	216.8	213.6	188.8

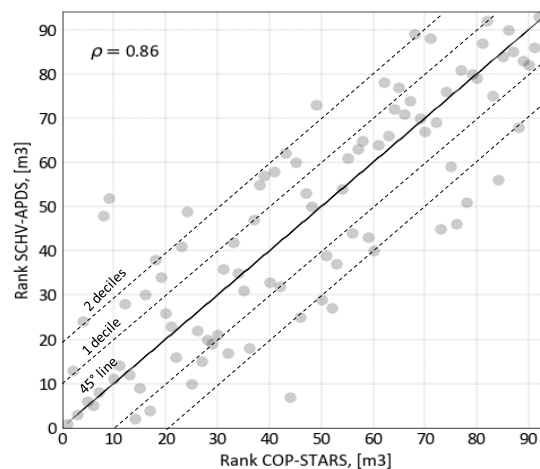
Table 3.2 summarizes statistics from the histograms in Figures 3.18, 3.19 and 3.20. Here is worthy to highlight that the mean and p50 of the SCHV from APDS has a percent error of less than 1% when is compared to the corresponding statistics of STARS's COP and SCHV. APDS also exhibits a larger interquartile range (IQR) than STARS, the larger

variance could be the effect of APDS being more sensitive than STARS to the reservoir heterogeneity. APDS is an algorithm that trades accuracy for efficiency.

Figure 3.23a. shows a scatter plot between the COP from STARS and the SCHV from APDS. They have a good linear relationship with  $\rho = 0.86$ . APDS also predicts very well the COP from STARS. Approximately 70% of the values lie in a +/- 5% band of the value predicted by the thermal simulator, and 95% of the values lie in a +/- 10% band. Figure 3.23b. shows a rank correlation coefficient  $\rho_s = 0.86$ , which indicates that APDS can preserve moderately well the rank of this set of geostatistical realizations. Approximately 80% of the rank predicted by APDS is inside a 2 deciles band of the rank predicted by STARS using COP.



a)

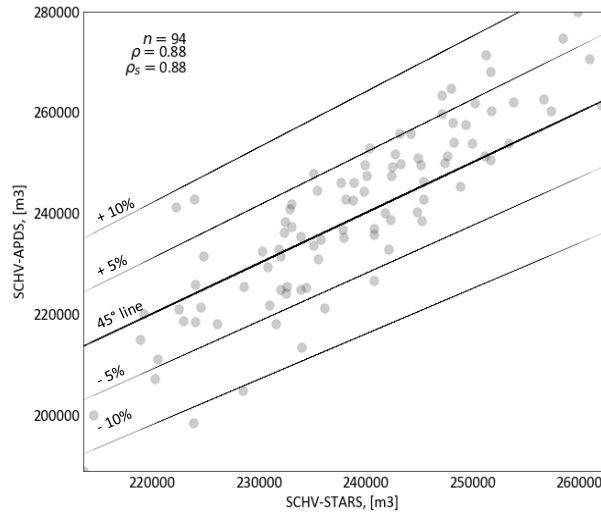


b)

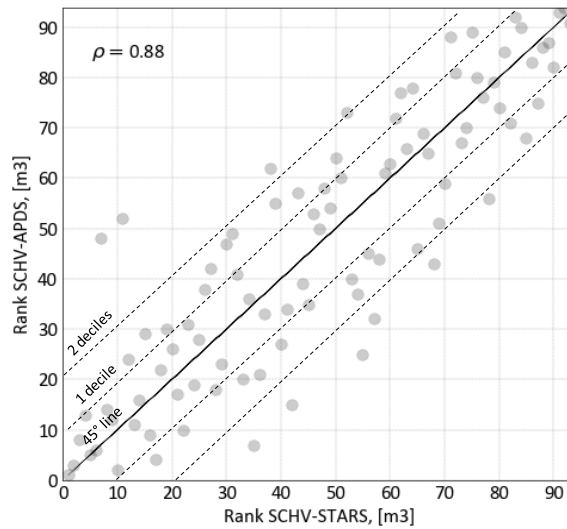
Figure 3.23: a) Scatter plot of COP from STARS and APDS from SCHV, b) Scatter plot of COP from STARS ranks and SCHV from APDS ranks.

Figure 3.24a. shows the scatter plot between the SCHV from STARS and the SCHV from APDS. They have a good linear relationship with  $\rho = 0.88$ , which is slightly higher than the previous case. The improvement is expected because in this case the comparison involves the same property. Figure 3.24a. also shows that 81% of the APDS's SCHV values are in a +/- 5% band of the value predicted using the thermal flow simulator. The percentage rises to 97% when a +/- 10% band is used. The Spearman's correlation coefficient of  $\rho_s = 0.88$  (Figure 3.24b) corroborates that APDS can preserve fairly well the rank of this set of geostatistical realizations.

Figure 3.24a shows that poor performing realizations in terms of STARS's SCHV are slightly underestimated by APDS, while good performing realizations are slightly overestimated. This behavior seems to be a consequence of using a single deceleration exponent value to control the steam-chamber interface velocity for all the geostatistical realizations as explained in Section 3.2.5.



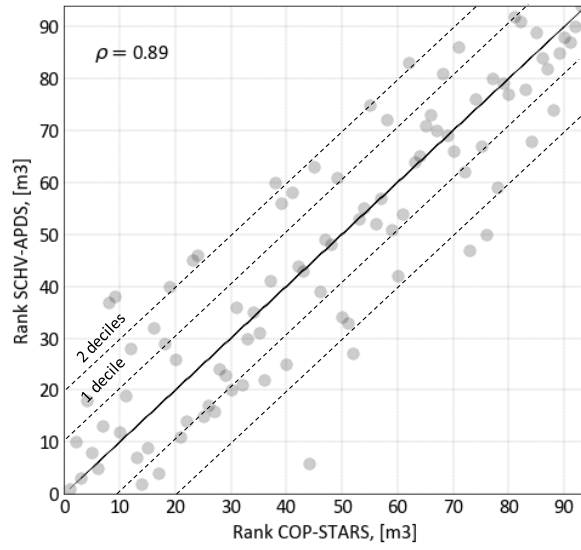
a)



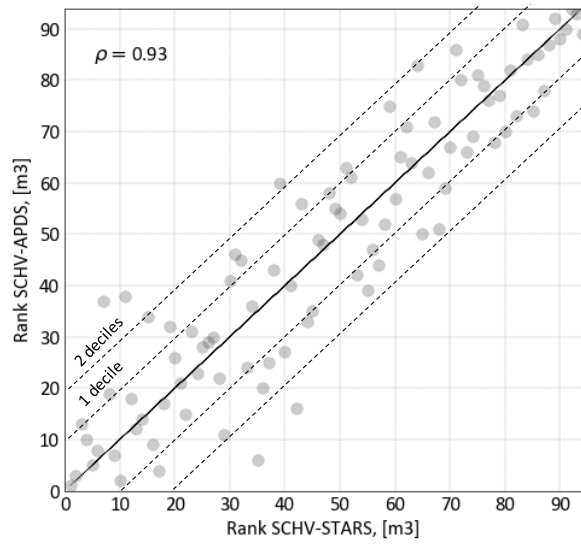
b)

Figure 3.24: a) Scatter plot of SCHV from STARS and SCHV from APDS. b) Scatter plot of SCHV ranks from STARS and SCHV ranks from APDS.

The rank correlation coefficient improves when the comparison is done at later times in the steam-chamber evolution. Figure 3.25a. shows that STARS's COP after 5 years and APDS's SCHV after 7 years have  $\rho_s = 0.89$ , while STARS's SCHV after 5 years and APDS's SCHV after 7 years have  $\rho_s = 0.93$ . Both values strongly indicate that APDS is rank preserving with respect to the similar metric calculate with STARS.



a)



b)

Figure 3.25: a) Scatter plot of COP from STARS after 5 years and SCHV from APDS after 7 years. b) Scatter plot SCHV ranks from STARS after 5 years and SCHV ranks from APDS after 7 years.

### 3.4.5 Computational Time

#### 3.4.5.1 Study-Case Running Time

Running the thermal flow simulator for 100 realizations with the engineering assumptions previously described took an average of 33 hours per realization. Since it was possible to run 3 realizations in parallel, the total effective simulation running time was 46 days. The current APDS Python prototype run the case-study in 5 hours, which results in an average time of 3 minutes per realization. APDS did not use parallel computing. Based on these numbers, it is concluded that in this case-study the graph-based algorithm was 3 orders of magnitude faster than the conventional thermal flow simulator.

It is worthy to mention that an independent implementation of APDS written in the C# programming language. It took 20 seconds approximately to process one realization of the geological model used in this case-study (Wilde, B. personal communication, September 20, 2018). On this implementation, APDS was 4 orders of magnitude faster than STARS.

### 3.5 Discussion

#### 3.5.1 APDS Level of Physics

APDS shows encouraging results that indicates the assumptions and simplifications implemented capture most of the physical phenomena occurring in the reservoir that are relevant to the steam-chamber expansion. Differences to the thermal flow simulator outputs are explained by flow in porous media and heat transfer thermal mechanisms that APDS does not address directly, as well as by the nature of the algorithm that works one cell at the time.

As mentioned before, the ranking function can be expanded to more closely reproduce the STARS results, but the improvement of the results should counterbalance the decrease in computational efficiency. Interestingly, maintaining a flexible ranking function offers the opportunity of tailoring the APDS level of physics (or complexity) to the particular decision problem that the reservoir manager must solve.

Figure 3.26 illustrates that in terms of complexity, APDS is superior to many analytical and semi-analytical models, especially given its capacity to handle reservoir heterogeneities. It is by design inferior to full physics flow thermal flow simulators, because it is intended to be faster than them. The opportunity appears because the range of APDS complexity is not difficult to adjust. A low complex physics APDS could be useful when the decision requires a 3-level discrimination (good, fair, poor) of the projects. For instance, to screen very large areas looking for sweet-spots during a SAGD exploration phase. A medium complex physics APDS could be useful when the decision requires a 5-level discrimination (very-good, good, fair, poor, very-poor) of the projects. For instance, to rank SAGD-Pads in a specified area. Finally, a high complex APDS could be useful when is necessary to approximate as close as possible thermal simulator results but within a constrained timeframe. For example, deciding the orientation and/or the vertical locations of well-pairs.

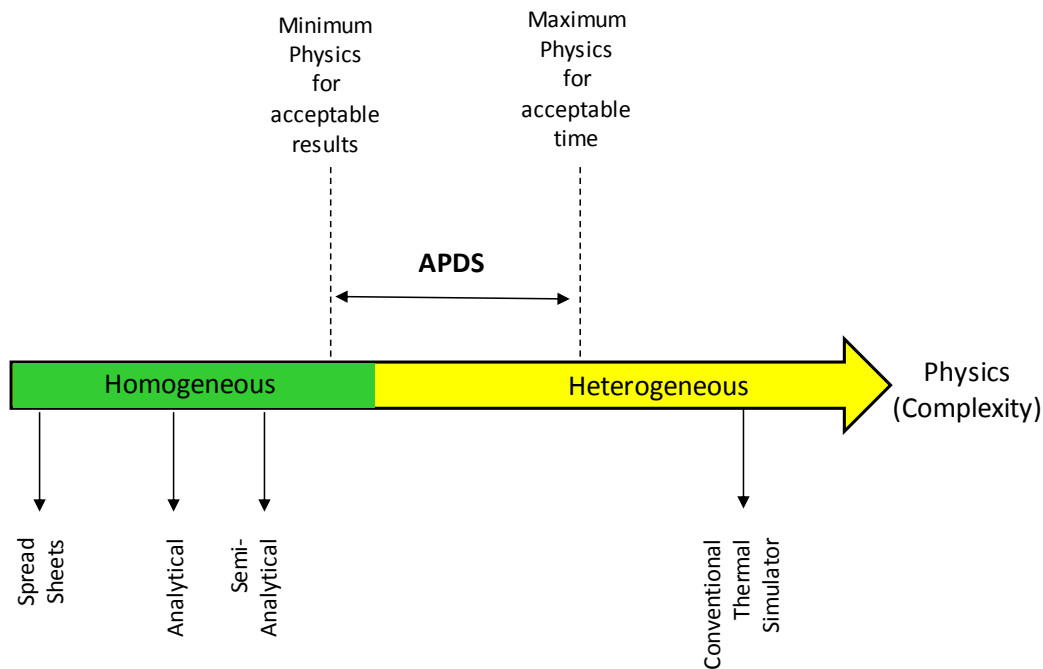


Figure 3.26: Conceptual level of physics of different transfers functions for SAGD.

### 3.5.2 APDS Validation

The visual and numerical comparisons of the steam-chambers generated with STARS and APDS confirm the ability of the later to predict the evolution of the SAGD steam-chamber in complex heterogeneous reservoirs.

The steam-chamber volume (SCHV) obtained from APDS exhibits strong and positive correlation with two different metrics (cumulative oil production and steam-chamber volume) calculated from STARS. The result strongly favors the idea of using APDS as a transfer function to support SAGD decision making workflows in the present of geological uncertainty.

### 3.5.3 APDS Prototype and Computational Time

In the case-study, APDS was 3 orders of magnitude faster than STARS to model the steam-chamber expansion and to provide a response variable. The cost was a reduction in the precision of the results.

Further gains in computational processing time can be reached by parallelizing APDS. The modular structure of the algorithm is very convenient for this as is shown in Figure 3.28. A geological model with  $L$  reservoir realizations can be converted to graphs by running in parallel several modules type I (i.e. graph generators). Then, the SAGD projects, for example,  $N$  potential well-trajectories under evaluation, can be processed by multiple modules type II (i.e. steam-chamber generators) running in parallel too. The outputs would be gathered by post-processing modules type III to assemble the probability distributions of the response variables.

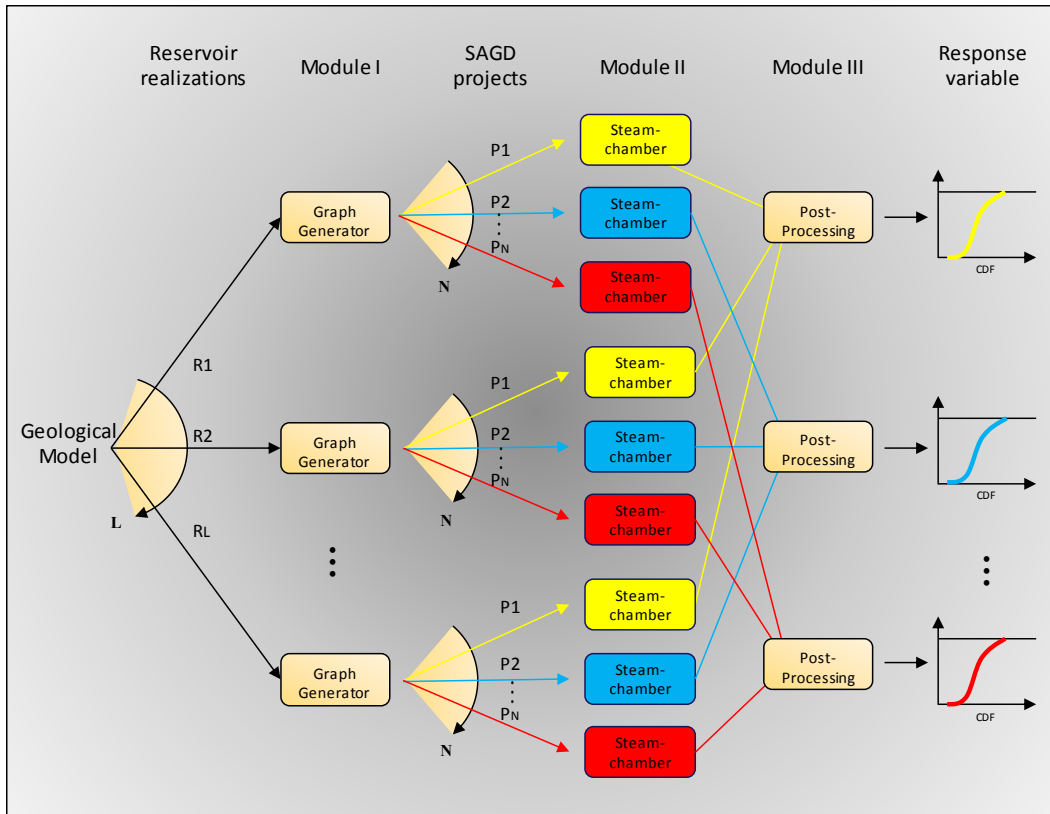


Figure 3.27: Parallelization computing scheme for APDS. Note that the output are cumulative distribution functions (CDF) of the response variables, one per each SAGD project.

Figure 3.27 also illustrates that the output of transferring the geological uncertainty are  $N$  cumulative distribution functions, one per SAGD project. It makes evident that the problem of selecting a project in the present of geological uncertainty is equivalent to the problem of making a choice between the probability distributions of the response variables (Johnstone & Lindley, 2013).

The next chapter introduces a practical decision-making rule to guide the selection of the CDF. It accounts for the risk-reward trade-off and the decision maker's preferences.

## 4 Mean-Variance Criterion and Stochastic Dominance Rules for PRM

### 4.1 Introduction

Considering the risk and reward trade-off for decision making in the presence of uncertainty could be thought of as common-sense knowledge. However, this principle is seldom implemented in petroleum reservoir management (PRM), even though the decisions involve significant geological uncertainty. The geological uncertainty reflects a lack of knowledge in the geometry and properties of the reservoir. Although the geological uncertainty is characterized by geostatistical methods, this information is often not transferred through PRM workflows.

One reason for this situation, already discussed in the previous chapters, is the excessive computation time of transferring the geological uncertainty. Another one is the lack of a practical decision-making criterion that actively manages the risk that arises from geological uncertainty. The importance of the latter reason should not be underestimated; it is the decision-making criterion adopted that ultimately determines which project is selected and implemented.

The decision-making criterion introduced to PRM in this dissertation considers the geological uncertainty in the selection of projects. It is consistent with expected utility theory and combines Mean-Variance Criterion (MVC) and Stochastic Dominance Rules (SDR). It differs from other research that applied the utility framework to PRM (e.g. Güyagüler and Horne 2004; Ozdogan and Horne 2006) because a specific utility function is not required.

This chapter has the following structure. First, PRM problems are stated in terms of a formal decision-making model under uncertainty. In this framework, the concepts of projects, geological uncertainty characterization, transfer of geological uncertainty, preferences over the outcomes and utility theory are discussed. Secondly, the theory of MVC and SDR are introduced to PRM. At the end, a conceptual example explains how MVC and SDR work together to guide the selection of a SAGD project.

## 4.2 Decision-Making Model in Presence of Geological Uncertainty

Figure 4.1 shows a PRM workflow translated to the words of a formal decision-making model under uncertainty with four elements: a set of feasible actions that represent the projects from which a choice must be made by the reservoir manager, a set of outcomes that refers to the consequences of every project under analysis, a preference ordering of the outcomes and a concept of rationality or decision rules that governs the decision process (Stirling, 2012). These components are described below.

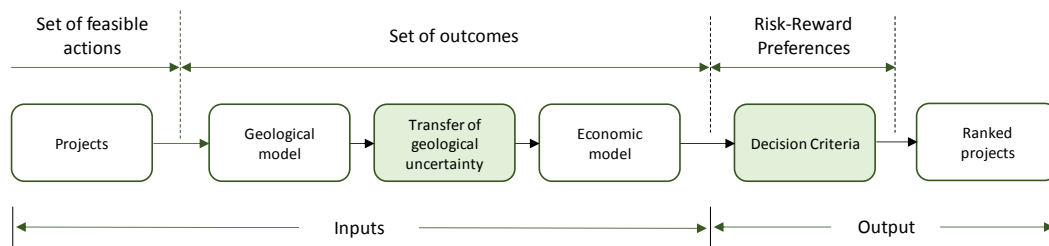


Figure 4.1: Components of a Petroleum Reservoir Management Decision-Making workflow.

### 4.2.1 Set of Feasible Actions or Projects.

The set of contender projects from which the reservoir manager must make a choice is the space of feasible actions of the decision-making model. There are many different types of projects that a reservoir manager is concerned with including drilling a single producer well or defining the integrated development of several fields (SPE, 2007). Notwithstanding the differences, all projects have an intrinsic geological spatial nature.

The spatial nature of the projects leads to a space of feasible actions that is often extremely high dimensional. For instance, the well location problem in a 3D grid has a combinatorial nature that even for small cases quickly leads to an intractable number of configurations. da Cruz (2000) explained how the number of possible combinations of 10 wells in a 30 x 30 grid is in the order of  $10^{29}$ .

The dimension of the space of feasible actions in PRM makes it impractical to perform an exhaustive global search for selection purposes. Optimization algorithms including Genetic Algorithms (Goldberg, 1989) and Particle Swarm Optimization (Kennedy &

Eberhart, 1995) have been studied (Echeverría-Ciurri, Conn, Mello, & Onwunalu, 2012; Isebor, Echeverría-Ciurri, & Durlofsky, 2013; H. Wang, Echeverría-Ciurri, Durlofsky, & Cominelli, 2012).

In some cases, accepted reservoir engineering principles can eliminate many possible projects from consideration and thus the set of feasible actions may be a well-defined set of contenders (Raiffa & Schlaifer, 1961).

#### 4.2.2 Set of Outcomes

The results of the projects cannot be anticipated with certainty because they depend on the unknown reservoir properties. Defining the set of outcomes requires performing two complex and demanding tasks, one is to build a geological model and the other is to process the projects and the geological model through transfer functions (e.g. conventional flow simulation or APDS) to obtain a probability distribution of the response variable that will be used to make the decision.

##### 4.2.2.1 The Geological Model

The geological model is a set of geostatistical realizations that taken all together provides an assessment of the geological uncertainty (Pyrz & Deutsch, 2014). By construction, every realization in the geological model is an equally likely to be drawn representation of the reservoir; and yet, any one realization could never be an accurate representation of the true reservoir.

The methodology and software to generate geological models of petroleum reservoirs are mature and well established. An up to the date collection and explanation of the geostatistical simulation techniques can be found in Pyrcz & Deutsch (2014). There are other important references devoted to the theory and practice of geostatistics and its algorithms (Caers, 2011; Chiles & Delfiner, 2012; Deutsch & Journel, 1998; Goovaerts, 1997).

#### 4.2.2.2 Transfer of Geological Uncertainty

Transferring the geological uncertainty to a production forecast (that might be later converted to a monetary value) is achieved by running a full physics flow simulator on each geostatistical realization with the set of projects being assessed (da Cruz, 2000). An optimization framework is considered when this comprehensive approach is too computationally demanding and time consuming.

An alternative to the full physics flow simulator is to run a relatively simpler and faster flow model such as streamline simulation or a simplified physics model (Pyrzcz & Deutsch, 2014). The precision of the results will be compromised but the relative ranking of the realizations may be preserved. If a good correlation between the response variable obtained from the alternative method and the result obtained by the full physics dynamic simulator can be demonstrated, then the cumulative density function of the faster method would be suitable to assist decision making.

Experimental design and response surfaces (Damsleth, Hage, & Volden, 1992) have been explored to obtain the distribution of the response variable, but the process requires careful calibration with the dynamic flow simulator and it is impractical to be used over a set of realizations. Ranking the realizations through a quick-to-calculate transfer function and selecting a few representative realizations for post-processing with a more complex transfer function is a common practice (Pyrzcz & Deutsch, 2014), but since all the realizations are equally probable and any one realization could be misleading this method should be used very carefully. Computing a static measure such as recoverable hydrocarbon volume in place or a measure of connectivity of the reservoir-quality rock for all the realizations is also valuable to understand the global characteristics of the geological model (Pyrzcz & Deutsch, 2014).

#### 4.2.3 Preferences and Concept of Rationality

Preferences and the concept of rationality are the foundation of a decision-making model. After transferring the geological uncertainty, selecting a project from the set of feasible

actions is equivalent to make a choice between the probability distributions of the chosen response variable (Johnstone & Lindley, 2013).

To make that choice, the investor's preferences over the space of outcomes can be encoded in a utility function (Kochenderfer, 2015). A decision maker will make a rational decision if he chooses a project that maximizes the expected utility. A decision-making model to support PRM should belong to the utility theory framework to fully take advantage of the quantification of the geological uncertainty.

The concept of maximum expected value as an optimal criterion for decision making under uncertainty was proposed by the mathematicians Blaise Pascal and Pierre de Fermat in the 17<sup>th</sup> century (Machina, 1987). Although appealing, this criterion does not explain real decisions under uncertainty, especially with asymmetric consequences of risk associated with large projects.

The concepts of the utility function and the maximum expected utility were proposed by Daniel Bernoulli in 1738. However, only in 1947, John von Neumann and Oskar Morgenstern developed the formal theory of expected utility (Von Neumann & Morgenstern, 2007). They demonstrated axiomatically that the preferences of a decision maker can be encoded in a real-valued utility function. Then, a rational decision maker must act as if their objective is to maximize the expected utility (Johnstone & Lindley, 2013).

In PRM the decision-making problem can be formulated as:

$$\operatorname{argmax}_{a \in A} E[u(x(a, w))] = \operatorname{argmax}_{a \in A} \int f(x(a, w)) \cdot u(x(a, w)) dx \quad (4.1)$$

Here,  $a$  represents projects from the set of feasible actions  $A$ ;  $w$  represents realizations from the geological model;  $x(a, w)$  represents the payoff calculated after transferring the geological uncertainty;  $f(x(\cdot))$  is the probability density function of  $x(\cdot)$  and  $u(x(\cdot))$  is the utility function. Equation 4.1 emphasizes that the payoff of  $x(\cdot)$  depends on the decisions  $a \in A$  and on the geological uncertainty characterized by a set of geostatistical realizations  $w$ .

The utility function is difficult to quantify in practice; however, as shown in Figure 4.2, they can be classified in three groups according to the preferences of the decision maker:

risk-averse, risk-neutral and risk-taker utility functions. A decision maker with risk-averse utility function (a concave function, i.e.  $u''(x) \leq 0$ ) will not play a fair game. “A fair game is defined as a game in which the price of a ticket to play the game is equal to the expected prize” (Levy, 2016). A decision maker with risk-neutral utility function (linear function) is indifferent between playing the fair game or not. A decision maker with risk-taker utility function (convex function, i.e.  $u''(x) \geq 0$ ) will play the fair game. The evidence indicates that most investors exhibit some degree of risk aversion (Levy, 2016); therefore, in this research the decision-making model for PRM is formulated only for risk-averse decision makers. Note that all utility functions are non-decreasing functions (i.e.  $u'(x) \geq 0$ ).

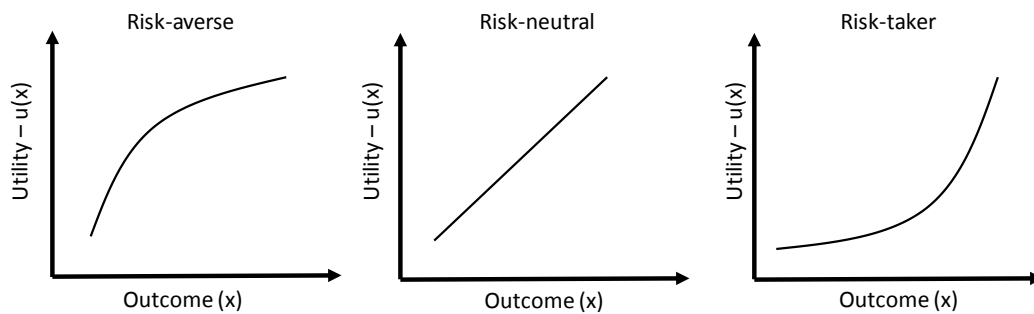


Figure 4.2: Types of utility functions,  $u(x)$ .

Considering that the utility function of companies is difficult to determine or simply not known, an alternative is to look for decision criteria that use only partial information on the decision maker’s preferences (e.g. monotonicity, risk aversion, etc.) and/or the distribution of the response variable to rank candidate projects. MVC (Markowitz, 1959) and SDR (Hadar & Russell, 1969; Hanoch & Levy, 1969; Rothschild & Stiglitz, 1970) are two criteria that allow decision makers to make rational choices between projects with uncertain outcomes without knowing the exact form of the utility function.

### 4.3 Utility Theory in PRM

In the oil and gas industry, the use of expected utility as a criterion for drilling investment was introduced in 1968 (Newendorp & Campbell, 1968). However, the authors of the paper

commented that implementing utility theory was problematic because there were no effective methods to construct or determine a decision maker's utility curve.

This problem remains unsolved. Walls (1995) assumed an exponential utility function,  $u(x) = -e^{-x/R}$ , and proposed inferring the risk tolerance parameter,  $R$ , using an industry specific questionnaire or by reconstructing the risky alternatives that were selected by the firm for capital allocations (Walls, 2005). To circumvent the problem of inferring  $R$ , some authors perform sensitivity analysis over a range of  $R$  to evaluate the robustness of the decisions to different risk attitudes (Güyagüler & Horne, 2004; Ozdogan & Horne, 2006). Begg, Bratvold, & Campbell (2003) and Bratvold, Begg, & Campbell (2003) provide an extensive review of utility theory, and introduced indifference curves to portfolio decision-making in the oil and gas industry. They assumed risk-averse investors with exponential utility functions in their research.

#### 4.4 Mean Variance Criterion and Stochastic Dominance Rules

MVC and SDR are two approaches for making choices without a complete knowledge of the decision maker's utility function (Hadar and Russell 1969). The MVC is the cornerstone of the construction of Markowitz's efficient frontier (Markowitz, 1959) in modern portfolio selection theory. It allows the construction of efficient portfolios based on the maximization of a function of expected return and of its variability (Levy & Sarnat, 1970). SDR is suitable for ranking response variable distribution functions with limited information of the decision maker's preferences.

SDR is superior to MVC when the task is to compare two distributions. SDR is inferior to the MVC when the task is to construct efficient portfolios by combining individual assets (Levy, 2016). Note that the optimization algorithm proposed by Markowitz cannot be applied to the selection of petroleum reservoir projects under geological uncertainty because they have very limited divisibility. For example, one well cannot be further divided into smaller parts, therefore it is meaningless to calculate an efficient portfolio containing fractions of different wells.

#### 4.4.1 The Mean-Variance Criterion (MVC)

MVC states that given the response variable probability distribution functions of projects F and G, F will be preferred to G, if the following conditions are met. It is also required that both equalities do not met simultaneously (Levy & Sarnat, 1970).

$$E_F(x) \geq E_G(x) \text{ and } \text{Var}_F(x) \leq \text{Var}_G(x) \quad (4.2)$$

Where  $E$  and  $Var$  stand for expected value and variance, respectively. MVC reduces a set of opportunity projects to those that are optimal in a Markowitz sense. The set of optimal projects is called the efficient frontier as shown in Figure 4.3. Each project on the efficient frontier dominates all projects located to its “southeast” because those have both, lower expected value and higher variance or standard deviation. For instance, in Figure 4.3. Project A dominates projects B, C and D located in the hatched region. MVC makes explicit that investors must consider the trade-off between risk and return when selecting from uncertain projects.

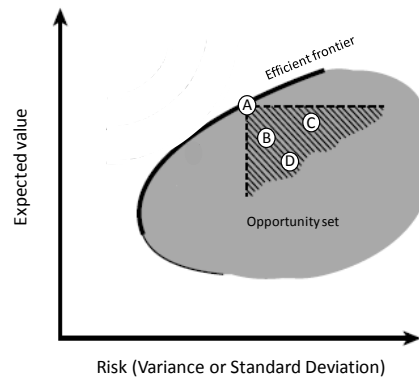


Figure 4.3: Illustration of Markowitz's efficient frontier (Modified after Johnstone & Lindley (2013)).

MVC should be applied with caution, the following example modified after Levy & Sarnat (1970) illustrates a shortcoming of this criteria. Given the payoff for projects F and G on Table 4.1, any decision maker by common sense will prefer F over G, because having the same probabilities, F has higher payoffs than G in all cases. However, according to MVC, both projects belong to the efficient set and theoretically some decision makers

could choose F and others G. Note that project F has both higher expected payoff and higher variance than project G, then the MVC's inequalities in Equation 4.2 do not hold.

Table 4.1: Payoff matrix for projects F and G (Modified after Levy and Sarnat (1970)).

	Prospect F		Prospect G	
	Payoff	Probability	Payoff	Probability
	3	1/3	1	1/3
	6	1/3	2	1/3
	9	1/3	3	1/3
<b>E (X)</b>	6		2	
<b>Var (X)</b>	6		0.67	

The Figure 4.4 provides another clarifying example. It depicts the response variable CDF's of two projects named A and B. For any rational decision maker, project A is preferred to project B because the minimum value of A is higher than the maximum value of B. However, MVC cannot resolve which project is better because not only  $E_A(x) > E_B(x)$  but also  $Var_A(x) > Var_B(x)$ . The analysis of these type of situations motivated the formulation of SDR.

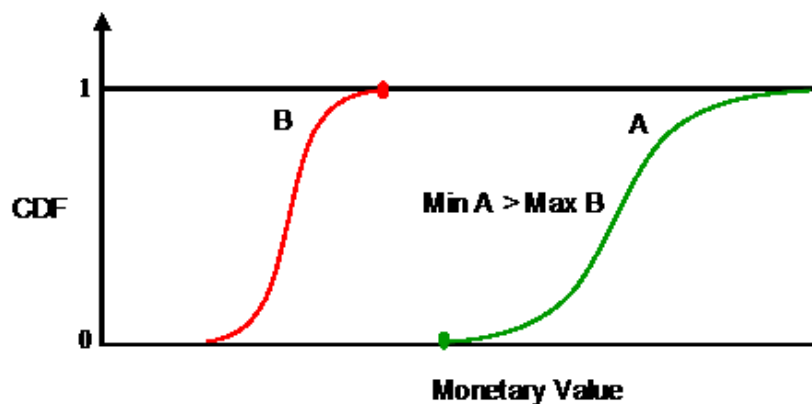


Figure 4.4: MVC criterion fails to discern which project is preferred between A and B.

## 4.4.2 Stochastic Dominance Rules (SDR)

SDR ranks uncertain projects based on partial information about the investor's preferences or the response variable distribution (Levy, 2016) and is consistent with maximizing expected utility. This section on SDR is based on the work of Levy (2016) and Levy & Sarnat (1970).

### 4.4.2.1 First Degree Stochastic Dominance (FSD)

FSD rule states that given two cumulative distributions functions (CDF)  $F(x)$  and  $G(x)$ ,  $F$  dominates  $G$ , if and only if:

$$F(x) \leq G(x), \forall x \Leftrightarrow E_F[u(x)] \geq E_G[u(x)], \forall u'(x) \geq 0 \quad (4.3)$$

The underlying space of uncertainty is the same;  $F(x)$  and  $G(x)$  represent the cumulative distributions of payoff calculated from the same set of realizations for projects  $F$  and  $G$ .  $E_F[u(x)]$  and  $E_G[u(x)]$  represent the expected utility for the projects  $F$  and  $G$ , respectively. FSD assumes that investors always prefer more money rather than less money (Levy, 2016), thus, FSD decisions are valid for all non-decreasing utility functions (i.e.  $u'(x) \geq 0$ ). If  $F(x)$  and  $G(x)$  intersect, then FSD does not provide a choice to the investor.

Figure 4.5 depicts the CDFs for projects in Table 4.1. FSD unambiguously indicates that investors should prefer  $F$  over  $G$  since for any quantile  $F$  dominates  $G$ . Even though  $F$  has higher variance than  $G$ , it does not change the decision; on the contrary, since the lowest payoff of  $F$  is at least equal to the highest payoff of  $G$ , the higher variance represents desirable upsides of project  $F$ . Also note that for the example on Figure 4.4, SDR indicates that  $A$  dominates  $B$  by FSD because  $A(x) \leq B(x), \forall x$ .

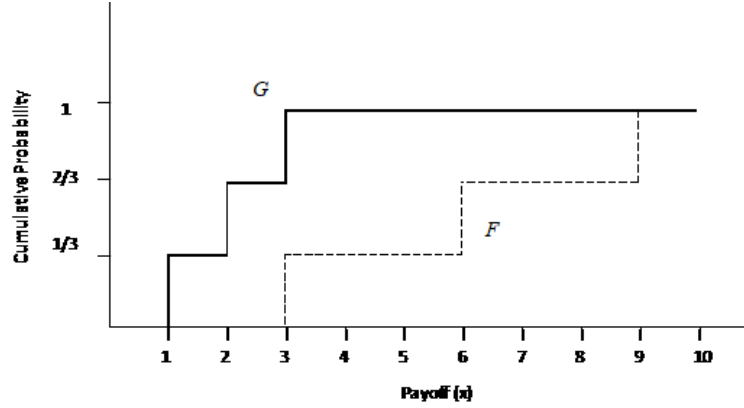


Figure 4.5: Project  $F$  dominates project  $G$  by FSD because  $F(x) \leq G(x)$ ,  $\forall x$ .

As stated above, FSD requires that the CDFs under comparison do not cross each other, although they can touch each other. For that reason, in Figure 4.6a neither  $F$  dominates  $G$ , nor  $G$  dominates  $F$  by FSD. However, in Figure 4.6b,  $F$  dominates  $G$  by FSD even though there is a range of  $x$  where  $F(x) = G(x)$ .

The relationship between FSD and the utility function can be extracted from Equation 4.4, that was derived from the expected utility definition applied to projects  $F$  and  $G$  (details are provided in Appendix B).

$$E_F[u(x)] - E_G[u(x)] = \int_a^b [G(x) - F(x)] u'(x) dx \quad (4.4)$$

From the application of FSD,  $[G(x) - F(x)] \geq 0$ . Moreover,  $u(x)$  is a non-decreasing function with  $u'(x) \geq 0$ . Then, the integral is non-negative and we can conclude that:

$$E_F[u(x)] - E_G[u(x)] \geq 0 \text{ or } E_F[u(x)] \geq E_G[u(x)] \quad (4.5)$$

Thus, Equation 4.4 and Equation 4.5 show that by applying FSD, a decision maker maximizes the expected utility.

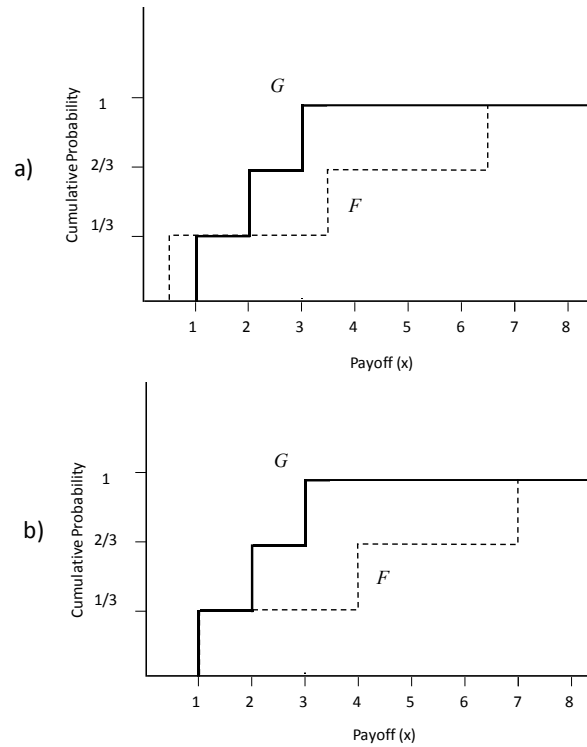


Figure 4.6: a) Since CDFs cross each other, there is not FSD, b) Although CDFs touch each other,  $F$  dominates  $G$  by FSD.

#### 4.4.2.2 Second Degree Stochastic Dominance (SSD)

SSD rule states that if the investor has a convex utility function (i.e. He is a risk averse investor), then  $F$  dominates  $G$ , if and only if:

$$\int_a^x [G(t) - F(t)]dt \geq 0, \forall x \in [a,b] \quad (4.6)$$

$$\Leftrightarrow E_F[u(x)] \geq E_G[u(x)], \forall u''(x) \leq 0$$

Equation 4.6 entails that  $F$  will be preferred over  $G$ , even if the CDF's intercepts multiple times, as long as the cumulative difference between them is non-negative for all values of  $x$  (Levy & Sarnat, 1970). In Figure 4.7a we can conclude that project  $F$  dominates  $G$  by SSD. In Figure 4.7b, neither  $F$  nor  $G$  dominates the other by SSD.  $F$  does not dominate  $G$  because the cumulative first differences between the two CDF's is negative in the range  $3 < x < 5$ .  $G$  does not dominate  $F$ , because  $G$  has a lower left tail than  $F$ . The SSD

formulation implies that a distribution with lower left tail cannot dominate distributions that start at its right (Levy, 2016).

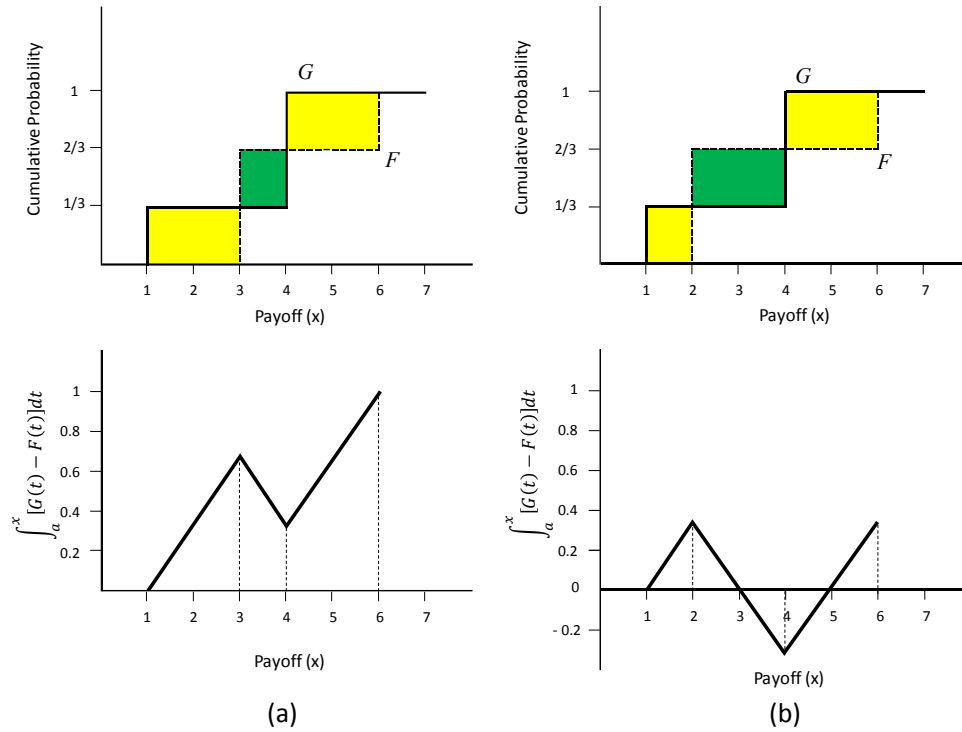


Figure 4.7: a)  $F$  dominates  $G$  by SSD, b) Neither  $F$  nor  $G$  dominates the other by SSD.

Insights about the relationship between SSD and the utility function can be gained from the analysis of CDFs shown in Figure 4.8. Firstly, by visual inspection it is possible to conclude that  $F$  dominates  $G$  by SSD because the cumulative difference between the CDFs is non-negative over the entire domain  $a \leq x \leq c$ .

Note that in this case the right-side of Equation 4.4 can be expanded as shown in Equation 4.7.

$$\begin{aligned}
 E_F[u(x)] - E_G[u(x)] &= \int_a^b [G(x) - F(x)] u'(x) dx \\
 &+ \int_b^c [G(x) - F(x)] u'(x) dx
 \end{aligned} \tag{4.7}$$

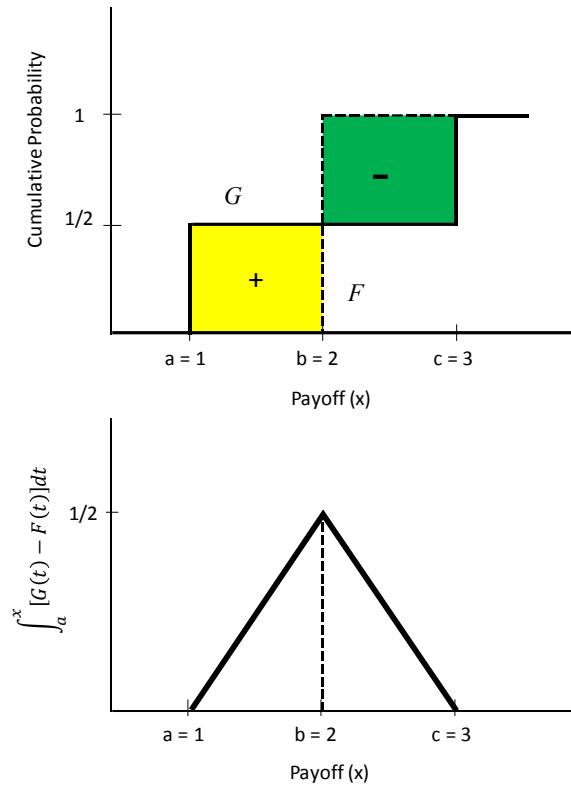


Figure 4.8:  $F$  dominates  $G$  by SSD (Modified after Levy (2016)).

The cumulative difference  $[G(x) - F(x)]$  is positive in the range  $a \leq x \leq b$  and negative in the range  $b \leq x \leq c$ . Now, by the risk-aversion assumption, the utility function is concave, which means that  $u''(x) < 0$  and therefore  $u'(x)$  is a declining function of  $x$ . This observation implies that in Equation 4.7, the first integral has a larger absolute value than the second integral, and thus the right side of Equation 4.7 is positive. Since the integral is positive, we can conclude again that:

$$E_F[u(x)] - E_G[u(x)] \geq 0 \text{ or } E_F[u(x)] \geq E_G[u(x)] \quad (4.8)$$

Thus, Equation 4.4, Equation 4.7 and Figure 4.8 show that by applying SSD, a decision maker maximizes the expected utility.

Besides FSD and SSD, higher order stochastic dominance rules have been derived (e.g. third or fourth order stochastic dominances), but their economic interpretation is not as clear as for FSD and SSD: they rely on extraordinarily precise distributions. For these

reasons, only the first two degrees of stochastic dominance are considered in this dissertation as criteria for PRM problems.

#### 4.4.2.3 Stochastic Dominance Matrix (SDM)

After ranking a set of projects using SDR, the results can be summarized in a Stochastic Dominance Matrix (SDM) as shown on Figure 4.9. In SDM, projects on the columns dominates projects on the rows, conversely, projects on the rows are dominated by projects on the columns. Projects from left to right are ordered from higher to lower expected value. The color and number represent the stochastic dominance degree. Green and zero (0) mean there is no dominance, blue and one (1) mean FSD, red and two (2) mean SSD. For example, project A dominates B by SSD and it dominates all other projects by FSD.

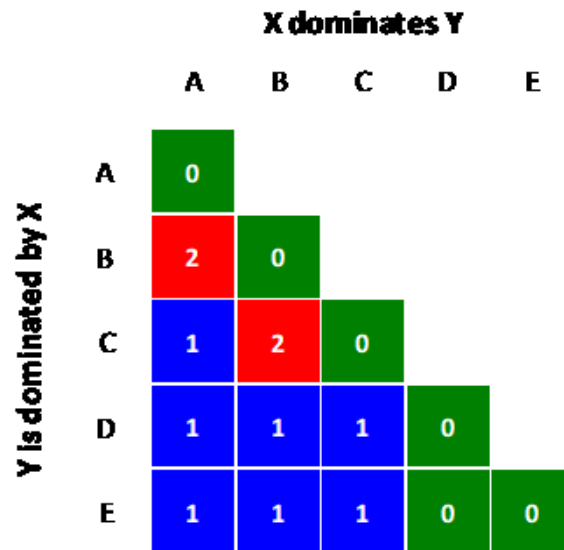


Figure 4.9: Stochastic Dominance Matrix.

Based on the above discussion, this dissertation proposes using MVC-SDR sequentially in PRM decision-making workflows. MVC compares the first two moments of the response variable probability function is applied to the set of feasible actions to identify an initial efficient frontier, and then SDR is applied to the projects on the efficient frontier to further reduce its size. Section 4.6 provides an example of the methodology.

## 4.5 MVC and SDR in PRM

In the oil and gas industry, portfolio theory optimization (Markowitz, 1959) that is based on MVC was proposed to support budget allocations and investment/divestment decisions that result in efficient portfolios of assets (Bratvold et al., 2003; Edwards, 1993). However, while this method developed for financial instruments is readily applicable to assets, it cannot be used directly to solve project selection problems in the presence of geological uncertainty. Capolei, Suwartadi, Foss, & Jørgensen (2015) implemented an objective function based on MVC to identify the efficient frontier of a production optimization problem in the presence of geological uncertainty and suggested the Sharpe ratio to trade-off risk and return. The efficient frontier in their work represents different operational strategies to maximize the net present value (NPV) of a waterflooding project. In the case study, they reported the issue that the strategy obtained with MVC and the Sharpe ratio has a maximum NPV that was smaller than the minimum NPV of one competing strategy in the efficient frontier. Chang, Bouzarkouna, & Devegowda (2015) implemented a mean-variance approach to find the solution of well placement problems considering geological uncertainty. They obtained an efficient frontier but did not try to further reduce its size. As far as the author knows, MVC-SDR have not been previously implemented to solve PRM problems.

## 4.6 Example of MVC-SDR Methodology

This example is designed to explain the MVC-SDR methodology step by step. The next chapter presents a realistic case-study that integrates APDS to MVC-SDR to guide the solution of a representative SAGD problem commonly found in the exploitation of oil sands.

Consider the problem of selecting one SAGD well-pad to be drilled from a set of thirteen possible options illustrated in Figure 4.10. It is assumed that a geological model is available and that the probability density function (PDF) of the response variable (net present value in this case) is also available by transferring the geological uncertainty through flow simulation (or APDS) and economic modeling for every realization for all well pads.

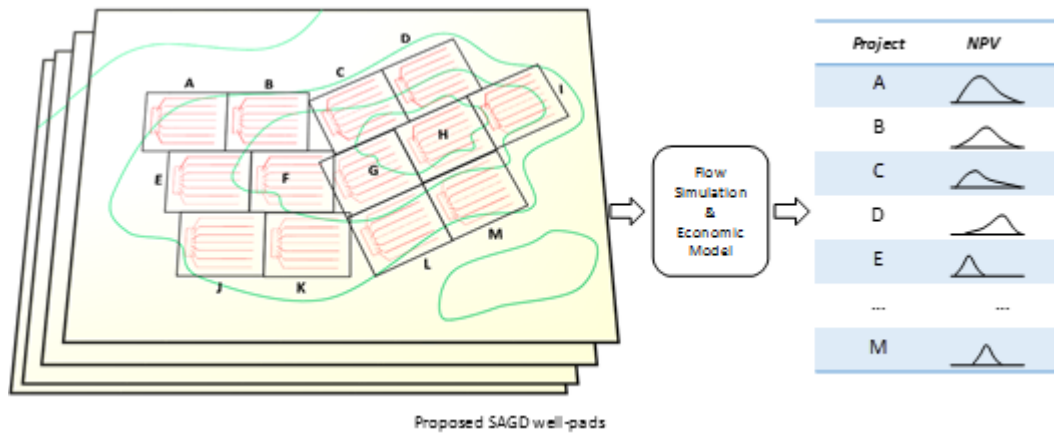


Figure 4.10: SAGD well-pad locations and assumed net present value probability distribution functions.

With the given information, the MVC-SDR proceeds as follow:

(1) Compute the mean and variance values of each option and use MVC to establish Markowitz's efficient frontier. The red dots in Figure 4.11 represent the projects on the efficient frontier. Note that each red-dot project dominates all the other projects located to its southeast. For example, B dominates D, H and L. Projects on the efficient frontier are not dominated in Markowitz's sense by any other project.

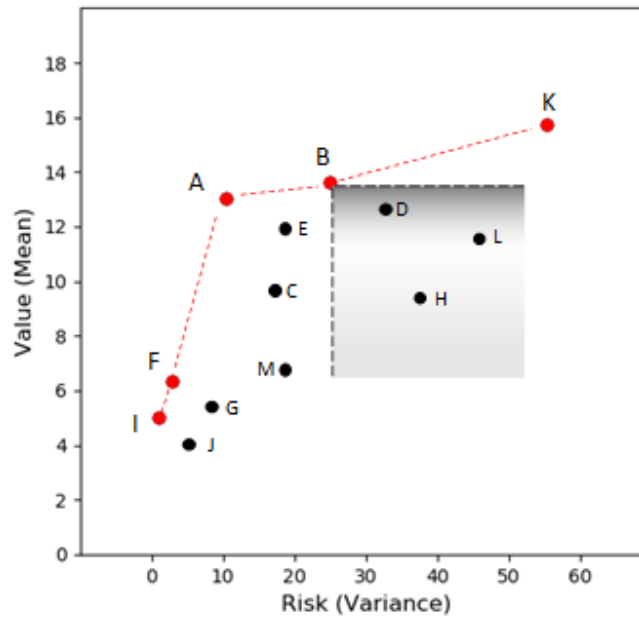


Figure 4.11: Red dots are projects on the efficient frontier. Project B dominates D, L and H because it has higher mean and less variance.

(2) Apply the first and second degree SDR to possibly eliminate some of the projects on the efficient frontier.

**FSD.** Figure 4.12 shows the PDFs and CDFs for the well-pads I, F, A, B and K. A percentile to percentile comparison between the pairs of projects I-A and F-A demonstrates that A dominates I and F by FSD. Then, projects I and F should be discarded from the efficient frontier, while projects A, B and K should remain. It is noteworthy that K and B do not dominate F.

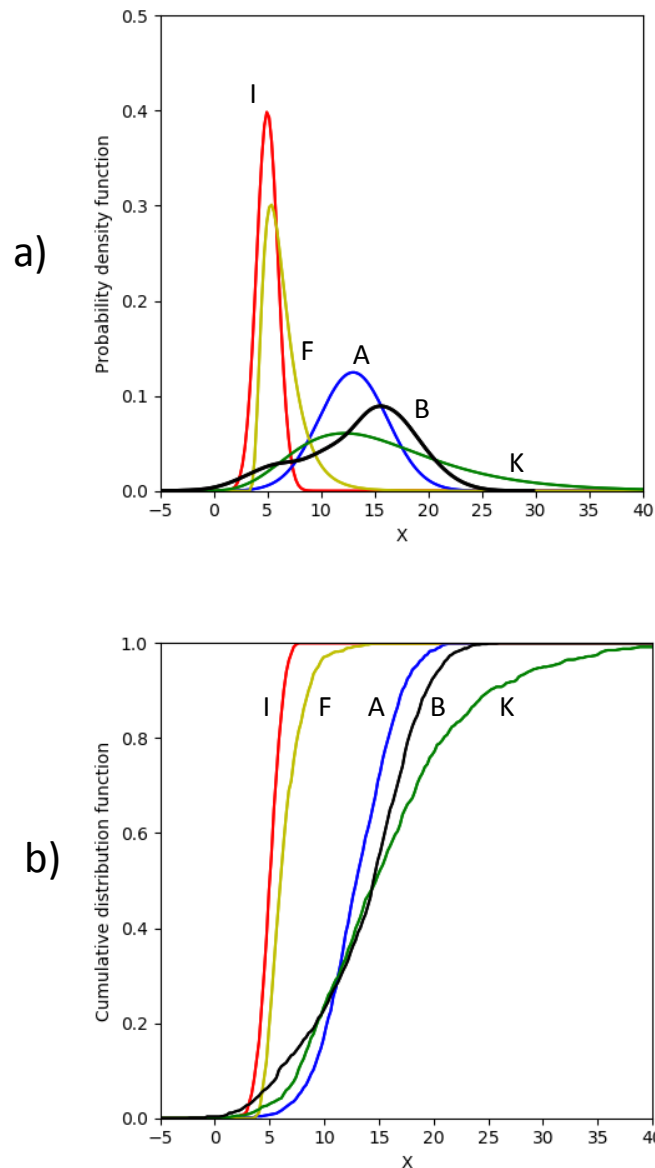


Figure 4.12: PDF (top) and CDF (bottom) of projects on the efficient frontier. After FSD, projects I and F should be discarded. Projects A, B and K remain in the efficient set.

**SSD.** Figure 4.13 shows the integral of the CDF for projects A, B and K. Observe that the curve K is always to the right side of curve B; thus, K dominates B by SSD. Projects B should be discarded from the efficient frontier, while projects A, K should remain. Observe that in this case, project A does not dominate projects B or K by SSD; but similarly, A is not dominated by any other project. SDM in Figure 4.14 summarizes the results of applying FSD and SSD.

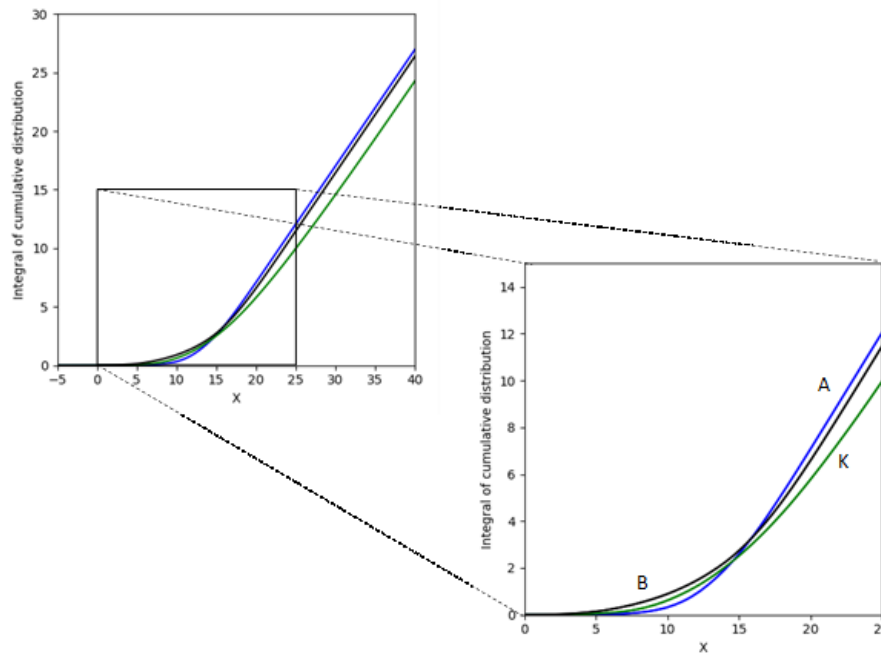


Figure 4.13: Integral of CDF for projects A, B and K. After SSD, project B should be discarded. Projects A and K remain in the efficient set.

	K	B	A	F	I
K	0				
B	2	0			
A	0	0	0		
F	2	0	1	0	
I	2	0	1	1	0

Figure 4.14: Stochastic Dominance Matrix

After applying MVC-SDR, the number of contender projects is reduced from 13 to 2. While most reservoir managers should agree with this result, the final choice between A and K depends on the specific reservoir manager's utility function.

#### 4.7 Discussion

The MVC-SDR decision-making model is general enough to be applied to any kind of PRM problem. In the example above, SAGD well-pad selection is demonstrated.

MVC and SDR considers the risk and return trade-off according to the utility theory framework. They work without knowing the exact form of the decision-maker's utility function. This is an advantage over models that require the utility function. While most decision-makers might agree with the use of a risk-averse function, they probably will not agree with the level of risk (risk tolerance) that they are willing to accept.

MVC-SDR leads to decisions that are considered rational to risk-averse reservoir managers. This desirable property comes at the expense of losing the ability to discriminate between very similar projects. In the example, the result is two projects from which the manager should make the final decision.

Geostatistical reservoir models to quantify the geological uncertainty have increased in complexity over the years; for that reason, reservoir managers might have more difficulty selecting projects. MVC-SDR will not always help them to find a single project, but they can reduce the number of alternatives from which the final decision must be made.

To obtain robust results from MVC-SDR the response variables CDF's must be stable and representative. Therefore, transferring of the geological uncertainty should be done over many geostatistical realizations, it is recommended to use at least 100 realizations.

## 5 Case-Study: SAGD Vertical Well Placement

### 5.1 Introduction

A graph-based APDS is formulated, implemented and validated. It can efficiently transfer geological uncertainty into SAGD steam-chambers over hundreds of geostatistical realizations. Making a selection among a group of SAGD competitor projects is equivalent to make a choice among their corresponding response variable CDFs. For this purpose, the MVC-SDR criterion is proposed because it considers the decision maker's preferences on the risk-reward information embedded in the CDFs.

The case study documented here applies all the aforementioned concepts. The problem consists in finding the best vertical location for a SAGD well-pair project in a target volume. The example is a challenge commonly found in the exploitation of Canadian oil sands.

### 5.2 SAGD Vertical Placement Well Problem

#### 5.2.1 Problem Setting

Consider a reservoir manager that must decide the elevation of a 500 m SAGD horizontal well-pair inside a 40 meter wide x 10 meter thick target volume shown in Figure 5.1. The manager faces the challenge illustrated in the Figure 5.2, they would like to drill the producer well as close as possible to the base formation to increase the drainable oil column, but the risk of having an ineffective well length is higher there (Figure 5.2.a). An intermediate well location reduces the risk of losing effective well length, but near-well barriers could negatively impact the steam-chamber growing (Figure 5.2.b). In contrast, a higher producer well location in the target volume would likely contact good quality reservoir, but at the expense of a reduced hydrocarbon column (Figure 5.2.c). Figure 5.2 has a vertical exaggeration of 8.

The geological uncertainty is characterized by a set of 100 geostatistical realizations. The reservoir manager must make the decision considering the risk and return trade-off and their preferences. Hereafter, the problem is setup with the decision-making model elements previously described.

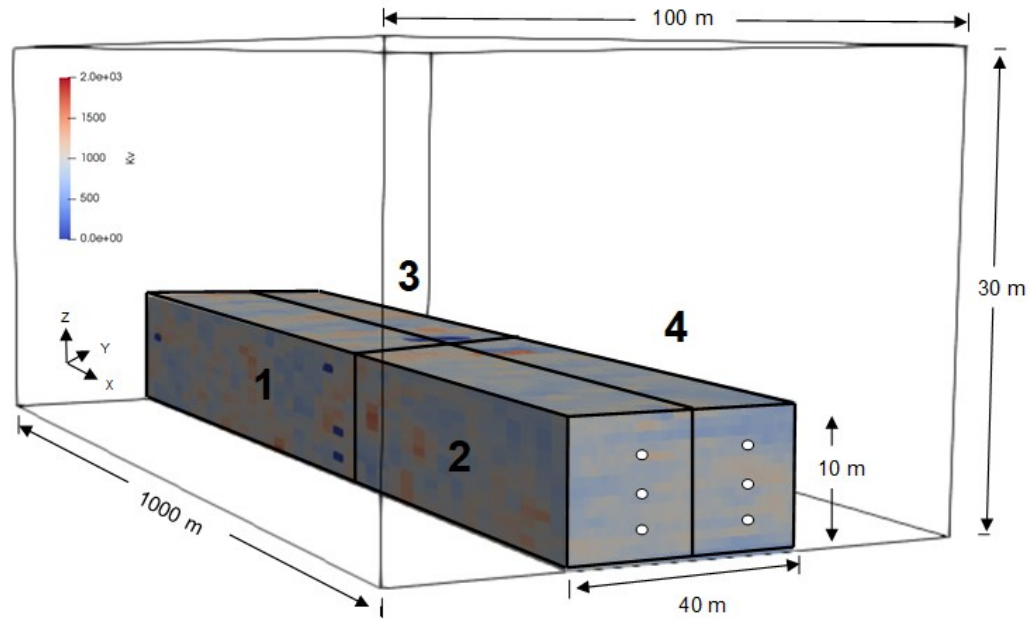


Figure 5.1: Target volume for vertical placement case study.

## 5.2.2 Set of Feasible Actions

The set of feasible actions from which a decision must be made are all possible well locations inside the target volume depicted in Figure 5.1. The target volume was discretized in quadrants and the wells locations were modeled using levels every meter. Consequently, wells were indexed by quadrant and levels; for example, W15 refers to a well located in the first quadrant and the level 5. Figure 5.1 has a vertical exaggeration of 8.

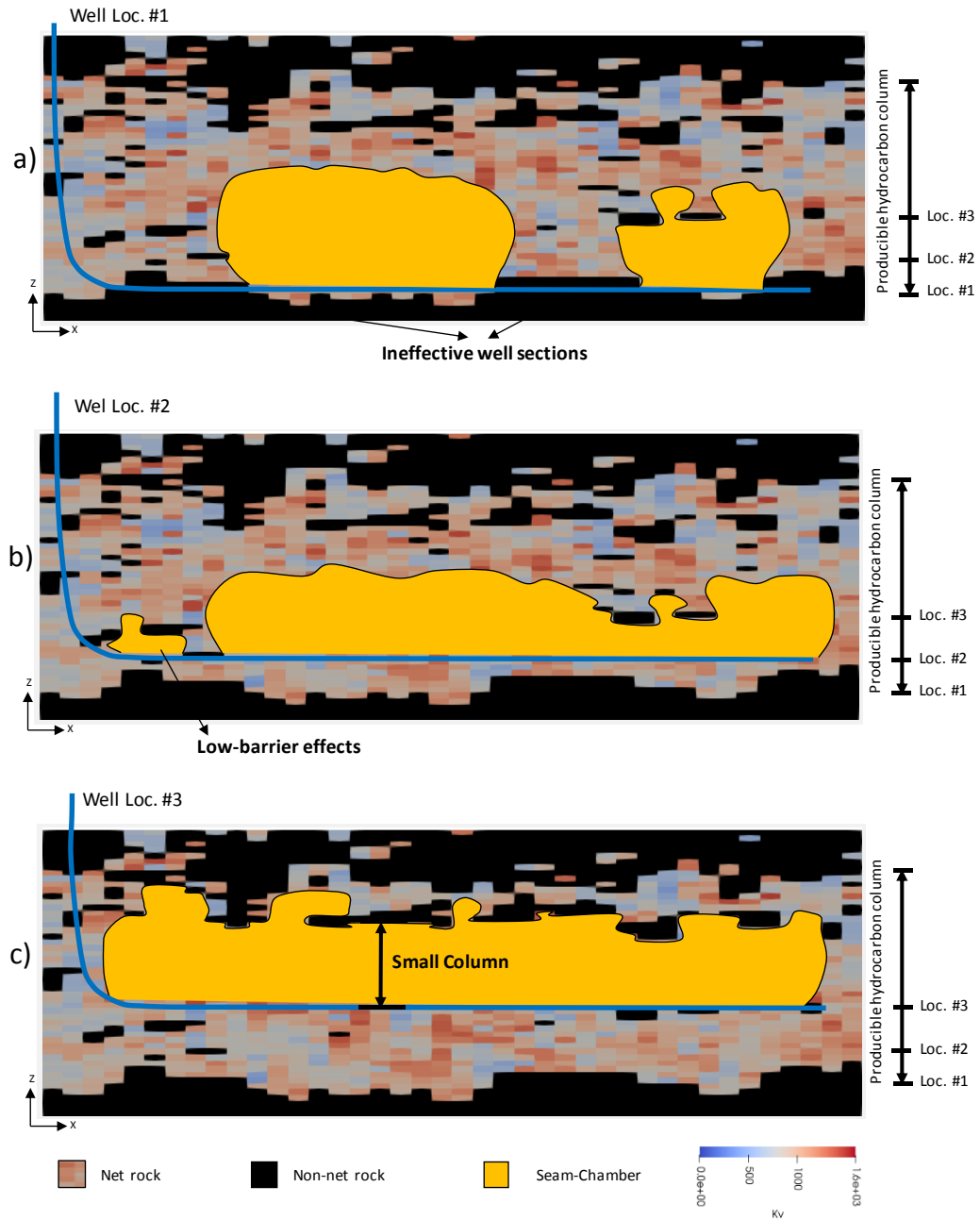


Figure 5.2: Description of vertical placement well location challenge. a) Location #1 has ineffective well length, b) Location #2 intersects low-placed barriers, c) Location #3 has a small hydrocarbon column.

### 5.2.3 Geological Model

The geological model with 100 reservoir realizations is described in Section 3.4.1. Figure 5.3 shows some cross-sections through the target volume from different geostatistical realizations.

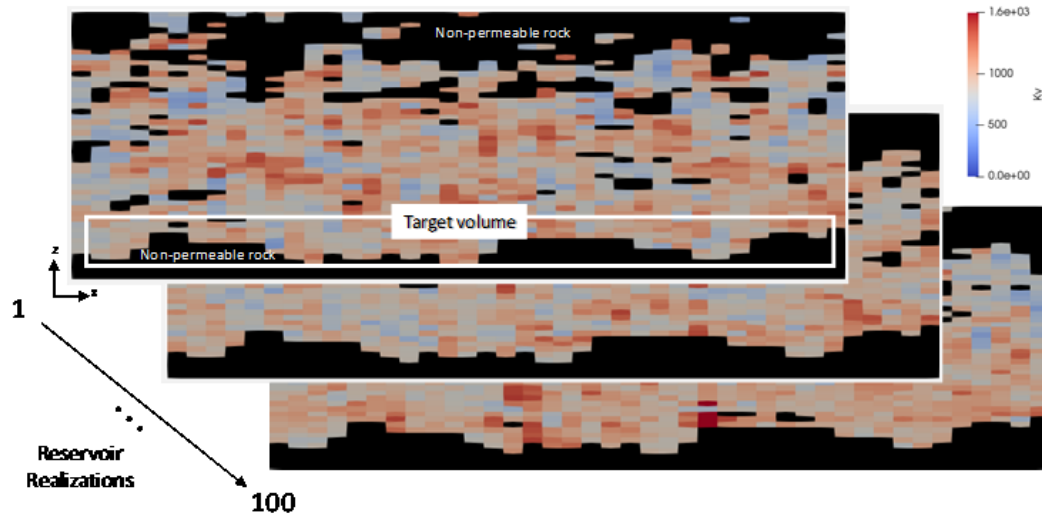


Figure 5.3: Cross-section through the target volume on several geostatistical realizations.

### 5.2.4 Transferring the Geological Uncertainty with APDS

APDS was used to transfer the geological uncertainty. After modeling the steam-chamber for 5 years, the heated hydrocarbon volume (also called heated steam-chamber volume - SCHV) was calculated and converted to a monetary value using a net present value per barrel (NPV/bbl) of 5 US\$/bbl. The NPV/bbl is based on the supply costs study for a 30,000 BPD SAGD project published by the Canadian Energy Research Institute (CERI, 2018) and assuming a WTI price of 65 US\$/bbl. The typical design parameters of a 30,000 BPD SAGD project with its supply cost summary are reported in Tables 5.1 and 5.2 (CERI, 2018), respectively.

Table 5.1: Typical design parameters for a 30,000 BPD SAGD project. (Obtained from CERI (2018)).

	Measurement Units	SAGD
<b>Project Design Parameters</b>		
Stream day capacity	bbl of bitumen per day	30,000
Production Life	years	30
Capacity Factor (Annual Average)	%	90%
<b>Capital Expenditures (2017 CAD Dollars)</b>		
<i>Initial</i>	Millions of dollars	\$1,200.0
	Dollars per bbl of capacity	\$40,000.0
<i>Sustaining</i>		
(Annual Average)	Millions of dollars/year	\$43.8
Operating Working Capital	Days payment	45
<b>Operating Costs (2017 CAD Dollars)</b>		
Total Operating Costs	Millions of dollars/year	\$123.2
Non-Energy Operating Costs	Millions of dollars/year	\$86.2
<b>Energy Requirements</b>		
Natural Gas	GJ per day	35,910
Electricity Purchased	MWh/d	300
Electricity Sold	MWh/d	0
<b>Other Project Assumptions</b>		
Abandonment and Reclamation	percent of total capital	2%

APDS provides for each potential producer well location a set of 100 cumulative heated hydrocarbon volume curves. Figures 5.4 and 5.5 show the curves for wells located 5 and 6 meters above the grid base, respectively. Note that every curve corresponds to one geostatistical realization. Figure 5.6 shows the box-plots of the heated hydrocarbon volumes after 5 years for all 40 possible well locations.

Table 5.2: Supply cost summary for a 30,000 BPD SAGD project. (Obtained from CERI (2018)).

<b>Supply Cost</b>		SAGD 10% ROR (a)
Net Present Value (C\$ Millions)		\$0
Discount Rate		10%
Base Year		2017
<b>Costs (C\$/b)</b>		Discounted
Return on Investment		Included
Fixed Capital (Initial & Sustaining)		\$19.33
Operating Working Capital		\$0.41
Fuel (Natural Gas)		\$4.57
Other Operating Costs (incl. Elec.)		\$9.02
Abandonment Costs		\$0.03
Royalties		\$7.81
Income Taxes		\$2.87
Emissions Compliance Costs		\$0.67
	Subtotal	<u>\$44.70</u>
	Electricity Sales	0.0
	Subtotal	0.0
<b>Total Supply Cost (C\$/b)</b>		<b><u>\$44.70</u></b>
Blend Product @ Hardisty in C\$/b		\$49.90
Blend Product @ Hardisty in US\$/b		\$39.92
Blend Product's WTI Equivalent @ Edmonton in US\$/b		\$54.92
<b>WTI Equivalent (US\$/b)</b>		<b><u>\$60.17</u></b>

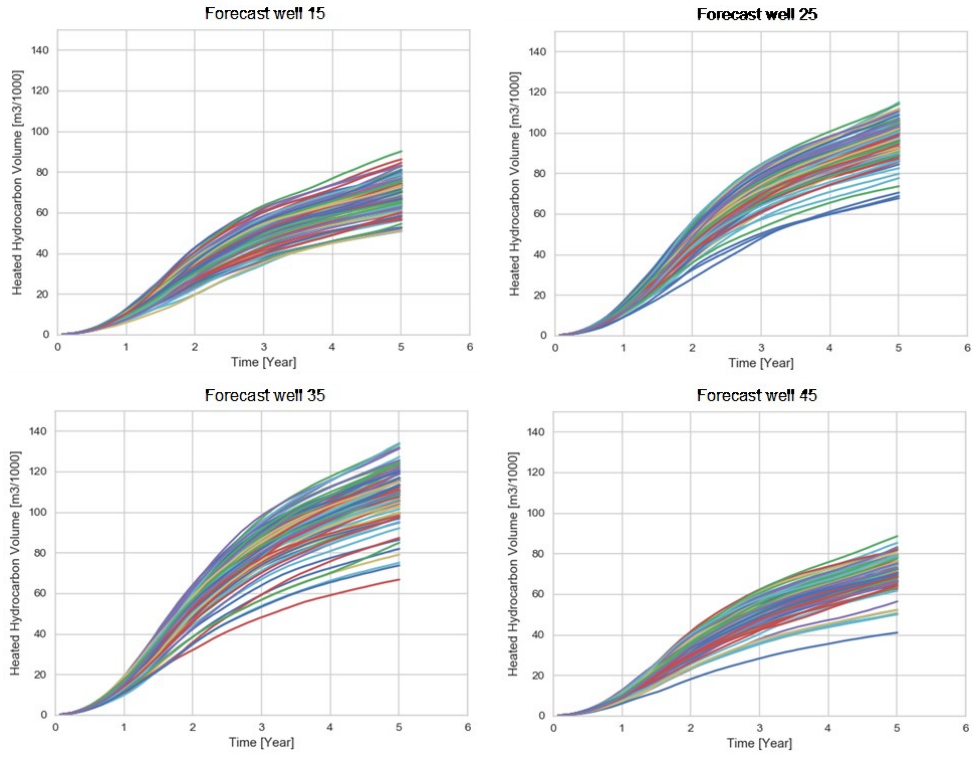


Figure 5.4: Heated hydrocarbon volume forecast for wells in level 5 of target volume.

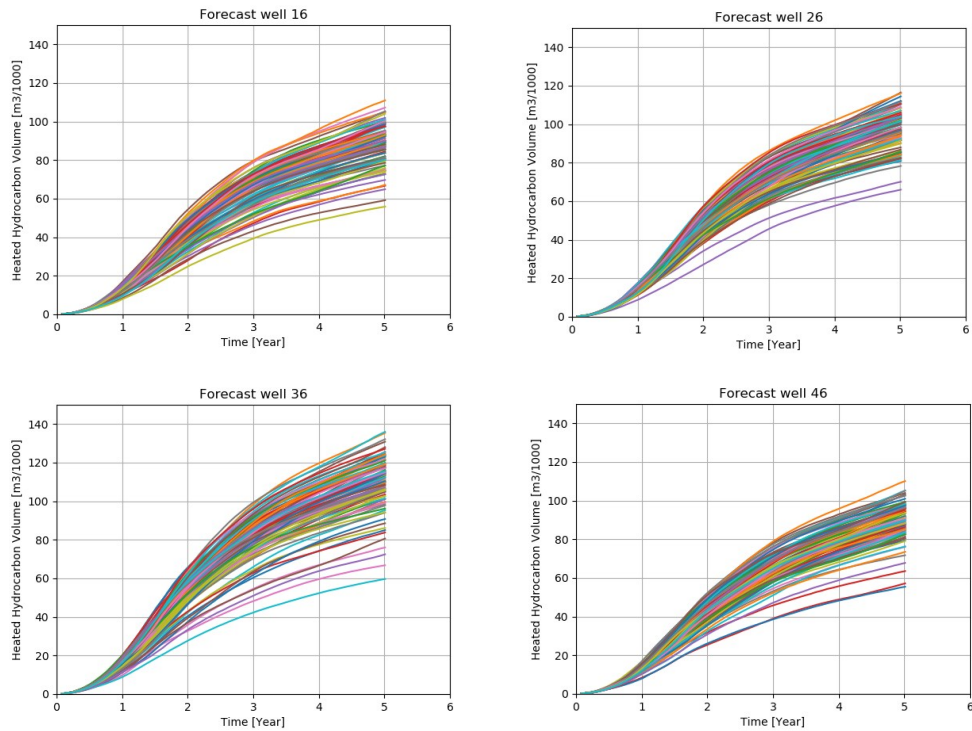


Figure 5.5: Heated hydrocarbon volume forecast for wells in level 6 of target volume.

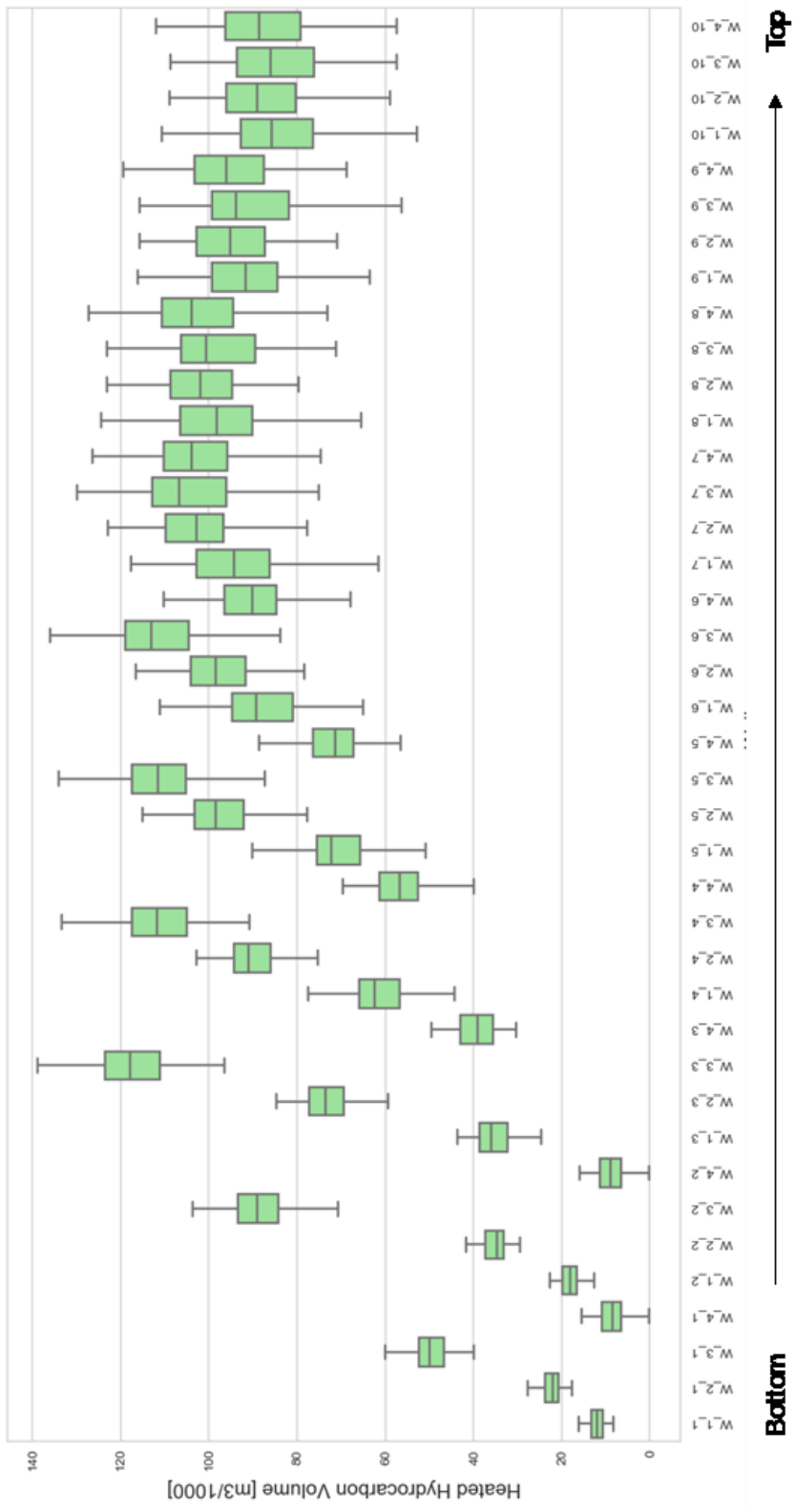


Figure 5.6: Box-plots of heated hydrocarbon volume for wells in target zone.

Note that wells located in levels 1 and 2 have small volumes and small interquartile ranges. These wells tend to intercept non-productive formations and have long ineffective sections that do not contribute to bitumen production. Figure 5.7 shows a steam-chamber generated by a well located in the second quadrant and the level 2.

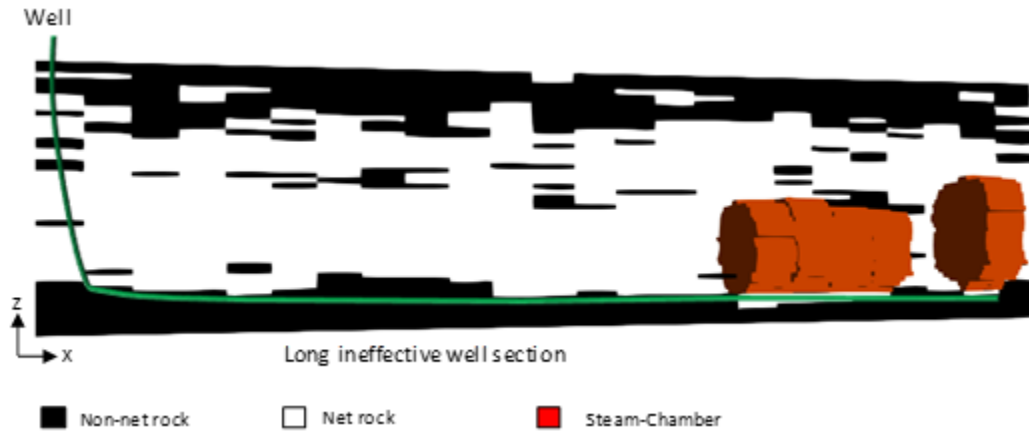


Figure 5.7: Steam-chamber of well located in second quadrant and level 2. The long ineffective well section has a negative effect on the steam-chamber development.

Wells in levels 3 to 7 contact sandy formation sections and their box-plots show higher volumes and higher dispersion than the previous group. Figure 5.8 shows a steam-chamber generated by a well located in the second quadrant and the level 7.



Figure 5.8: Steam-chamber of well located in second quadrant and level 7.

Wells above level 7 have a reduced hydrocarbon column and they will produce less bitumen than the previous groups. Figure 5.9 shows a steam-chamber generated by a well located in the second quadrant and the level 10. Note the large amount of unrecoverable bitumen below the producer well. Heated hydrocarbon volume was converted to net present value before applying the decision criteria.



Figure 5.9: Steam-chamber of well located in second quadrant and level 10. Note the large amount of unrecoverable bitumen below the producer well.

### 5.2.5 MVC

MVC was applied to the set of 40 potential locations to find the initial efficient frontier depicted in Figure 5.10. The 13 efficient locations are  $EF = \{W11, W12, W21, W22, W13, W31, W23, W24, W25, W26, W27, W34, W33\}$ . Note that MVC fails to reject locations in levels 1 and 2 that any reasonable reservoir manager would never select, for example, W11, W12, W21 or W22.

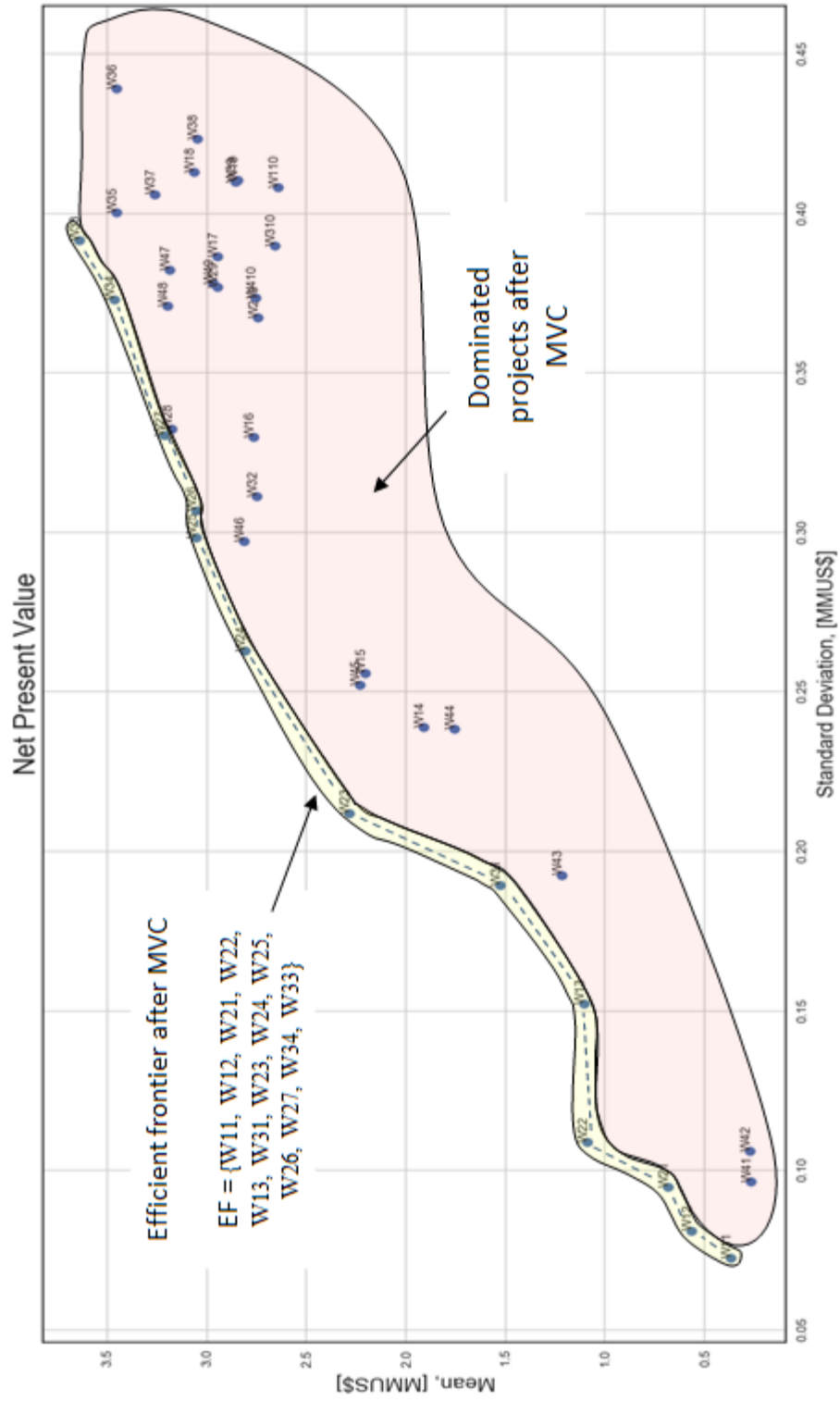


Figure 5.10: Efficient frontier and dominated locations after MVC.

## 5.2.6 SDR

SDR was applied to the remaining 13 efficient locations with the results summarized in the SDM on Figure 5.11. The SDM shows that locations W27, W33 and W34 dominate by FSD or SSD all other locations. Figure 5.12 shows the mean-variance plot with all the initial well locations partitioned into 3 optimal locations, 10 dominated locations after SDR and 27 dominated locations after MVC.

MVC-SDM indicates that in the target volume the optimal windows to drill the wells are in the quadrants 2 and 3. It is worthy to note that these optimal zones were obtained by using all the geostatistical realizations. SDR ensures that every decision maker with a convex utility curve will agree with the result. The final choice of the well to be drilled depends on the specific reservoir manager's utility function.

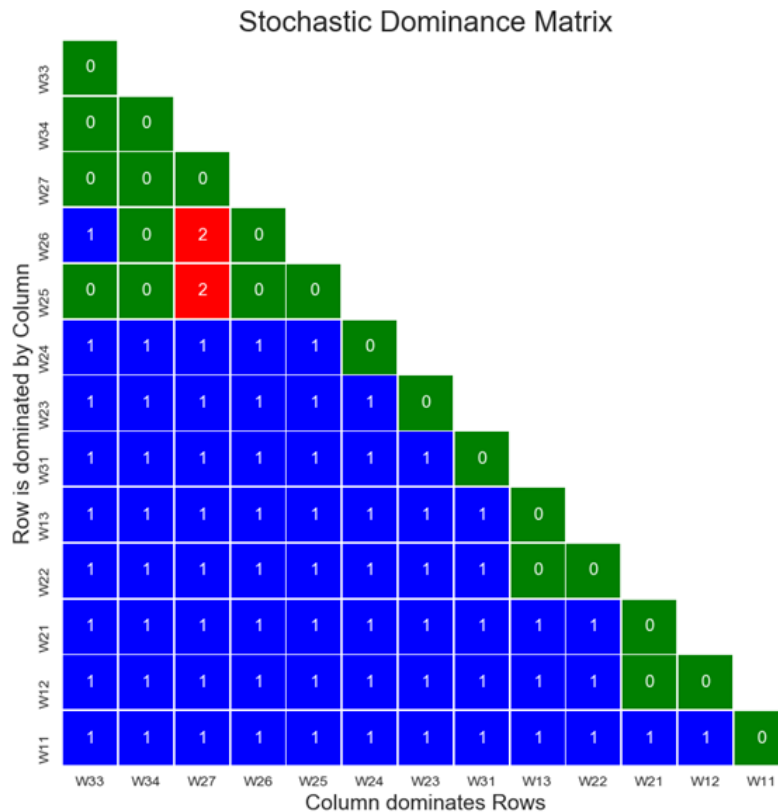


Figure 5.11: Stochastic Dominance Matrix. W33, W34 and W27 dominates by FSD and/or SSD the remaining well locations.

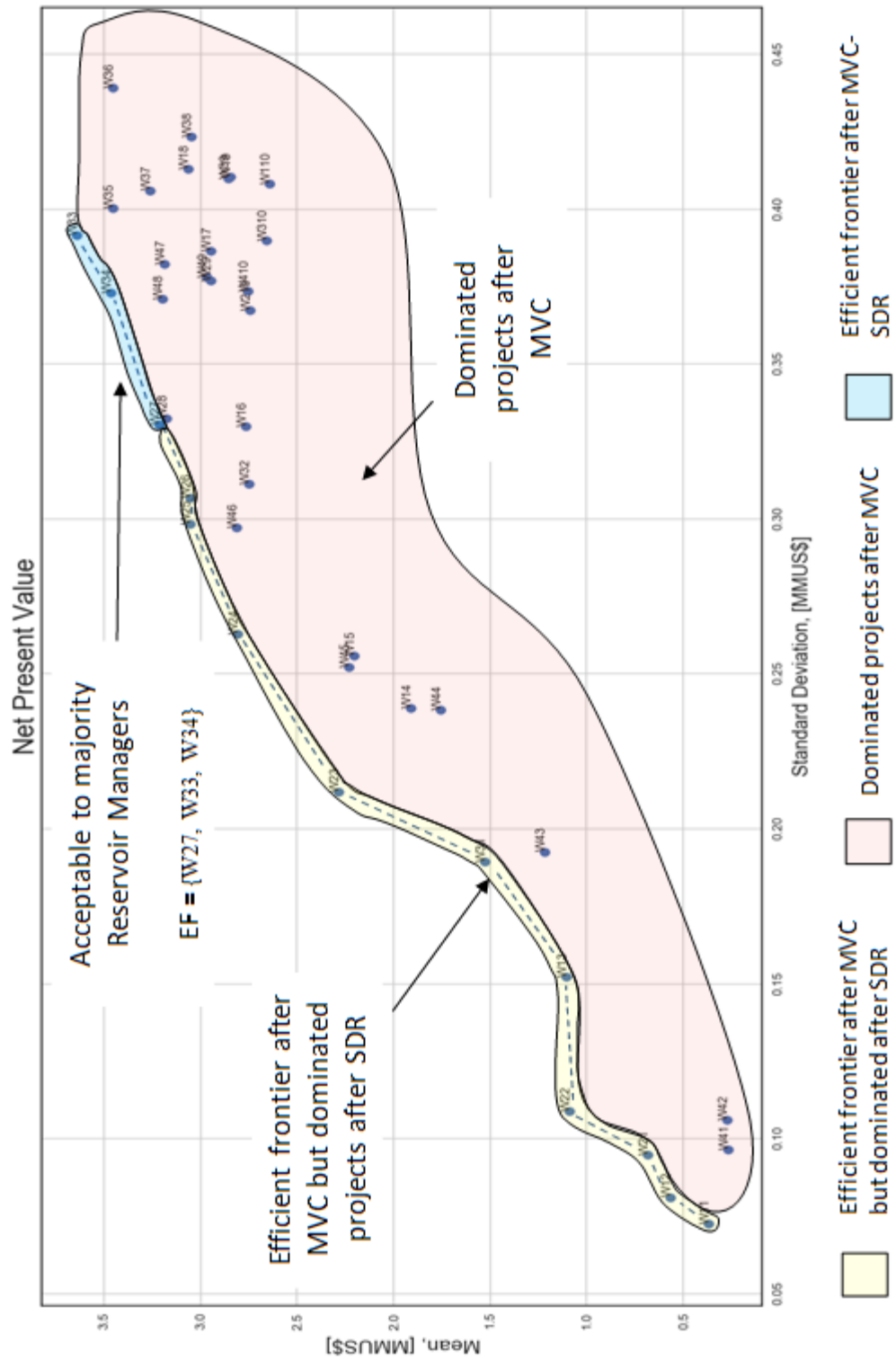


Figure 5.12: Mean-Standard Deviation space. MVC-SDR results on an optimum set with 3 locations. EF = {W33, W34, W27}

### 5.3 Computational Time

40 potential well locations were assessed through the entire set of 100 geostatistical realizations resulting in a total of 4,000 steam-chamber models. The current APDS Python prototype runs the case-study in 13 hours, which is an average time of 11.7 seconds per steam-chamber modeled.

The analysis benefited from the modular design of the algorithm, because the graphs had been already generated for the validation study presented in Section 3.4. Moreover, considering that the standard operation of a SAGD well-pair is around 10 years (Zhao, Law, & Coates, 2003), additional computational time was saved by modeling the steam-chamber only for 15 years.

### 5.4 Discussion

This case study shows that the combined MVC-SDR criterion is viable for decision making under geological uncertainty. It also confirms that APDS is an efficient transfer function for SAGD projects.

In the example, MVC-SDR reduced the initial set from 40 candidate well locations to 3 possible well locations. The final set of locations should be acceptable to risk-averse reservoir managers given the reward-risk trade-off preference assumptions underlying the formulation of the MVC-SDR criterion. The definitive selection of a single location requires knowing the particular reservoir manager's utility function.

The examples presented in this case study and in Section 4.6 make manifest that the MVC-SDR criterion do not always lead to a single project; for that reason, the criterion are primarily applicable to problems with a well-defined finite set of decision options. It is not suitable for problems that use optimization algorithms for searching extremely large combinatorial decision spaces.

The workflow presented in this case study can also be applied to solve other SAGD problems, such as selecting the length and orientation of the producer-injector well-pair or analyzing the producer-injector inter-well distance.

Regarding computational time, the APDS prototype took on average 11.7 seconds to model each steam-chamber without using parallel computing. This processing time appears encouraging to undertake problems with larger finite decision spaces. However, is not yet efficient enough to embed APDS into an closed-loop field optimization work flow (e.g. Echeverria-Ciurri et al. 2012; Wang et al. 2012; Shirangi and Durlofsky 2015). It is recommended to look for substantial efficiency gains in the scale of 1-3 additional orders of magnitude compared to a conventional thermal flow simulator. The obvious first step is to use a compiled language such as C, C++, C# or Fortran and to take advantage of the graphs staying very similar for small changes in well locations.

## 6 Case Study: SAGD Reservoir Characterization with APDS

### 6.1 Introduction

The APDS capability of modeling the steam-chamber propagation, that is the dynamic response of the reservoir to the steam injection, motivates using APDS as a companion tool of methodologies for 4D-seismic data integration in SAGD reservoir characterization.

Time-lapse seismic, or 4D-seismic, is an important source of dynamic data for monitoring heavy-oil reservoirs. It captures changes in the subsurface conditions caused by SAGD operations that are reliable manifestations of the steam-chamber presence. The analysis of seismic attributes recorded at different times might reveal anomalies by the absence or unexpected location of the steam that can be enforced into geostatistical realizations to improve reservoir characterization (Hadavand & Deutsch, 2017).

A practical methodology for enforcing these anomalies in geostatistical reservoir models was proposed by Hadavand & Deutsch (2017). They implemented the technique on a real SAGD project located in the Athabasca region, northeastern Alberta, Canada (Hadavand et al., 2018). Assessing the effect of the geostatistical-anomaly enforcement methodology requires comparing the estimation of the steam-chamber before and after applying the enforcement through all the geostatistical realizations. This procedure cannot be performed with full physics thermal flow simulators due its computational cost. However, APDS is efficient enough to perform this task and serve as a tool for assisting 4D-seismic integration in SAGD reservoir characterization.

Additionally, this case study uses a high resolution realistic geological model that represents the fluvial and estuarine depositional system of the McMurray (Ranger & Gingras, 2010). It exhibits sectors of blocky clean sands with horizontal barriers/baffles of different lengths, and sectors with heterogeneous inclined layers alternating shale and sands. The complexity of the reservoir model illustrates how APDS handles complex geological settings.

## 6.2 Assessment of Geostatistical Anomaly Enforcement with APDS

APDS is used to assess the result of the geostatistical anomaly enforcement methodology. It allows to compare the geometry of the steam-chamber before and after updating the geostatistical realizations with 4D-seismic information. Improvements in the SAGD reservoir characterization is shown by local improvements in the estimation of the steam-chamber propagation (Hadavand et al., 2018). The result of the validation procedure is summarized in a probability of steam-chamber presence volume after the 4D-seismic integration. This probability volume carries quantitative information about the evolution of the steam-chamber that is valuable to support SAGD reservoir management decisions.

### 6.2.1 Geological Model

The following analysis requires two sets of geostatistical realizations or geological models. An initial set of realizations that is conditioned only to static-well data including core and logs; and an updated set of realizations that additionally considers the dynamic information obtained from 4D-seismic data. In this chapter, the former set of geostatistical realizations is called the pre-enforced model and the latter the post-enforced model.

This case study was performed on a SAGD well-pair reservoir volume (i.e. pre-enforced and post-enforced geological models) prepared for a drainage area located in the Athabasca region, northeastern Alberta, Canada. The formation of economic interest is the McMurray formation. Figure 6.1 shows one pre-enforced realization of the vertical permeability for the entire drainage area indicating the extracted volume.

The geostatistical workflow to generate these reservoir models was set-up by several research assistants at the Centre for Computational Geostatistics (CCG) at the University of Alberta, Canada, particularly Hadavand, M., Silva, D. and Pinto, F. Geostatistical techniques recently introduced to the practice of geomodeling were applied. Hierarchical Truncated PluriGaussian (HTPG) (Silva, D., 2018) for modeling categorical variables and Projection Pursuit Multivariate Transform (PPMT) (Barnett et al., 2014) with Sequential Gaussian Simulation (SGS) for modeling the continuous variables. The Anomaly Recognition Tool (ART) (Hadavand, 2017) was used to update the set of geostatistical

realizations. The workflow is described in detail in Hadavand et al. (2018) and Hadavand & Deutsch (2017) and the geological setting of the McMurray formation is found in Baniak & Kingsmith (2018), Hassanpour (2013) and Moreton & Carter (2015).

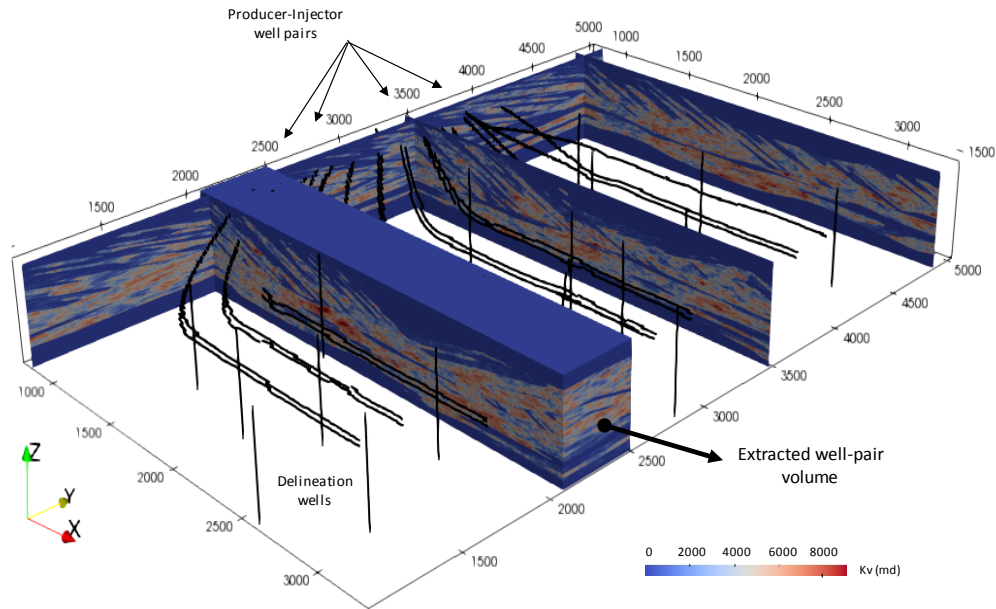


Figure 6.1: Reservoir realization of the pre-enforced geological model for the entire drainage area. The figure indicates the well-pair volume extracted for this case study.

### 6.2.1.1 Pre-enforced Geological Model

The extracted geological models (pre-enforced and post-enforced) consist of 50 geostatistical realizations of one SAGD well pair volume. Each realization has 1.78 million cells: 344 x 29 x 178 cells in the x, y and z directions, respectively. The grid blocks are 5 m x 5 m x 0.5 m in the x, y and z directions, respectively.

Figure 6.2 shows vertical and horizontal cross-sections of one extracted pre-enforced reservoir realization. The image has a data aspect ratio between the x-axis to y-axis and x-axis to z-axis of 5 in both cases. Unless otherwise specified, all figures in this chapter have the same aspect ratio. The numerical model exhibits a pattern commonly found in Canadian oil sand operations, there is a sand-rich interval at the bottom of the formation and a sequence of interlayered sand-shale/siltstone and abandoned mud channels at the top (Yi Su, Wang, & Gates, 2017). This interlayered sequences of sand and shale are common in

point bar depositional environments. They are denoted as Inclined Heterolithic Strata (IHS) (Moreton & Carter, 2015) and have a major effect in the steam-chamber propagation. IHS impacts negatively the economic performance of SAGD projects (Y. Su, Wang, & Gates, 2013; Yi Su et al., 2017).

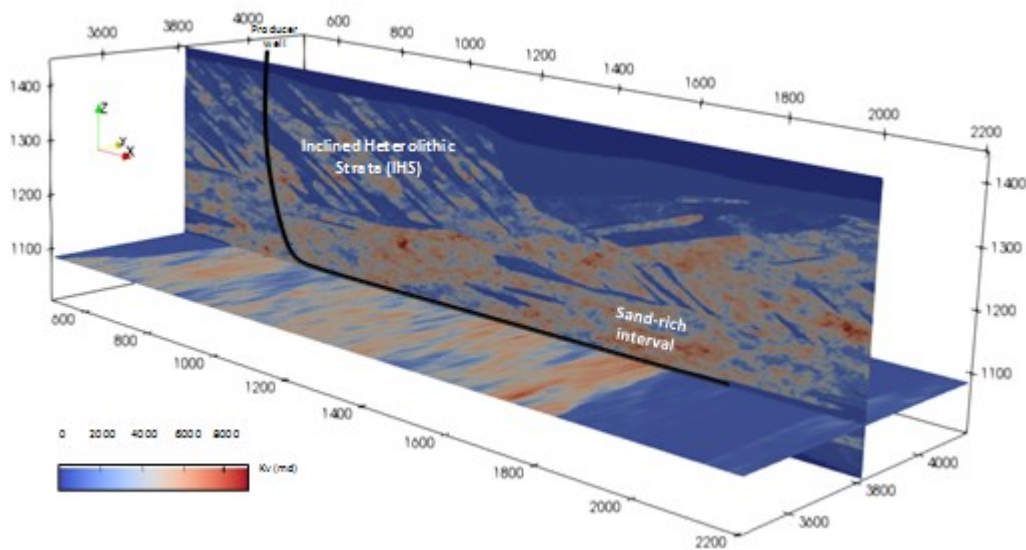


Figure 6.2: Reservoir realization of the pre-enforced geological model for the extracted well-pair volume used in the case study.

Figure 6.3 shows three vertical cross-sections along the axis of the SAGD well-pair. The top image (Figure 6.3.a) is a clean cross-section showing only the producer-injector well pair trajectory. It shows the location of low permeability rocks or non-net reservoir (i.e. shales) represented by solid blue areas, and net-reservoir. The non-net rocks are barriers to the flow of steam and bitumen.

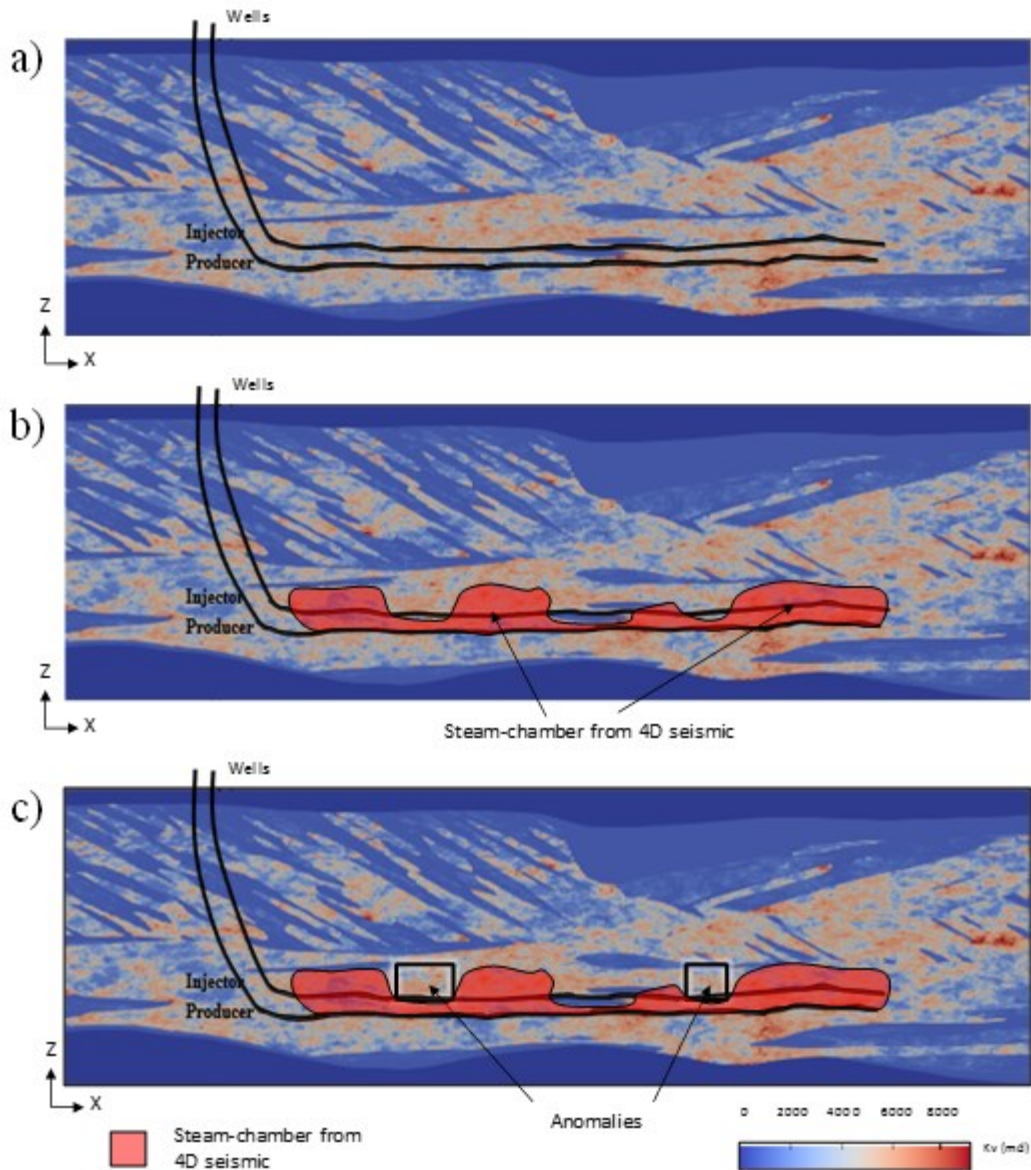


Figure 6.3: a) Vertical cross-section of pre-enforced geological model showing location of well-pair and net-reservoir and non-net reservoir distribution. b) Sketch of the steam-chamber obtained from 4D-seismic. c) The absence of the steam-chamber in net-reservoir sections near the wells represent potential anomalies.

Figure 6.3.b sketches a steam-chamber inferred from 4D-seismic. In most areas along the well-pair axis the steam-chamber has a good conformance with the distribution of net and non-net reservoirs. However, there are some areas in which the steam-chamber has a poor development even though the pre-enforced reservoir model has predominantly net-reservoir. These areas do not seem to agree with the dynamic information carried by the 4D-seismic and thus they are potential reservoir anomalies (Figure 6.3.c) according to the

geostatistical anomaly enforcement methodology (Hadavand & Deutsch, 2017). The work presented here is based on Hadavand & Deutsch (2017) and is not based on the actual 4D-seismic that was not accessible to the author.

#### 6.2.1.2 Post-enforced Geological Model

Geostatistical Anomaly Enforcement proposes two main types of anomalies: positive (Type +1) and negative (Type -1). Positive anomalies caused by flow conduits locally makes the steam-chamber growing faster than expected. Negative anomalies caused by barriers or baffles locally hampers the steam-chamber (Hadavand et al., 2018). Accordingly, the potential reservoir anomalies depicted in Figure 6.3.c are Type -1.

Not all local anomalies reflect changes in fluid saturations and reservoir properties, some of them are caused by operational steam-injection strategies, the well-pair trajectory or the well-pair completion design, among other factors. For that reason, the identification and final decision about the anomalies that should be enforced, called reservoir anomalies, relies on professional judgment (Hadavand et al., 2018; Hadavand & Deutsch, 2017).

The anomalies showed on Figure 6.3.c were judged as reservoir anomalies, and therefore the pre-enforced geological model was updated with this dynamic information. Figures 6.4 and 6.5 shows two updated realizations. Both, pre-enforced and post-enforced realizations are depicted to facilitate the comparison. Note the presence of enforced barriers/baffles in the updated reservoir realizations.

#### 6.2.2 Assessing SAGD Reservoir Characterization Improvement with APDS

The evidence of an improvement in reservoir characterization is a better local match in the areas with enforced anomalies between the steam-chamber obtained from 4D-seismic and the modeled steam-chambers over all the post-enforced geostatistical realizations. A fidelity analysis based on the effective directional permeability demonstrates improvements in the anomaly reproduction (Hadavand & Deutsch, 2017). However, the consequences or effects of the enforced features (i.e. barriers or conduits) should be evaluated by a direct comparison of the steam-chamber geometry.

As previously discussed, modeling the steam-chambers using conventional thermal flow simulation requires significant computational cost especially with many realizations. On the other hand, APDS can efficiently model the steam-chamber propagation on the updated geostatistical realizations to assess the quality of the 4D-seismic integration in the SAGD reservoir characterization.

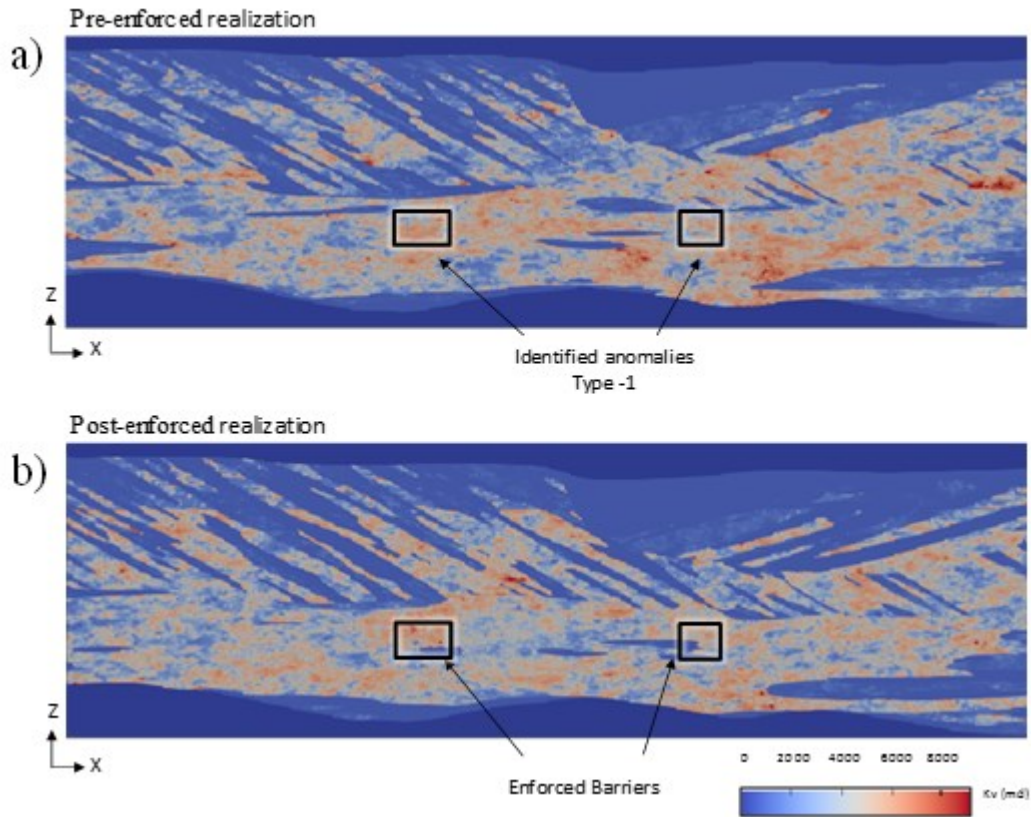


Figure 6.4: Vertical cross-section of: a) Pre-enforced realization showing location of anomalies Type -1. b) Post-enforced realization showing enforced barriers.

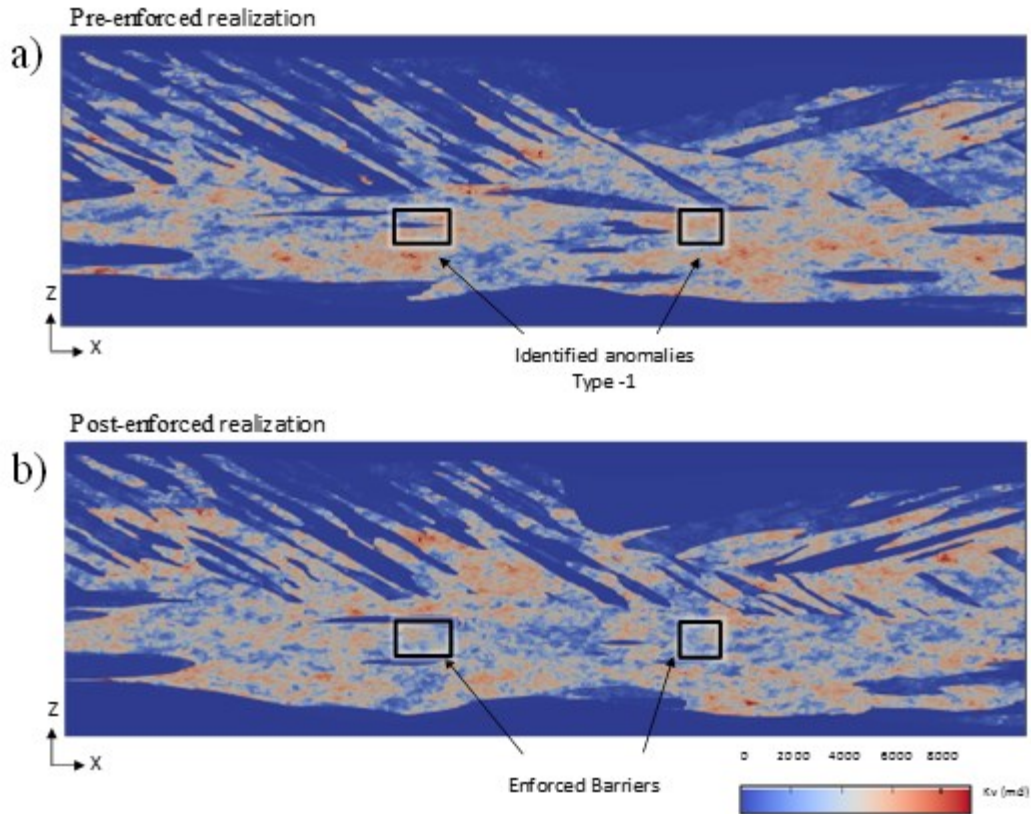


Figure 6.5: Vertical cross-section of: a) Pre-enforced realization showing location of anomalies Type -1. b) Post-enforced realization showing enforced barriers.

Figure 6.6 illustrates the idea with three vertical cross-sections along the axis of the well-pair. Here, net reservoir is represented by the lighter color and non-net reservoir is the darker color. Figures 6.6.a and 6.6.b sketch the steam-chambers obtained from the 4D-seismic and APDS, respectively. Since the steam-chambers exhibit a good local agreement, especially in the areas influenced by the enforced barriers, it is inferred that the reservoir characterization was improved because it honors the 4D-seismic dynamic information.

A local disagreement between the steam-chambers would call to reconsider the location or the existence of that particular anomaly. In such cases, the feedback provide by APDS not only supplements the geostatistical anomaly enforcement methodology, but actively helps to improve reservoir characterization.

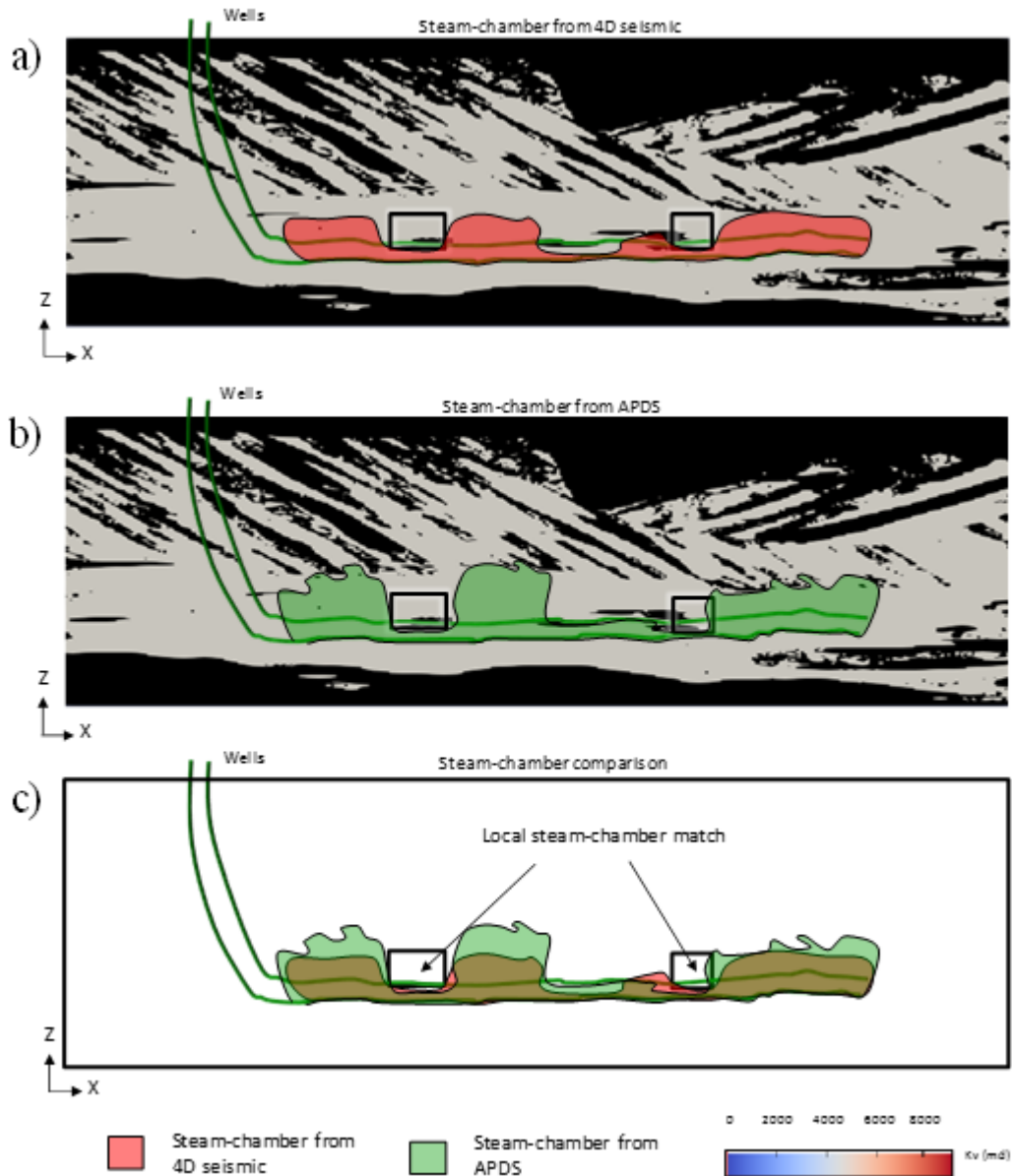


Figure 6.6: Vertical cross-section of post-enforced realization showing: a) 4D-seismic steam-chamber and anomalies Type -1, b) APDS steam-chamber and anomalies Type -1, and c) Comparison of the steam-chambers.

Figure 6.7 shows the 3D-steam-chambers modeled with APDS for a 3 year period on six post-enforced geostatistical realizations. They show the capacity of APDS to handle complex geometries in 3D. Note the presence of cold pockets (volumes where the steam has not reached) caused by reservoir heterogeneities that might deteriorate the SAGD project economic performance. Figure 6.8 shows vertical cross-sections along the axis of the well-pair of each post-enforced realization to ease the comparison with the 4D-seismic

steam-chamber (dashed line). The arrows indicate locations of the enforced anomalies. The effect of the dynamic data integration is seen in all the steam-chambers, with the only exception of the left anomaly in the realization #2. The steam-chamber propagation was deterred by the enforced anomalies resulting in good local matches with the 4D-seismic steam-chamber, which demonstrates the improvement in reservoir characterization.

It is impractical to individually compare each realization. The information about the APDS steam-chamber presence in the post-enforced realizations can be embedded in a steam-chamber probability volume. When this probability volume is compared to the 4D-seismic steam-chamber, reservoir volumes influenced by enforced barriers should have low probability of steam-chamber presence. Conversely, reservoir volumes with good petrophysical properties should have a high probability of steam-chamber presence.

Figure 6.9 shows a vertical cross-section along the axis of the SAGD well-pair of the steam-chamber probability volume after 3 years calculated using the post-enforced geological model. It has low probability of steam-chamber development in zones influenced by the enforced barriers and high probability of steam-chamber development in good quality reservoir zones. Hence, after considering all the post-enforced geostatistical realizations, APDS helps to demonstrate that the 4D-seismic anomaly enforcement methodology improves SAGD reservoir characterization.

SAGD reservoir decisions, such as: optimization of steam-injection strategies (Gates, Kenny, Hernandez-Hdez, & Bunio, 2007; Li, Mamora, Li, & Qui, 2011) , installation of flow control devices (Banerjee & Hascakir, 2018; Burke & Ghazar, 2018) or targeting bypassed oil with well workovers or sidetracks (Lumley & Behrens, 1998) benefits from an improved geological model.

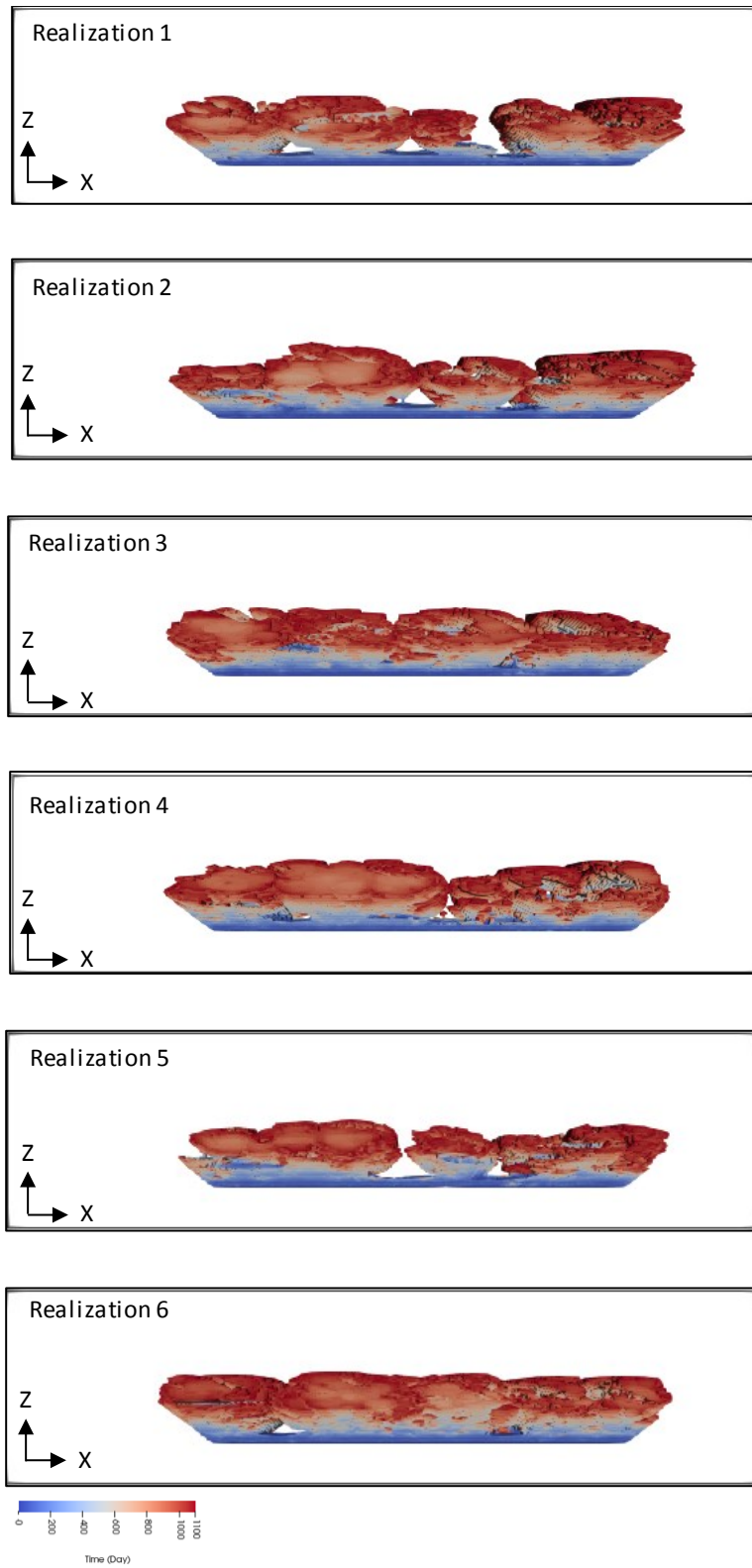


Figure 6.7: 3D-steam-chambers modeled with APDS for a 3 year period on six post-enforced geostatistical realizations.

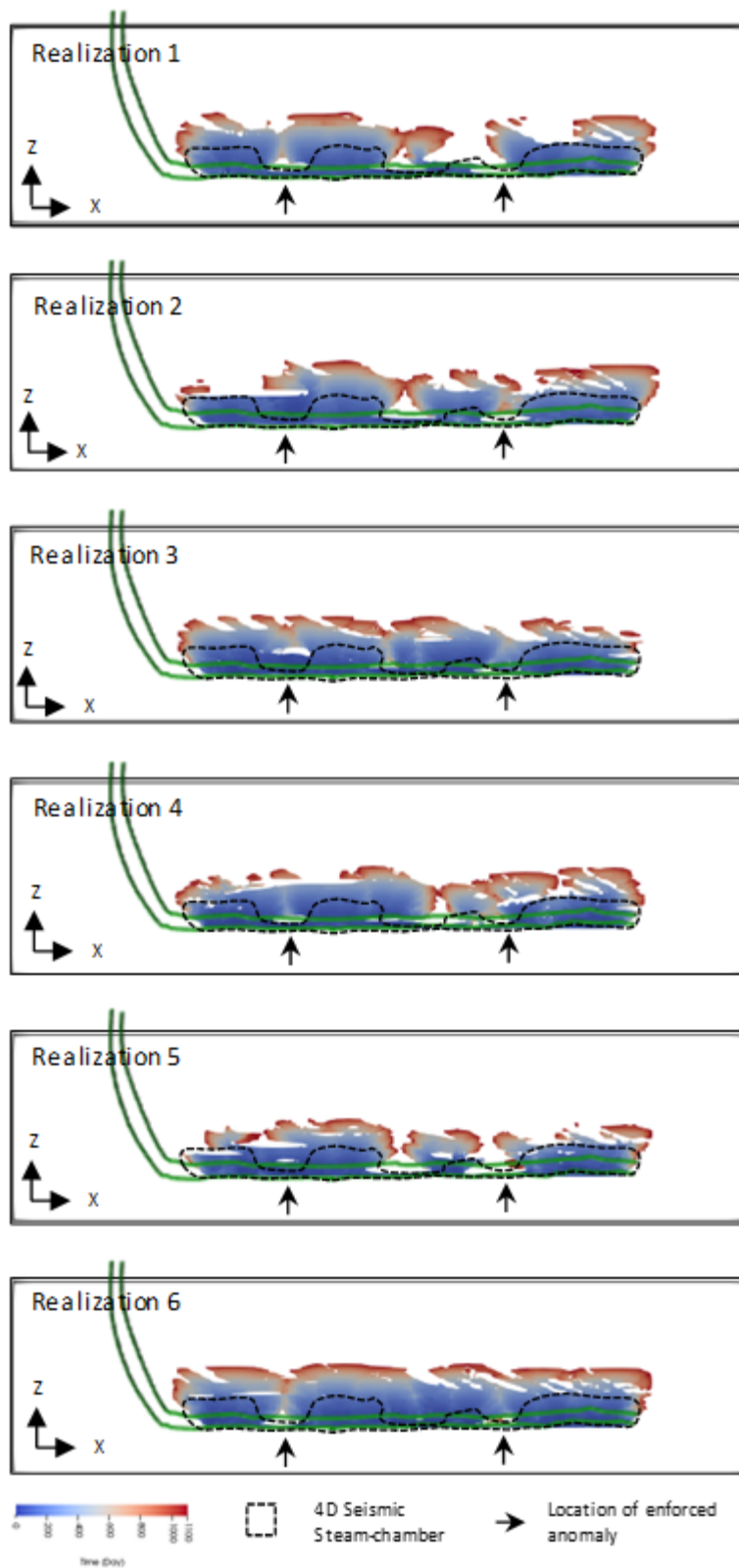


Figure 6.8: Vertical cross-sections along the axis of the well-pair showing the steam-chamber modeled with APDS for 3 years on 6 post-enforced realizations.

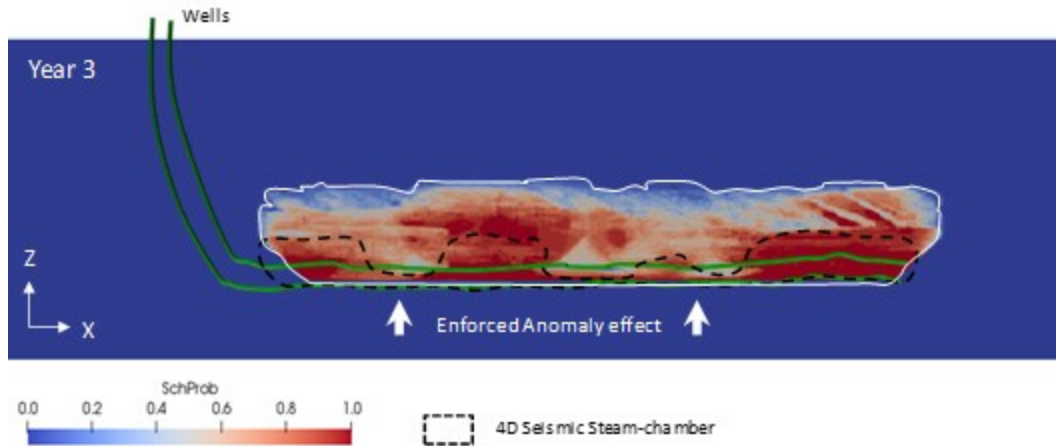


Figure 6.9: Probability of steam-chamber presence after 3 years.

APDS has the capability of modeling the steam-chamber in an almost continuous timeline. This makes it is easy to generate images of the probability of steam-chamber presence at any time of interest. For instance, Figure 6.10 condenses information about the first 5 years of steam-chamber propagation and also includes the tenth year. Note that APDS shows that the negative impact of the enforced barriers in the steam-chamber expansion is stronger at earlier times, and the impact diminishes as time advances.

Nowadays is common practice to monitor the SAGD steam-chamber with periodical seismic surveys. For instance, in the 4D-seismic integration field-case study of the Surmont project located in the Athabasca region, northeastern Alberta, Canada, (Hadavand et al., 2018) reported eight seismic surveys, one baseline and seven monitors. The resulting set of seven incremental 4D-seismic data and APDS would almost certainly enhance the assimilation of the dynamic data in the reservoir characterization workflow. Even more, if a good agreement between the initial 4D-seismic data sets and APDS is demonstrated, there is a venue for optimizing the frequency of the seismic survey recording. The economic impact would be a reduction of the overall SAGD project operational cost.

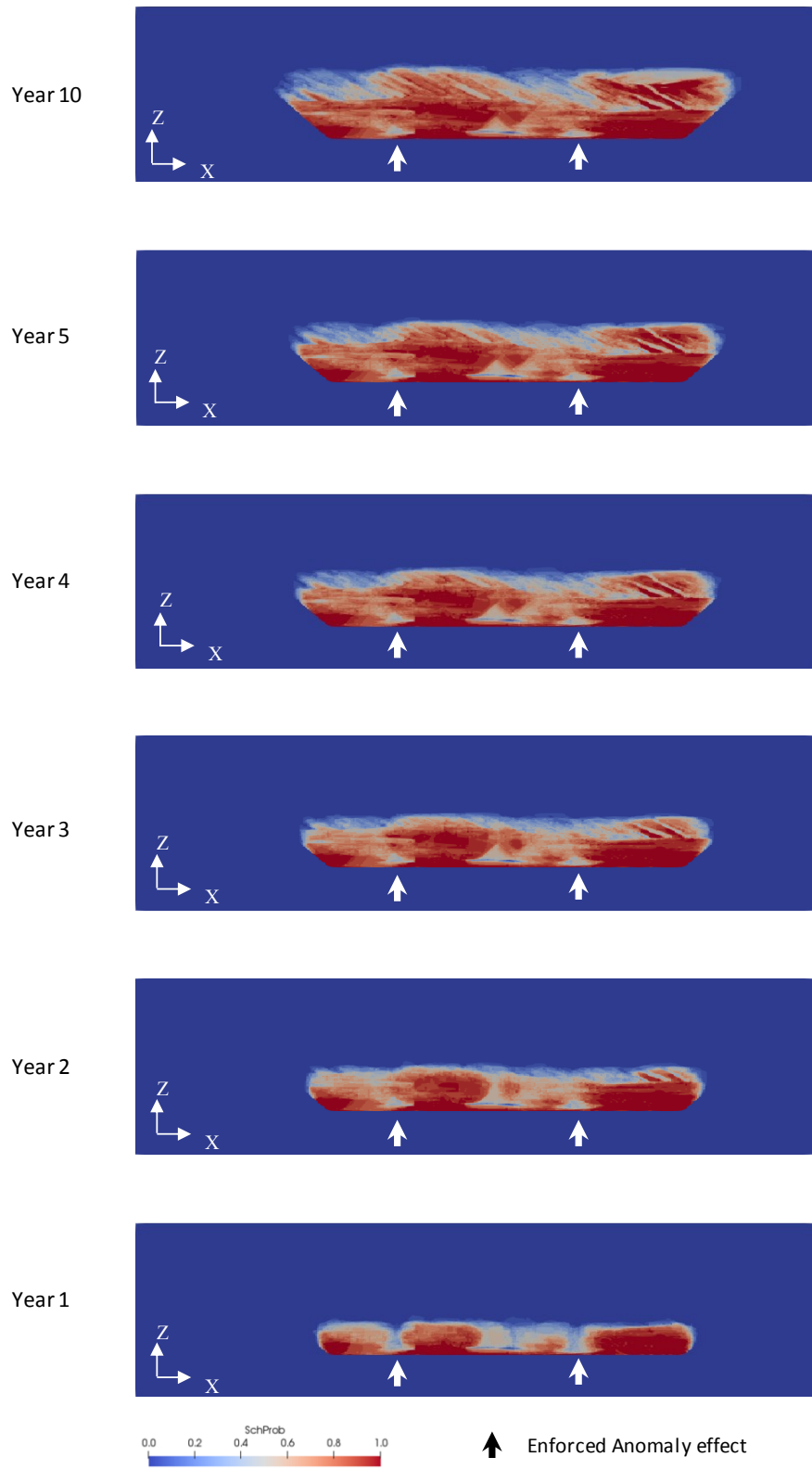


Figure 6.10: Probability of steam-chamber presence modeled at six different years.

### 6.2.3 APDS Modeling of Steam-Chamber in Point Bar Systems

The high resolution geological model illustrated in Figure 6.1 is representative of several commercial Canadian SAGD operations exploiting the McMurray Formation (Yi Su et al., 2017). Their distinctive characteristic is an IHS interval deposited on top of a blocky sand zone (Moreton & Carter, 2015). IHS are shallow-dipping heterogeneous point bar deposits whose strata show original depositional dip (Labrecque, Jensen, Hubbard, & Nielsen, 2011). The heterogeneity takes the form of alternating sand and shale layers as shown in the Figure 6.11. Observe that the sandwich-like pattern is very evident in all the vertical cross-sections presented in this case study.

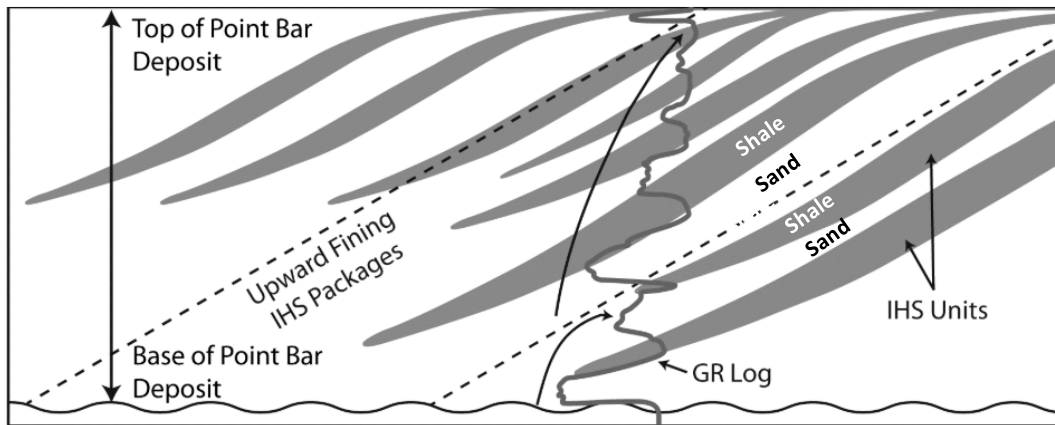


Figure 6.11: Upward-fining HIS packages with hypothetical gamma ray log (Modified after Labrecque et al. (2011)).

Extensive conventional thermal flow simulation (Y. Su et al., 2013; Yi Su et al., 2017) demonstrates that IHS have a pivotal effect in the shape of the steam-chambers which ultimately impacts negatively the thermal efficiency and well utilization in SAGD operations. Thus, it is worthy to understand qualitatively the APDS ability for modeling the steam-chamber in point bar systems.

Yi Su et al. describes the expected steam-chamber growing pattern in a point bar deposit obtained from several thermal flow simulations (Yi Su et al., 2017). Figure 6.12 shows a vertical cross-section of one of the reservoir models they used. Note the similarities with the top image in Figure 6.13. Initially, the steam-chamber grows relatively uniformly in the lower clean sand interval, although it might be locally affected by barriers. After that,

the steam penetrates the IHS in the form of ‘fingers’. The combined effect leads to amorphous steam-chambers. The expansion rate of the steam-chamber is faster in the blocky sand than in IHS. The authors reported that their simulation results are consistent with field observations in the Underground Test Facility (UTF) project Phase B pilot.

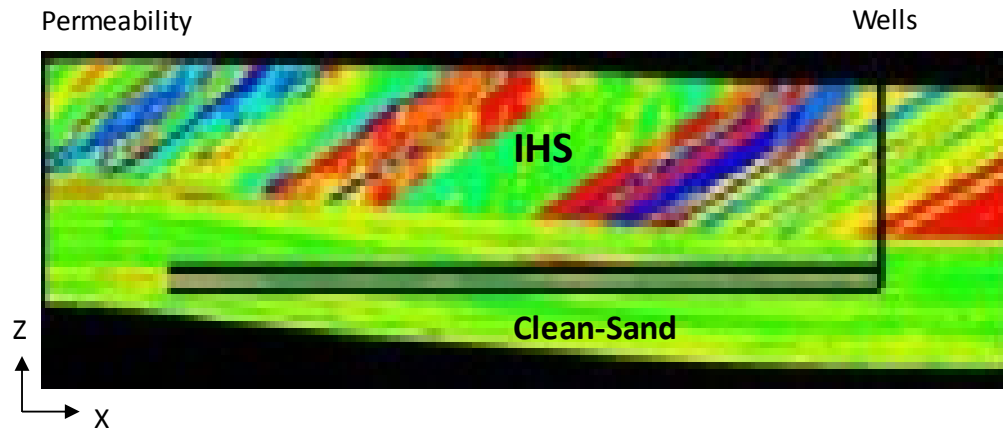


Figure 6.12: Vertical cross-section of one reservoir model used by Yi Su et al. (2017) in the thermal flow simulations. Permeability scale was not presented in original figure. (Modified after Yi Su et al. (2017)).

Figures 6.13 and 6.14 show the propagation of the APDS steam-chamber every six months for 5 years on a vertical cross-section along the axis of the well-pair. During the first 2 years, the overall steam-chamber expansion is uniform. Locally the propagation is hampered by two horizontal barriers located near the wells. Around the second year, the steam reaches the top of the basal clean zone and starts moving up like ‘fingers’ into the IHS. By the end of the fifth year, the steam had penetrated some distance into most IHS sand layers, but some of them, isolated by shales, are by passed and remain as cold spots. By visually comparing the height of the steam-chamber between years 2 and 5, it is possible to infer that the rate of expansion was faster in the clean basal zone than in the IHS.

The above discussion on Figures 6.11 to 6.14 supports concluding that APDS generates steam-chambers that compare satisfactorily to the results obtained from conventional thermal flow simulation in complex geological settings.

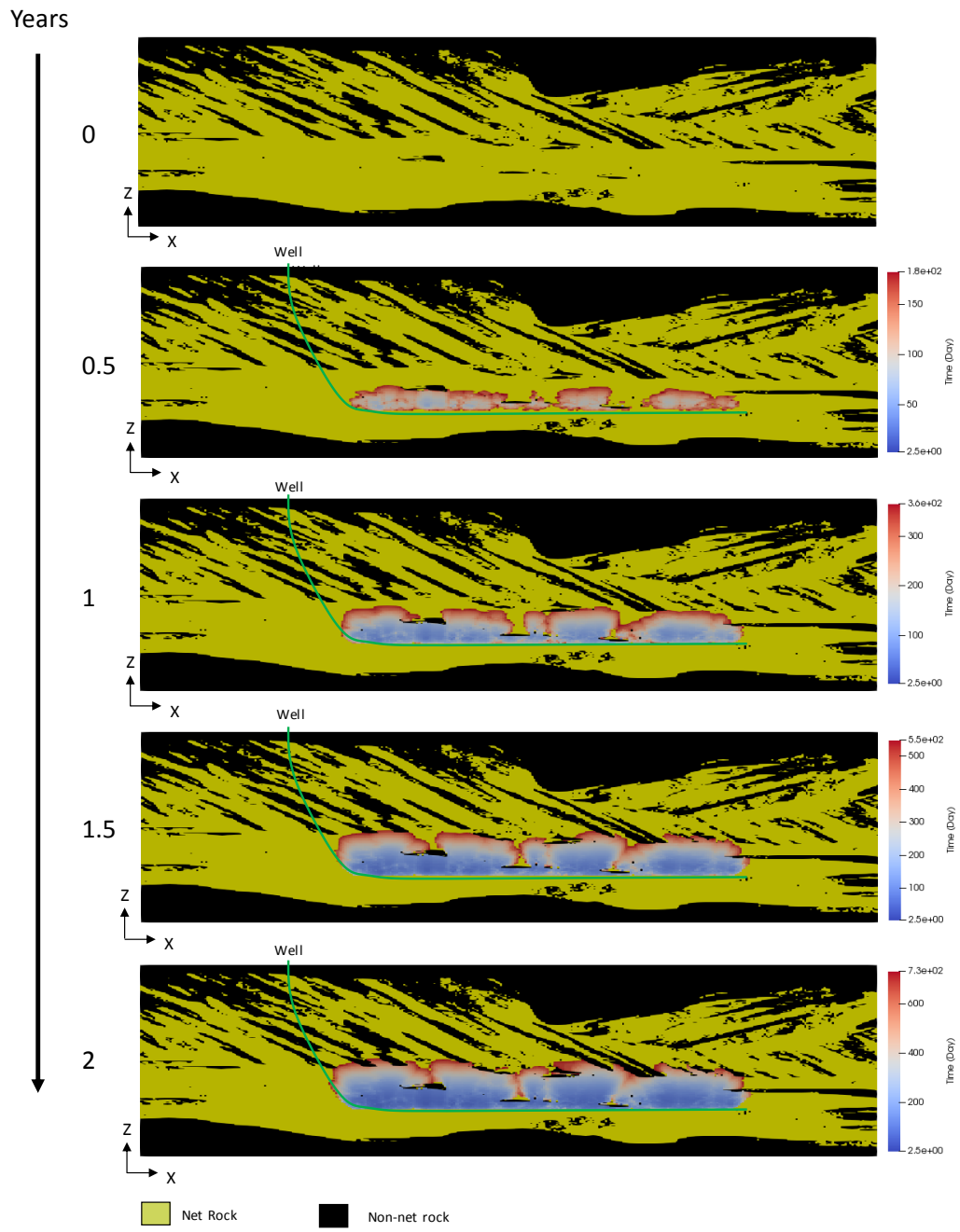


Figure 6.13: Vertical cross-section of post-enforced realization showing the steam-chamber every 6 months. Years 1 and 2.



## 6.2.4 Computational Time

Running this case-study for 50 post-enforced realizations took 2.8 hours, that is, an average of 3.4 minutes per steam-chamber modeled. Steam-chambers were modeled for 15 years. The total computational time was allocated 77 % building the graphs and 23% modeling the steam-chambers. The result indicates that when looking for efficiency gains, the APDS graph generator module is a candidate for parallel computing.

## 6.3 Discussion

This case study demonstrates how 4D-Seismic Anomaly Enforcement methodology and APDS complement each other to improve geostatistical SAGD reservoir modeling. The updated models are expected to improve SAGD reservoir decisions related to optimization of steam-injection strategies, installation of flow control devices and/or execution of well workovers or sidetracks among others. Better informed reservoir manager decisions should increase the profitability of SAGD operations.

The probability of steam-chamber presence volume is introduced. It condenses in one single image the information about the steam-chamber location of an entire set of geostatistical realizations. APDS easily captures in a sequence of images the steam-chamber propagation at any time period of interest. An obvious choice is to match these probability volumes with the recording time of seismic monitoring surveys to improve the assimilation of dynamic data in the SAGD reservoir characterization. In this line of reasoning, APDS might also help to quantify the value of information (VOI) of the seismic surveys. Reservoir managers could optimize the number and frequency of seismic data acquisition, resulting in a reduction of the projects operational costs.

The APDS ability to predict the steam-chamber location in a complex point bar depositional system is discussed. The qualitative analysis is encouraging regarding the APDS outputs, because the general expected expansion steam-chamber pattern found by other researches (Y. Su et al., 2013; Yi Su et al., 2017) using conventional thermal flow simulation is correctly reproduced. As a future work, it is desirable running the

conventional simulator in the post-enforced geological model to perform a precise quantitative comparison.

Regarding computational time, the APDS prototype takes an average of 3 minutes to model each steam-chamber without using parallel computing. Around 77 % of the time is consumed by the graph generator module. Using parallel computing for this module is an easy to implement option to reduce computational time in a few factors. However, as mentioned in Section 5.4, to obtain substantial efficiency gains measurable in terms of orders of magnitude, the initial approach is to re-engineer APDS using a compiled programming language.

## 7 Summary of Contributions and Future Work

This chapter summarizes the main contributions of the dissertation. It discusses strengths and limitations of the APDS algorithm and the proposed MVC-SDR decision-making criterion. Ideas for future work are provided to expand this research.

### 7.1 Summary of Contributions

At the heart of petroleum reservoir management (PRM) resides the challenge of selecting the best project from a group of feasible candidates in the presence of geological uncertainty. The challenge is particularly relevant in low oil price investment environments where many upstream projects are economically marginal and must be optimized. Companies are now more cautious. Investors are aware that they should consider not only the rewards of the projects, but also their risks. For these reasons, the selection of the projects to be implemented in the field should consider the geological risk and the capacity of the companies to tolerate it.

This thesis advocates for decision-making workflows in reservoir management that actively manage the geological uncertainty. That is, the geological uncertainty is transferred to probability distributions of the response variable, and the decision criteria that governs the final selection considers the decision maker's preferences toward the project's return-risk trade-off.

In the context of the SAGD recovery technology, this thesis contributes to improve reservoir management decision-making practices in several ways. 1) The formulation, implementation and validation of a graph-based simplified physics simulator named APDS, for efficiently transferring the geological uncertainty into steam-chamber evolution paths that can directly support SAGD reservoir management or be converted to a monetary response variable to input decision-making workflows, 2) the introduction and validation of a practical decision-making criterion consistent with the utility theory framework that combines MVC-SDR for active geological risk management, and 3) the thesis demonstrates that APDS can complement a 4D-seismic integration methodology to

improve reservoir characterization. Reservoir manager decisions supported on a better geological model should increase the profitability of SAGD operations.

### 7.1.1 APDS Formulation

SAGD is a thermal recovery process to produce bitumen from oil-sands. In this technology, steam is injected in the reservoir to reduce the viscosity of the bitumen that drains by gravity to a production well. In the subsurface, a steam-chamber evolves and grows with time. Understanding the geometry and rate of growth of the steam-chamber is necessary to manage an economically successful SAGD project; for that reason, Chapter 2 of this thesis formulates a graph-based algorithm called APDS to model the steam-chamber evolution. It uses graph theory, simplified porous media flow equations, heat transfer concepts and ideas from discrete simulation.

Even though graph theory has been used since 1956 (Fatt, 1956) to model the flow of fluids in porous media at pore-scale to predict macroscopic transport properties (Oren et al., 1998), the use of graphs proposed in this dissertation at the macroscopic scale of the cells of the numerical model to predict a large scale reservoir response such as the steam-chamber in SAGD is a novel contribution to the technical literature.

Chapter 2 formulates APDS, presents the pseudocode of the algorithm, and a step-wise application example that demonstrates how the steam-chamber evolution is predicted in homogeneous and heterogeneous reservoirs. APDS is intended to be mathematically simple and yet to have reasonably good predictive capabilities; for that reason, it will not match the sophistication and complexity of a conventional thermal flow simulator. However, APDS formulation is flexible enough to allow adjusting the complexity of the algorithm to the problem at hand and the timeframe available to provide a solution. Section 7.3 in future work, later in this chapter, offers specific ideas to expand the physical complexity modeled in APDS.

Finally, Chapter 2 discusses the use of APDS in SAGD projects to support operational strategies, geomechanical analysis, well-pair location decision making and 4D-seismic integration. The case studies in Chapters 5 and 6 successfully demonstrate the last two applications.

### 7.1.2 APDS Implementation and Validation

Being mathematically sound and based on well-established engineering principles of flow in porous media, material balance and heat-transfer does not guarantee a practical, successful or immediate implementation. Sometimes, there is a time gap between the formulation of an algorithm and its implementation and/or adoption. To mention one example, the principles of streamline simulation were established in 1934 (Muskat & Wyckoff, 1934), but according to Batycky, Blunt, & Thiele (1997) the technology only resurfaces to the reservoir simulation practice in the nineties after the introduction of the practical concept of time of flight along the streamlines (Pollock, 1988).

In the case of APDS, its successful implementation requires assumptions and practical simplifications that must be compatible with the graph-based structure of the algorithm. The implementation presented in Chapter 3 is considered a contribution to the practice of SAGD reservoir simulation on its own. In the future, starting from the same APDS formulation presented in this thesis, other researches might suggest different assumptions and/or simplifications to implement the algorithm.

A case study performed with a realistic multi-realization geological model validates the predictive capabilities of APDS. Visual and numerical comparisons with the results obtained from a conventional full physics thermal flow simulation are satisfactory. APDS was 3 orders of magnitude faster than the conventional simulator to model the steam-chamber expansion and to provide predictions of reservoir response. The cost was a reduction in the precision of the results. These results favor using APDS to support SAGD decision making workflows in the presence of geological uncertainty.

Finally, Chapter 3 discusses the APDS prototype written in the Python programming language. The structure of the prototype with 3 modules (graph generator, steam-chamber generator and post-processing) is convenient to further reduce computational running time by parallelizing APDS.

### 7.1.3 Decision-Making Criterion for Active Management of Geological Uncertainty

Reservoir managers want to select and implement projects that add value. The selection is difficult because project performance depends on the geological uncertainty. The geological uncertainty can be quantified with geostatistical methods, but this information is not often used because the decision-making models are not always formulated to exploit the geological risk.

Chapter 4 of this dissertation claims that for PRM, the decision process must be guided by a criterion tuned to the risk-reward preferences of the companies. For that reason, a decision-making criterion consistent with the utility theory framework is formulated and introduced. The proposed criterion ranks the projects to be implemented by combining MVC and SDR optimality criteria. The main advantages of the MVC-SDR model are that (1) it does not rely on a specific utility function and (2) the results are reasonable to all risk-averse reservoir managers. The shortcoming is a reduced ability to rank projects with very similar CDFs.

This thesis presents two examples that demonstrate MVC-SDR as a viable criterion for decision making under geological uncertainty. The first example in Chapter 4 considers the problem of selecting one SAGD well-pad to be drilled from a set of several possible options. It is designed intentionally simple with the goal of explaining the MVC-SDR methodology step by step. The second example in Chapter 5 considers the problem of finding the best vertical location for a SAGD well-pair project in a target volume. This example uses a realistic geological model and showed that APDS was computationally efficient enough to model 4000 steam-chambers in 13 hours. This is a reasonable computational time for supporting problems that require transferring the geological uncertainty over a well-defined finite set of decision options.

The examples show that the MVC-SDR criterion do not always lead to a single project; for that reason, it not suitable for problems that use optimization algorithms for searching extremely large combinatorial decision spaces. MVC-SDR will not always help reservoir managers to find a single optimum project, but they can reduce considerably the number

of alternatives from which the final decision must be made. The final choice depends on the specific reservoir manager's utility function.

#### 7.1.4 Assisting 4D-Seismic Integration in Reservoir Characterization

4D-seismic is an important source of dynamic data for monitoring heavy-oil reservoirs. It provides images of the SAGD steam-chamber at different times that might reveal anomalies caused by barriers/baffles and conduits. These anomalies can be enforced into geostatistical realizations using the practical integration of 4D-seismic methodology proposed by Hadavand & Deutsch (2017).

Chapter 6 demonstrates with a realistic case study, that after the geostatistical anomaly enforcement, APDS can efficiently model the steam-chamber propagation on the updated geostatistical realizations to assess the quality of the 4D-seismic integration in the SAGD reservoir characterization. In fact, APDS not only supplements the geostatistical anomaly enforcement methodology, but it actively helps to improve reservoir characterization by providing valuable feedback about the location of the anomalies. The updated models are expected to improve SAGD reservoir decisions related to optimization of steam-injection strategies, installation of flow control devices and/or execution of well workovers or sidetracks among others.

Chapter 6 also introduces the probability of steam-chamber presence volume. This practical contribution permits to condensate in one single image the information about the steam-chamber location of an entire set of geostatistical realizations. The APDS capability of modeling the steam-chamber in an almost continuous timeline makes it is easy to generate probability volumes at any time of interest. They can be synchronized with the recording time of seismic monitoring surveys to improve the assimilation of dynamic data in the reservoir characterization.

## 7.2 Limitations and Future Work

Reflections on the limitations of APDS and MVC-SDR are included in the closing section of each chapter. This final section recalls some of those limitations, discusses new ones, but mainly focusses on offering specific ideas to overcome them.

Future works that might improve the methods and algorithms developed on this thesis or build upon the results obtained include:

- Improve current APDS outputs or develop new ones. For instances, production oil forecast and steam-oil-ratio forecast.
- Improve or expand the APDS physical complexity to offer higher flexibility without affecting the computational efficiency. For example: include relative permeabilities curves, improve handling of high-water saturation cells or develop a new two-phase APDS algorithm.
- Integrate APDS to well-established methodologies to improve reservoir characterization, such as the Ensemble Kalman Filter (EnKF).
- Couple APDS with models that describe aspects of the SAGD physics not considered in the ranking function, for example, the steam properties variations along the injector wellbore trajectory.
- Develop additional case studies applying APDS to larger or more complex SAGD problems. For example, study the optimization of SAGD-Pads placement.
- Improve APDS computational efficiency
- Regarding the decision-making model: calibrate the decision-maker's position on risks coming from the geological uncertainty and use APDS to determine the value of information (VOI) of monitoring seismic surveys.

These future work ideas are described in the next sections.

## 7.2.1 Production Oil Forecast

APDS combines the sequence of graph nodes ordered by time with their volumetric information to approximate the cumulative oil forecast. The calculation requires the recoverable oil saturation ( $\Delta S_o$ ) of every cell; that is, the difference between the initial oil saturation ( $S_{oi}$ ) and the residual oil saturation ( $S_{or}$ ).  $S_{oi}$  is available from the input geological model, but  $S_{or}$  must be assumed.

APDS assumes that when a cell is heated, all its recoverable oil is produced instantaneously. This assumption causes discrepancies to the conventional thermal simulator results, because the oil saturation ( $S_o$ ) is a time-dependent variable. The oil saturation remaining in the steam-chamber changes through time until it reaches  $S_{or}$ .

Implementing the time-dependent average  $\overline{S_{or}}$  proposed by Cardwell & Parsons (1949) might improve the APDS oil production forecast.

$$\overline{S_{or}} = \frac{(b-1)}{b} \left( \frac{v_s \phi Z}{bkgt} \right)^{1/(b-1)} \quad (7.1)$$

Here,  $\overline{S_{or}}$  is the average residual oil saturation after time  $t$ ,  $v_s$  is the kinematic viscosity of the oil at the steam temperature,  $\phi$  is the porosity,  $Z$  is the drainage height,  $k$  is the permeability,  $g$  is the gravity constant, and  $b$  is the exponent in Cardwell and Parson's equation for relative permeability,  $k_r = S^b$ . After applying a typical value for  $b$  of 3.5 (Butler, 1991), the average residual oil saturation in the steam-chamber after a time ( $t$ ) can be approximate by:

$$\overline{S_{or}} = 0.43 \left( \frac{v_s \phi h}{kgt} \right)^{0.4} \quad (7.2)$$

Note that the variable  $Z$  was replaced by the height of the steam-chamber  $h$  that can be calculated at any time  $t$  from APDS.

## 7.2.2 Steam-Oil Ratio (SOR) Forecast

SOR is a key economic performance indicator of a SAGD project. The current APDS implementation does not provide the steam consumption of the process. However, all the inputs to estimate the SOR are readily available from APDS.

After calculating the oil production forecast, the steam consumption can be estimated by adding the heat to expand the steam-chamber, the heat storage ahead of the interface of the steam-chamber and the heat loss to the over-burden. The following equations from Butler (1991).

### 7.2.2.1 Heat to Expand the Steam-chamber ( $Q_{sch}$ )

The heat to raise the steam-chamber from the reservoir temperature to the steam-temperature is calculated with the following equation,

$$Q_{sch} = \frac{Q_o}{\phi \Delta S_o} M (T_{st} - T_r) \quad (7.3)$$

Where,  $T_{st}$  and  $T_r$  are the steam temperature and the initial reservoir temperature, respectively.  $M$  is the volumetric heat capacity of the reservoir,  $Q_o$  is the cumulative recoverable oil,  $\phi$  is the porosity and  $\Delta S_o$  is the recoverable oil saturation.

Note that APDS provides  $Q_o$ ,  $\Delta S_o$  was discussed in Section 7.3.1,  $\phi, M, T_r$  are inputs from the geological model, and  $T_{st}$  is set by the reservoir manager.

### 7.2.2.2 Heat Storage Ahead of the Steam-chamber Interface ( $Q_{stg}$ )

The heat to raise the oil temperature ahead of the steam-chamber from  $T_r$  to  $T_{st}$  is calculated with the following equation,

$$Q_{stg} = \frac{KA_i}{U} (T_{st} - T_r) \quad (7.4)$$

Where,  $K$  is the thermal conductivity of the reservoir,  $A_i$  is the area of the steam-chamber interface,  $U$  is the interface velocity, and  $T_r$  and  $T_{st}$  were previously defined. To solve this equation, APDS provides estimate values of  $A_i$  and  $U$ .

### 7.2.2.3 Heat Loss to the Overburden ( $Q_{ovb}$ )

The heat losses to the overburden above the steam-chamber is calculated with the following equation,

$$Q_{ovb} = \frac{4}{3} K A_{ob} (T_{st} - T_r) \sqrt{\frac{t}{\pi \alpha}} \quad (7.5)$$

Where,  $A_{ob}$  is the area in contact with the overburden at the time  $t$ ,  $\alpha$  is the thermal diffusivity of the overburden and the other variables were previously defined. To solve this equation, APDS provides estimate values  $A_{ob}$ .

### 7.2.3 Oil Relative Permeability ( $K_{ro}$ )

The travel cell time is one component of the APDS ranking function that controls the steam-chamber propagation. After combining Equations 2.1 and 2.2 it can be expressed as,

$$Travel\ Cell\ time = (V_c \phi \Delta S_o) \left( \frac{v_{hv}}{A_t k_o g \sin \beta} \right) \quad (7.6)$$

Where all variables in this equation were previously defined. Note the effective oil permeability ( $k_o$ ) variable in the denominator. APDS currently uses a constant oil relative permeability value ( $k_{ro}$ ) in the range 0.2 to 0.4 to convert the absolute oil permeability ( $k_{abs}$ ) to  $k_o$ . This simplification should cause differences from the results obtained with a thermal flow simulation.

SAGD is a thermal recovery process where high temperatures impact  $k_{ro}$ . Therefore, it is worthy to expand the APDS physics with an oil/water relative permeability correlation at the edge of the steam-chamber. The following correlation proposed by Mosavat, Mohsenzadeh, & Al-Wahaibi (2016) that modifies Corey's equation could render good results. Corey's correlation is given by.

$$k_{rw} = (S_w^*)^4 \quad (7.7)$$

$$k_{ro} = (1 - S_w^{*2}) (1 - S_w^*)^2 \quad (7.8)$$

Where,  $k_{rw}$  is water relative permeability,  $S_w$  water saturation and  $S_w^*$  is the normalized water saturation that depends on the irreducible water saturation  $S_{wirr}$ . The equation of  $S_w^*$  is,

$$S_w^* = \left( \frac{S_w - S_{wirr}}{1 - S_{wirr}} \right) \quad (7.9)$$

Mosavat et al. (2016) developed the following temperature-dependent oil/water relative permeability correlations that are function of water saturation and oil-water viscosity ratio. They reported that the correlations were obtained from curve-fitting SAGD experimental data publicly available.

$$k_{rw} = S_w^{*a} \quad (7.10)$$

$$k_{ro} = (1 - S_w^{*b}) (1 - S_w^*)^c \quad (7.11)$$

The parameters  $a, b, c$  are given by,

$$a = 1.32 + 0.00123\mu_R - 7.47 * 10^{-7}\mu_R^2 \quad (7.12a)$$

$$b = 1.02 - 0.000298\mu_R - 1.38 * 10^{-7}\mu_R^2 \quad (7.12b)$$

$$c = 2.22 + 0.00318\mu_R - 1.22 * 10^{-6}\mu_R^2 \quad (7.12c)$$

$$\mu_R(T) = \left( \frac{\mu_{oil}}{\mu_{water}} \right)_T \quad (7.13)$$

Where,  $\mu_R(T)$  is the viscosity ratio at temperature ( $T$ ).  $\mu_{oil}$  and  $\mu_{water}$  are the oil and water viscosity in  $cP$  at temperature  $T$ , respectively.

Implementing the  $k_{ro}$  correlation should improve the APDS results, so they better match a full physics thermal flow simulator. However, using a  $k_{ro}$  curve might result in mathematical instabilities in cells with initial high-water saturation. In such cases,  $k_{ro}$  will tend to zero and the travel cell time given by Equation 7.6 will tend to infinity. To overcome this issue, it is suggested to include in the APDS implementation a condition to assign very large ranking values to cells with travel cell time that tends to infinite.

It is recommended to search and test other oil/water relative permeability correlations that could be available in the technical literature. The correlation that better compares to the conventional full physics thermal flow simulator should be implemented.

#### 7.2.4 Cells with High Initial Water Saturation ( $S_{wi}$ )

APDS classifies cells with initial water saturation ( $S_{wi}$ ) above a user-defined cut-off, as isolated nodes in the graph, so they are treated like shales. This approximation is not completely satisfactory. Reservoir layers with initial high-water saturation slow-down the steam-chamber propagation, and after the connate water is drained, the steam can pass through them.

Regarding cells with high  $S_{wi}$ , a practical and more flexible alternative to the current APDS assumptions, it is to calculate the travel cell time using water properties or oil properties, depending on a pre-defined water saturation condition. For example, if  $S_{wi} > 40\%$ , then:

$$Travel\ Cell\ time = (V_c \emptyset \Delta S_w) \left( \frac{v_{water}}{A_t k_{abs} k_{rw} g \sin \beta} \right) \quad (7.14)$$

All variables in this equation were previously defined. If  $S_w \leq 40\%$ , then Equation 7.6 is used.

A more complex solution to high  $S_{wi}$  zones involves implementing a fractional flow model that considers both, oil and water saturations, into the travel cell time equation. As a starter point for future research, the fractional flow between one cell and its neighbors,

after neglecting the effect of the capillary pressure, can be calculated with the following equation (Butler, 1991).

$$f_w = \frac{q_w}{q_t} = \frac{1 - \varphi}{1 + \frac{\mu_w k_{ro}}{k_{rw} \mu_o}} \quad (7.15)$$

Where,

$$\varphi = \frac{k_{abs} k_{ro} A_t \Delta \rho g \sin \beta}{q_t \mu_o} \quad (7.16)$$

Where  $q_w$ ,  $q_t$  are water and oil flow rate, respectively. All other variables in these equations were previously defined. How to combine these equations with a material balance of both fluids (oil and water) at the cell-scale in a consistent way with other APDS assumptions is not solved yet. However, a solution of this type would certainly render a better representation of the actual physical phenomena occurring at the edge of the steam-chamber and it would be an important advance in the APDS formulation.

### 7.2.5 Assisting the Ensemble Kalman Filter (EnKF) Technique with APDS

EnKF is an inverse-modelling local optimization technique intended for sequential assimilation of static and dynamic into a model (Aanonsen, Nævdal, Oliver, Reynolds, & Vallès, 2009). It consists of two recursive steps, the forecast step to propagate state variables as a function of the updated parameters from one timestep to another, and the analysis or updating step for data assimilation (Zagayevskiy & Deutsch, 2015).

EnKF was applied to assimilate time-lapse temperature observations and 4D-seismic data in SAGD reservoir characterization by Zagayevskiy & Deutsch (2015). They discussed two challenges to implement EnKF. It requires an ensemble with a large number of geostatistical realizations, and they all need to be processed during the forecast step. The forecast step can be performed with a full-physics thermal flow simulator but is computationally too expensive. Using APDS should reduce drastically the computational overburden of running the forecast step with a marginal loss in the quality of the estimate.

A case study intended to explore the advantages and limitations of assisting EnKF with APDS is suggested.

### 7.2.6 Coupling APDS with a Thermal Wellbore Simulator

APDS assumes a uniform pressure profile along the injector wellbore. However, in SAGD projects, the pressure difference between the heel and toe of a long horizontal steam injector due to frictional losses can be significant. These pressure differences can affect the development of the shape of the steam chamber (Tan, Butterworth, & Yang, 2002).

It is anticipated that coupling a thermal wellbore simulator to APDS will improve the ability of the latter to predict the steam-chamber propagation. As a starter point for this research path, the following literature about modeling thermal wellbore conditions in SAGD is suggested (Ju & Zhao, 2016; Oballa, Coombe, & Buchanan, 1997; Tan et al., 2002; Vander Valk & Yang, 2007). The challenge is making compatible existing thermal wellbore simulators with the APDS formulation.

### 7.2.7 APDS Applications

The APDS applications discussed in this thesis used geological models representing SAGD well-pair volumes. To further test the limits of the APDS predictive capabilities and assess its potential use in commercial SAGD projects, additional case studies using larger scales are required.

In this regard, a challenging problem worthy of being revisited having APDS as a companion tool, is the placement of SAGD surface production pads and subsurface drainage areas to maximize the economic potential of an area tackled by Manchuk & Deutsch (2013).

### 7.2.8 APDS Computational Efficiency

The case studies presented in this thesis indicate that APDS is around 3 orders of magnitude faster than conventional full-physics thermal flow simulators to model the steam-chamber

expansion and to provide a response variable. This processing time appears encouraging to undertake problems with large finite decision spaces. However, is not yet efficient enough to embed APDS into a full-scale field optimization work flow. It is recommended to look for substantial efficiency gains in the scale of 1-3 additional orders of magnitude compared to a conventional thermal flow simulator. It is suggested to program APDS using a compiled language such as C, C++, C# or Fortran. Moreover, the structure of the program must ensure that APDS can be parallelized.

### 7.2.9 Decision-Maker Position on Geological Risk

The MVC-SDR criterion is primarily applicable to problems with a well-defined finite set of decision options. It helps reservoir managers to reduce the number of alternatives from which the decision must be made, but at the end, the final choice depends on the specific reservoir manager's utility function. Utility functions are also required as objective functions to account for geological uncertainty in closed-loop field optimization work flows. The reservoir manager's position on risk should be explicitly embedded in a utility function, so the PRM decision-making problem can be generically formulated as:

$$\operatorname{argmax}_{a \in A} E[u(x(a, w))] = \operatorname{argmax}_{a \in A} \int f(x(a, w)) \cdot u(x(a, w)) dx \quad (7.17)$$

Where,  $a$  represents projects from the set of feasible actions  $A$ ;  $w$  represents realizations from the geological model;  $x(a, w)$  represents the payoff calculated after transferring the geological uncertainty;  $f(x(\cdot))$  is the probability density function of  $x(\cdot)$  and  $u(x(\cdot))$  is the utility function.

Because there is no clear method to determine a decision maker's utility function, it is recommended to follow a pragmatic approach similar to Güyagüler & Horne (2004) and Ozdogan & Horne (2006). That is, the utility function is assumed to be exponential,  $u(x) = -e^{-x/R}$ , and the position on risk of the reservoir manager, represented by the risk tolerance parameter  $R$ , is calibrated performing a sensitivity analysis over a range of  $R$ . In the case of SAGD decision-making problems, this procedure will benefit from the APDS efficiency,

because it requires transferring the geological uncertainty over the set of geostatistical realizations, as many times as needed for the calibration of the R parameter.

#### 7.2.10 Value of Seismic Information on SAGD projects

The APDS probability of steam-chamber presence volumes condense the information about the steam-chamber location of an entire set of geostatistical realizations. They can be estimated at the recording time of different seismic monitoring surveys to improve the assimilation of dynamic data in reservoir characterization.

The bitumen forecast provided by APDS can be used to quantify the value of information as incremental 4D-seismic data become available (Hadavand, 2017). However, since the steam-consumption is the largest operational cost in SAGD projects, it is recommended to develop and validate the procedure to obtain the Steam-Oil Ratio (SOR) forecast from APDS (Section 7.3.2) before undertaking this VOI problem.

## References

- Aanonsen, S. I., Nævdal, G., Oliver, D. S., Reynolds, A. C., & Vallès, B. (2009). The Ensemble Kalman Filter in Reservoir Engineering- A Review. *SPE Journal*, *14*(03), 393–412. <https://doi.org/10.2118/117274-PA>
- Alusta, G. A., Mackay, E. J., Fennema, J., Armih, K., & Collins, I. R. (2012). EOR vs. Infill Well Drilling: Field application of new decision making technique. In *SPE Kuwait International Petroleum Conference and Exhibition*. Kuwait City, Kuwait: Dec. 10-12. <https://doi.org/10.2118/163298-MS>
- Azad, A., & Chalaturnyk, R. J. (2012). An Improved SAGD Analytical Simulator: Circular Steam Chamber Geometry. *Journal of Petroleum Science and Engineering*, *82–83*, 27–37. <https://doi.org/10.1016/j.petrol.2012.01.003>
- Azom, P. N., & Srinivasan, S. (2011). Modeling the Effect of Permeability Anisotropy on the Steam-Assisted Gravity Drainage (SAGD) Process. In *Canadian Unconventional Resources Conference*. Calgary, Alberta, Ca. <https://doi.org/10.2118/149274-MS>
- Azom, P. N., & Srinivasan, S. (2013). Modeling the Effect of Permeability Anisotropy on the Steam-Assisted Gravity Drainage (SAGD) Process in Multi-Layered Reservoirs. In *SPE Heavy Oil Conference Canada*. Calgary, Alberta, Ca. <https://doi.org/10.2118/149274-MS>
- Banerjee, S., & Hascakir, B. (2018). Flow Control Devices in SAGD Completion Design: Enhanced Heavy Oil/ Bitumen Recovery through Improved Thermal Efficiency. *Journal of Petroleum Science and Engineering*, *169*(May), 297–308. <https://doi.org/10.1016/j.petrol.2018.05.064>
- Baniak, G. M., & Kingsmith, K. G. (2018). Sedimentological and Stratigraphic Characterization of Cretaceous Upper McMurray Deposits in the Southern Athabasca Oil Sands, Alberta, Canada. *AAPG Bulletin*, *102*(2), 309–332. <https://doi.org/10.1306/0502171619317010>
- Batycky, R. P., Blunt, M. J., & Thiele, M. R. (1997). A 3D Field-Scale Streamline-Based Reservoir Simulator. *SPE Reservoir Engineering*, *12*(04), 246–254. <https://doi.org/SPE 36726>
- Begg, S. H., Bratvold, R. B., & Campbell, J. M. (2003). Shrinks Or Quants: Who Will

- Improve Decision-Making. In *Proceedings of SPE Annual Technical Conference and Exhibition*. Denver, Colorado: Oct. 5-8. <https://doi.org/10.2523/84238-MS>
- Bratvold, R. B., Begg, S. H., & Campbell, J. M. (2003). Even Optimists Should Optimize. In *Proceedings of SPE Annual Technical Conference and Exhibition*. Denver, Colorado: Oct. 5-8. <https://doi.org/10.2118/84329-MS>
- Burke, L., & Ghazar, C. (2018). Flow Control Devices in SAGD - A System-Based Technology Solution. In *SPE Thermal Well Integrity and Design Symposium*. Banff, Alberta, Canada.: Nov. 27-29. <https://doi.org/10.2118/193353-MS>
- Butler, R. M. (1985). A New Approach to the Modelling of Steam-Assisted Gravity Drainage. *Journal of Canadian Petroleum Technology*, 24(03), 42–51. <https://doi.org/10.2118/85-03-01>
- Butler, R. M. (1991). *Thermal Recovery of Oil and Bitumen*. Englewood Cliff, New Jersey: Prentice-Hall. Retrieved from [https://books.google.ca/books?id=\\_6RTAAAAMAAJ](https://books.google.ca/books?id=_6RTAAAAMAAJ)
- Butler, R. M., McNab, G. S., & Lo, H. Y. (1981). Theoretical Studies on the Gravity Drainage of Heavy Oil During in-situ Steam Heating. *The Canadian Journal of Chemical Engineering*, 59(4), 455–460. <https://doi.org/10.1002/cjce.5450590407>
- Butler, R. M., & Stephens, D. J. (1981). The Gravity Drainage of Steam-Heated Heavy Oil to Parallel Horizontal Wells. *Journal of Canadian Petroleum Technology*, 20(2), 90–96. <https://doi.org/10.2118/81-02-07>
- Caers, J. (2011). *Modeling Uncertainty in the Earth Sciences* (1st ed.). Hoboken, NJ: Wiley-Blackwell.
- Capolei, A., Suwartadi, E., Foss, B., & Jørgensen, J. B. (2015). A Mean-Variance Objective for Robust Production Optimization in Uncertain Geological Scenarios. *Journal of Petroleum Science and Engineering*, 125, 23–37. <https://doi.org/10.1016/j.petrol.2014.11.015>
- Cardwell, W. T., & Parsons, R. L. (1949). Gravity Drainage Theory. *Transactions of the AIME*, 179(01), 199–215. <https://doi.org/10.2118/949199-G>
- CERI. (2018). *Canadian Oil Sands Supply Costs and Development Projects*. Calgary, Alberta, Ca.
- Chalaturnyk, R. J., & Li, P. (2004). When Is It Important to Consider Geomechanics in SAGD Operations? *Journal of Canadian Petroleum Technology*, 43(4), 53–61.

<https://doi.org/10.2118/04-08-discussion>

- Chang, Y., Bouzarkouna, Z., & Devegowda, D. (2015). Multi-objective Optimization for Rapid and Robust Optimal Oilfield Development Under Geological Uncertainty. *Computational Geosciences*, 19(4), 933–950. <https://doi.org/10.1007/s10596-015-9507-6>
- Chiles, J.-P., & Delfiner, P. (2012). *Geostatistics: Modeling Spatial Uncertainty*. (S. S. W. Walter A. Shewhart, Ed.), *Wiley series in probability and statistics* (2nd ed.). Oxford: Wiley-Blackwell. Retrieved from <http://onlinelibrary.wiley.com/book/10.1002/9781118136188>
- CMG. (2010). *STARS User's Guide*. Calgary, Alberta: Computer Modelling Group Ltd.
- CMG. (2013). *CMG's SAGD Guide*. Calgary, Alberta: Computer Modelling Group Ltd.
- Cokar, M., Kallos, M. S., & Gates, I. D. (2013). A New Thermogeomechanical Theory for Gravity Drainage in Steam-Assisted Gravity Drainage. *SPE Journal*, 18(4), 736–742. <https://doi.org/10.2118/163136-PA>
- Collins, P. M. (2007). Geomechanical Effects on the SAGD Process. *SPE Reservoir Evaluation & Engineering*, 10(4), 367–375. <https://doi.org/10.2118/97905-PA>
- da Cruz, S. P. (2000). *Reservoir Management Decision-Making in the Presence of Geological Uncertainty*. Stanford University, United States. Retrieved from <https://pangea.stanford.edu/ERE/pdf/pereports/PhD/Cruz00.pdf>
- Damsleth, E., Hage, A., & Volden, R. (1992). Maximum Information at Minimum Cost: A North Sea Field Development Study With an Experimental Design. *Journal of Petroleum Technology*, (December), 1350–1356. <https://doi.org/10.2118/23139-PA>
- Dehdari, V. (2014). *Development and Applications of a Semi-Analytical Approximate Thermal Simulator*. Universty of Alberta, Canada.
- Deo, N., & Pang, C. - Y. (1984). Shortest-Path Algorithms: Taxonomy and Annotation. *Networks*, 14(2), 275–323. <https://doi.org/10.1002/net.3230140208>
- Deutsch, C. V., & Journel, A. G. (1998). *GSLIB. Geostatistical Software Library and User's Guide* (2nd ed.). New York: Oxford University Press.
- Dijkstra, E. W. (1959). A Note on Two Problems in Connection with Graphs. *Numerische Mathematik*. <https://doi.org/10.1007/BF01386390>
- Echeverria-Ciurri, D., Conn, A. R., Mello, U. T., & Onwunalu, J. E. (2012). Integrating

- Mathematical Optimization and Decision Making in Intelligent Fields. In *SPE Intelligent Energy International 2012* (Vol. 1). Utrecht, The Netherlands: 27-29 March. <https://doi.org/10.2118/149780-MS>
- Edwards, R. A. (1993). Applying Financial Portfolio Theory to the Analysis of Producing Properties.
- Even, S. (2011). *Graph Algorithms*. (G. Even, Ed.). Cambridge: Cambridge University Press. <https://doi.org/10.1017/CBO9781139015165>
- Fatt, I. (1956). The Network Model of Porous Media. *Petroleum Transactions, AIME*, 207, 144–181.
- Gallardo, E. C., & Deutsch, C. V. (2018). Approximate Physics-Discrete Simulation of the Steam-Chamber Evolution in Steam-Assisted Gravity Drainage. *SPE Journal, Preprint*(Preprint), 15. <https://doi.org/10.2118/194016-PA>
- Gates, I. D., Kenny, J., Hernandez-Hdez, I. L., & Bunio, G. L. (2007). Steam Injection Strategy and Energetics of Steam-Assisted Gravity Drainage. *SPE Reservoir Evaluation & Engineering*, 10(01), 19–34. <https://doi.org/10.2118/97742-PA>
- Goldberg, D. E. (1989). *Genetic Algorithms in Search, Optimization, and Machine Learning*. Reading, MA: Addison-Wesley.
- Goovaerts, P. (1997). *Geostatistics for Natural Resources Evaluation. Applied geostatistics series*. New York: Oxford University Press.
- Güyagüler, B., & Horne, R. N. (2004). Uncertainty Assessment of Well-Placement Optimization. *SPE Reservoir Evaluation & Engineering*, 7(1), 24–32. <https://doi.org/10.2118/87663-pa>
- Hadar, J., & Russell, W. R. (1969). Rules for Ordering Uncertain Prospects. *American Economic Review*, 59(1), 25–34. <https://doi.org/10.1126/science.151.3712.867-a>
- Hadavand, M. (2017). *Integration of 4D Seismic Data in Reservoir Characterization with Facies Parameter Uncertainty*. University of Alberta, Canada.
- Hadavand, M., Carmichael, P., Dalir, A., Rodriguez, M., Silva, D. F. S., & Deutsch, C. V. (2018). Integration of 4D Seismic in Steam-Assisted-Gravity-Drainage Reservoir Characterization. *SPE Reservoir Evaluation & Engineering*, (June 2017), 1–16. <https://doi.org/10.2118/191359-PA>
- Hadavand, M., & Deutsch, C. V. (2017). A Practical Methodology For Integration of 4D

- Seismic in Steam-Assisted-Gravity-Drainage Reservoir Characterization. *SPE Reservoir Evaluation & Engineering*, 20(2), 353–362. <https://doi.org/10.2118/184390-PA>
- Hanoch, G., & Levy, H. (1969). The Efficiency Analysis of Choices Involving Risk. *Review of Economic Studies*, 36(3), 107–335. <https://doi.org/10.2307/2296431>
- Hassanpour, R. . (2013). *Grid-free Facies Modelling of Inclined Heterolitic Strata in McMurray Formation*. University of Alberta, Alberta, Canada.
- Heidari, M., Pooladi-Darvish, M., Azaiez, J., & Maini, B. (2009). Effect of Drainage Height and Permeability on SAGD Performance. *Journal of Petroleum Science and Engineering*, 68(1–2), 99–106. <https://doi.org/10.1016/j.petrol.2009.06.020>
- Irani, M., & Cokar, M. (2016). Discussion on the Effects of Temperature on Thermal Properties in the Steam-Assisted-Gravity-Drainage (SAGD) Process. Part 1: Thermal Conductivity. *SPE Journal*, 21(2), 334–352. <https://doi.org/10.2118/178426-PA>
- Isebor, O. J., Echeverría-Ciaurri, D., & Durlofsky, L. J. (2013). Generalized Field Development Optimization Using Derivative-Free Procedures. In *SPE Reservoir Simulation Symposium*. The Woodlands, Texas: 1-4 February. <https://doi.org/10.2118/163631-PA>
- Johnstone, D., & Lindley, D. (2013). Mean–Variance and Expected Utility: The Borch Paradox. *Statistical Science*, 28(2), 223–237. <https://doi.org/10.1214/12-STS408>
- Ju, N., & Zhao, G. (2016). A Calculation Model for Steam Property Variation Along Wellbore Trajectory in SAGD Processes. In *Society of Petroleum Engineers - SPE Latin America and Caribbean Heavy and Extra Heavy Oil Conference 2016*. Lima, Peru: Oct. 19-20. <https://doi.org/10.2118/181155-MS>
- Kennedy, J., & Eberhart, R. (1995). Particle Swarm Optimization. In N. 27- Dec.1 (Ed.), *Neural Networks, 1995. Proceedings., IEEE International Conference on* (Vol. 4). Perth, WA, Australia. <https://doi.org/10.1109/ICNN.1995.488968>
- Khan, K. D., & Deutsch, C. V. (2016). Practical Incorporation of Multivariate Parameter Uncertainty in Geostatistical Resource Modeling. *Natural Resources Research*, 25(1), 51–70. <https://doi.org/10.1007/s11053-015-9267-y>
- Kochenderfer, M. J. (2015). *Decision Making Under Uncertainty: Theory and Application*. MIT Lincoln Laboratory series. Cambridge, Massachusetts: The MIT

- Press. Retrieved from <http://ieeexplore.ieee.org/servlet/opac?bknumber=7288640>
- Labrecque, P. A., Jensen, J. L., Hubbard, S. M., & Nielsen, H. (2011). Sedimentology and Stratigraphic Architecture of a Point Bar Deposit, Lower Cretaceous McMurray Formation, Alberta, Canada. *Bulletin of Canadian Petroleum Geology*, 59(2), 147–171. <https://doi.org/10.2113/gscpgbull.59.2.147>
- Levy, H. (2016). *Stochastic Dominance: Investment Decision Making Under Uncertainty* (3rd ed.). New York: Springer. <https://doi.org/10.1007/978-3-319-21708-6>
- Levy, H., & Sarnat, M. (1970). Portfolio Selection and Investors Utility: A Graphical Analysis. *Applied Economics*, 2(2), 113–119. <https://doi.org/10.1080/00036847000000020>
- Li, W., Mamora, D. D., Li, Y., & Qui, F. (2011). Numerical Investigation of Potential Injection Strategies to Reduce Shale Barrier Impacts on SAGD Process. *Journal of Canadian Petroleum Technology*, 50(3), 57–64. <https://doi.org/10.2118/133298-PA>
- Lumley, D. E., & Behrens, R. A. (1998). Practical Issues of 4D Seismic Reservoir Monitoring: What an Engineer Needs to Know. *SPE Reservoir Evaluation & Engineering*, 1(06), 528–538. <https://doi.org/10.2118/53004-PA>
- Machina, M. J. (1987). Choice Under Uncertainty: Problems Solved and Unsolved. *Journal of Economic Perspectives*, 1(1), 121–154. <https://doi.org/10.1257/jep.1.1.121>
- Majdi Yazdi, M., & Jensen, J. L. (2014). Fast Screening of Geostatistical Realizations for SAGD Reservoir Simulation. *Journal of Petroleum Science and Engineering*, 124, 264–274. <https://doi.org/10.1016/j.petrol.2014.09.030>
- Manchuk, J. G., & Deutsch, C. V. (2013). Optimization of Drainage-Area Configurations to Maximize Recovery from SAGD Operations. *Journal of Canadian Petroleum Technology*, 52(3), 233–242. <https://doi.org/10.2118/165573-PA>
- Markowitz, H. M. (1959). *Portfolio Selection. Efficient Diversification of Investments*. New York: John Wiley & Sons, Inc.
- Moreton, D. J., & Carter, B. J. (2015). *Characterizing Alluvial Architecture of Point Bars within the McMurray Formation, Alberta, Canada, for Improved Bitumen Resource Prediction and Recovery. Developments in Sedimentology* (1st ed., Vol. 68). Elsevier B.V. <https://doi.org/10.1016/B978-0-444-63529-7.00016-X>
- Mosavat, N., Mohsenzadeh, A., & Al-Wahaibi, Y. (2016). Estimating Oil/Water Relative

- Permeability at SAGD Steam Chamber Edge. In *SPE Heavy Oil Conference and Exhibition*. Kuwait City, Kuwait: Dec. 6-8. <https://doi.org/10.2118/184132-MS>
- Muskat, M., & Wyckoff, R. D. (1934). A Theoretical Analysis of Water-flooding Networks. *Transactions of the AIME*, 107(01), 62–76. <https://doi.org/10.2118/934062-G>
- Newendorp, P. D., & Campbell, J. M. (1968). SPE Criterion for Drilling Investments. *Society of Petroleum Engineers of AIME*.
- Oballa, V., Coombe, D. A., & Buchanan, L. (1997). Aspects of Discretized Wellbore Modelling Coupled to Compositional/Thermal Simulation. *Journal of Canadian Petroleum Technology*, 36(4), 45–51. <https://doi.org/10.2118/97-04-04>
- Oren, P.-E., Bakke, S., & Arntzen, O. J. (1998). Extending Predictive Capabilities to Network Models. *SPE Journal*, 3(04), 324–336. <https://doi.org/10.2118/52052-PA>
- Ortega-Arranz, H., Llanos R., D., & Gonzalez-Escribano, A. (2015). *The Shortest-Path Problem: Analysis and Comparison of Methods*. Morgan & Claypool. [https://doi.org/DOI 10.2200/S00618ED1V01Y201412TCS001](https://doi.org/DOI%2010.2200/S00618ED1V01Y201412TCS001)
- Ozdogan, U., & Horne, R. (2006). Optimization of Well Placement Under Time-Dependent Uncertainty. *SPE Reservoir Evaluation & Engineering*, 9(April), 26–29. <https://doi.org/10.2118/90091-PA>
- Pathak, V., Tran, D., & Kumar, A. (2014). Quantifying the Uncertainty Associated with Caprock Integrity during SAGD using Coupled Geomechanics Thermal Reservoir Simulation. In *SPE Heavy Oil Conference-Canada*. Calgary, Alberta: 10-12 June. <https://doi.org/10.2118/170130-MS>
- Peacock, M. J. (2010). Athabasca Oil Sands: Reservoir Characterization and its Impact on Thermal and Mining Opportunities. *Geological Society, London, Petroleum Geology Conference Series*, 7(1), 1141–1150. <https://doi.org/10.1144/0071141>
- Pollock, D. W. (1988). Semianalytical Computation of Path Lines for Finite-Difference Models. *Groundwater*, 26(6), 743–750. <https://doi.org/10.1111/j.1745-6584.1988.tb00425.x>
- Pyrcz, M. J., & Deutsch, C. V. (2014). *Geostatistical Reservoir Modeling* (2nd ed.). New York : Oxford University Press. Retrieved from <http://login.ezproxy.library.ualberta.ca/login?url=http://search.ebscohost.com/login>.

aspx?direct=true&db=cat03710a&AN=alb.8111105&site=eds-live&scope=site

- Raiffa, H., & Schlaifer, R. (1961). *Applied Statistical Decision Theory. Studies in managerial economics*. Boston: Division of Research, Graduate School of Business Administration, Harvard University.
- Ranger, M. J., & Gingras, M. (2010). *Geology of the Athabasca Oil Sands: Field Guide & Overview*. Canadian Society of Petroleum Geologists. Retrieved from <https://books.google.com.co/books?id=ZKwCswEACAAJ>
- Reis, J. C. (1992). A Steam Assisted Gravity Drainage Model for Tar Sands: Linear Geometry. *Journal of Canadian Petroleum Technology*, 31(10), 14–20. <https://doi.org/10.2118/92-10-01>
- Rothschild, M., & Stiglitz, J. E. (1970). Increasing Risk: I. A Definition. *Journal of Economic Theory*, 2(3), 225–243. [https://doi.org/10.1016/0022-0531\(70\)90038-4](https://doi.org/10.1016/0022-0531(70)90038-4)
- Sarma, P., Chen, W. H., & Xie, J. (2013). Selecting Representative Models from a Large Set of Models. In *SPE Reservoir Simulation Symposium*. The Woodlands, Texas: Feb. 18-20. <https://doi.org/10.2118/163671-MS>
- Schroeder, W., Martin, K., & Lorensen, B. (2006). *The Visualization Toolkit* (4th ed.). Kitware.
- Sharma, B. C., Khataniar, S., Patil, S. L., Kamath, V. A., & Dandekar, A. Y. (2002). A Simulation Study of Novel Thermal Recovery Methods in the Ugnu Tar Sand Reservoir, North Slope, Alaska. In *SPE Western Regional/AAPG Pacific Section Joint Meeting*. Anchorage, Alaska: May. 20-22. <https://doi.org/10.2118/76729-MS>
- Shirangi, M. G., & Durlofsky, L. J. (2015). Closed-Loop Field Development Optimization Under Uncertainty. In *SPE Reservoir Simulation Symposium*. Houston, Texas: Feb. 23-25. <https://doi.org/10.2118/173219-MS>
- Stirling, W. C. (2012). *Theory of Conditional Games*. New York: Cambridge University Press. Retrieved from <http://assets.cambridge.org/97811070/11748/cover/9781107011748.jpg>  
<http://catdir.loc.gov/catdir/enhancements/fy1201/2011041577-b.html>  
<http://catdir.loc.gov/catdir/enhancements/fy1201/2011041577-d.html>  
<http://catdir.loc.gov/catdir/enhancements/fy1201/20110>
- Su, Y., Wang, J., & Gates, I. D. (2017). SAGD Pad Performance in a Point Bar Deposit

- with a Thick Sandy Base. *Journal of Petroleum Science and Engineering*, 154(April), 442–456. <https://doi.org/10.1016/j.petrol.2017.03.052>
- Su, Y., Wang, J. Y., & Gates, I. D. (2013). SAGD Well Orientation in Point Bar Oil Sand Deposit Affects Performance. *Engineering Geology*, 157, 79–92. <https://doi.org/10.1016/j.enggeo.2013.01.019>
- Tan, T. B., Butterworth, E., & Yang, P. (2002). Application of a Thermal Simulator with Fully Coupled Discretized Wellbore Simulation to SAGD. *Journal of Canadian Petroleum Technology*, 41(1), 25–30. <https://doi.org/10.2118/02-01-01>
- Vander Valk, P. ., & Yang, P. (2007). Investigation of Key Parameters in SAGD Wellbore Desing and Operation. *Journal of Canadian Petroleum Technology*, 46(6). <https://doi.org/10.1007/BF01210950>
- Voloshin, V. I. (2009). *Introduction to Graph Theory*. New York: Nova Science Publishers, Inc. Retrieved from <http://login.ezproxy.library.ualberta.ca/login?url=http://search.ebscohost.com/login.aspx?direct=true&db=nlebk&AN=393233&site=ehost-live&scope=site>
- Von Neumann, J., & Morgenstern, O. (2007). *Theory of Games and Economic Behavior : 60th Anniversary Commemorative Edition* (Vol. 60th anniv). Princeton: Princeton University Press. Retrieved from <http://login.ezproxy.library.ualberta.ca/login?url=https://search.ebscohost.com/login.aspx?direct=true&db=e000xna&AN=509721&site=ehost-live&scope=site>
- Walls, M. R. (1995). Corporate Risk Tolerance and Capital Allocation: A Practical Approach to Implementing an Exploration Risk Policy. *Journal of Petroleum Technology*, (April), 307–311. <https://doi.org/10.2118/28281-PA>
- Walls, M. R. (2005). Corporate Risk-Taking and Performance: A 20 Year Look at the Petroleum Industry. *Journal of Petroleum Science and Engineering*, 48(3–4), 127–140. <https://doi.org/10.1016/j.petrol.2005.06.009>
- Wang, C., & Leung, J. (2015). Characterizing the Effects of Lean Zones and Shale Distribution in Steam-Assisted-Gravity-Drainage Recovery Performance. *SPE Reservoir Evaluation & Engineering*, 18(03), 329–345. <https://doi.org/10.2118/170101-PA>
- Wang, H., Echeverría-Ciaurri, D., Durlofsky, L., & Cominelli, A. (2012). Optimal Well

- Placement Under Uncertainty Using a Retrospective Optimization Framework. *SPE Journal*, 17(01), 112–121. <https://doi.org/10.2118/141950-PA>
- Wilde, B., & Deutsch, C. V. (2012). *Calculating an Improved Connected Hydrocarbon Volume with Line-of-sight for Ranking Realizations by SAGD Performance*. Edmonton, Canada.
- Xu, J., Chen, Z., Cao, J., & Li, R. (2014). Numerical Study of the Effects of Lean Zones on SAGD Performance in Periodically Heterogeneous Media. In *SPE Heavy Oil Conference-Canada*. Calgary, Alberta: 10-12 June. <https://doi.org/10.2118/170138-MS>
- Zagayevskiy, Y., & Deutsch, C. V. (2015). Assimilation of Time-Lapse Temperature Observations and 4D-Seismic Data with the EnKF in SAGD Petroleum Reservoirs. *Journal of Canadian Petroleum Technology*, 54(3), 164–182. <https://doi.org/10.2118/174547-PA>
- Zhao, L., Law, D. H. S., & Coates, R. (2003). Numerical Study and Economic Evaluation of SAGD Wind-Down Methods. *Journal of Canadian Petroleum Technology*, 42(1), 53–57. <https://doi.org/10.2118/03-01-05>

## Appendix A

### Computer Programs

This appendix presents the APDS prototype written in the Python programming language. The prototype is a collection of programs organized in 3 modules: Graph generator, Steam-chamber generator and Post-processing (Figure 3.6). APDS programs are self-documented, they have a heading describing the function of the program, the inputs and outputs. In the codes, star symbols (\*\*\*) indicates the start and the end of the program, and text inside number symbols (###), or after them, are explanatory comments. This appendix has the following structure:

1. Section A.1 presents the dependencies, requirements and licenses.
2. Section A.2 presents a workflow to run APDS.
3. Section A.3 contains the programs.

#### A.1 Dependencies, Requirements and Licenses

##### A.1.1 Dependencies and Requirements

APDS requires Python 3.X or higher such as the Anaconda distribution from Continuum Analytics, <https://www.continuum.io/downloads>. The following packages are required:

- NumPy- Python math library - <http://www.numpy.org/>
- SciPy - Python math library - <http://www.scipy.org/>
- Pandas - Python data analysis library - <http://pandas.pydata.org/>
- Spyder – Python environment with MATLAB-like features - <https://pypi.python.org/pypi/spyder>
- pqdict 1.0.0 - Dictionary Priority Queues. - <https://pypi.python.org/pypi/pqdict/>
- pygeostat is recommended from <https://ccgsrv.geostats.ualberta.ca/ccgkb/doku.php>

## A.1.2 Licenses

### A.1.2.1 CCG Software Terms of Use for APDS and pygeostat

Pygeostat Python code is licensed under CCG Software Terms of Use, which are copied below. Use and Support of Software from the Centre for Computational Geostatistics (CCG). Last Revised August 30, 2016.

The Centre for Computational Geostatistics (CCG) at the University of Alberta has evolved over the years, yet the basic idea remains the same: organizations provide research funding for access to research results. CCG software is intellectual property of CCG; the following principles apply to the use and support of CCG software.

#### 1. Openness within the CCG Community

All researchers within CCG share all software developed at the CCG openly within the CCG community. All software aims for high standards, but many programs are works in progress.

#### 2. Support of CCG Software

There is no support provided for CCG software. CCG researchers may address questions and reports of errors and deficiencies. CCG Research Partners receive greater consideration.

3. Software Use for Short Courses and the Citation Program in Applied Geostatistics Course participants use CCG software for exercises and projects, but should not use the software for commercial application outside of the CCG community after the training course.

#### 4. Use in Commercial Software

A CCG member may embed CCG software within commercial software that they develop or apply, if they take responsibility for the product.

#### 5. Software Use if a CCG Member Drops Support

It is an expectation of the CCG community that former CCG members discontinue the use of CCG software embedded within their practices and applications, unless they were the developer.

#### 6. Software Use by the Developer

A particular researcher within CCG can distribute their software as they see fit. Special care is required for derivative works built on previous CCG software.

#### 7. Released Software

Certain software is released as part of journal publications or on our website. Such software is released and licensed under <https://creativecommons.org/licenses/by-nc-nd/4.0/>

\*\*\*\*\*

The following text should be disclosed within CCG code and when CCG code is executed: This software is the intellectual property of the Centre for Computational Geostatistics (CCG). It is made available to the CCG community, but no support is provided. For more information, please refer to the terms of use on <http://www.ccgalberta.com/software-terms-of-use>.

\*\*\*\*\*

THE SOFTWARE IS PROVIDED "AS IS", WITHOUT WARRANTY OF ANY KIND, EXPRESS OR IMPLIED, INCLUDING BUT NOT LIMITED TO THE WARRANTIES OF MERCHANTABILITY, FITNESS FOR A

PARTICULAR PURPOSE AND NONINFRINGEMENT. IN NO EVENT SHALL THE AUTHORS OR COPYRIGHT HOLDERS BE LIABLE FOR ANY CLAIM, DAMAGES OR OTHER LIABILITY, WHETHER IN AN ACTION OF CONTRACT, TORT OR OTHERWISE, ARISING FROM, OUT OF OR IN CONNECTION WITH THE SOFTWARE OR THE USE OR OTHER DEALINGS IN THE SOFTWARE.

\*\*\*\*\*

Subroutines from GSLIB are redistributed under the license from GSLIB:

\*\*\*\*\*

Copyright (C) 2003, Statios Software and Services Incorporated. All rights reserved.

This program has been modified from the one distributed in 1996 (see below). This version is also distributed in the hope that it will be useful, but WITHOUT ANY WARRANTY. Compiled programs based on this code may be redistributed without restriction; however, this code is for one developer only. Each developer or user of this source code must purchase a separate copy from Statios. Copyright (C) 1996, The Board of Trustees of the Leland Stanford Junior University. All rights reserved.

\*\*\*\*\*

The programs in GSLIB are distributed in the hope that they will be useful, but WITHOUT ANY WARRANTY. No author or distributor accepts responsibility to anyone for the consequences of using them or for whether they serve any particular purpose or work at all, unless he says so in writing. Everyone is granted permission to copy, modify and redistribute the programs in GSLIB, but only under the condition that this notice and the above copyright notice remain intact.

### A.1.2.2 MIT License for pddict

From: <https://pqdict.readthedocs.io/en/latest/intro.html#license>

From: <https://opensource.org/licenses/MIT>

Permission is hereby granted, free of charge, to any person obtaining a copy of this software and associated documentation files (the "Software"), to deal in the Software without restriction, including without limitation the rights to use, copy, modify, merge, publish, distribute, sublicense, and/or sell copies of the Software, and to permit persons to whom the Software is furnished to do so, subject to the following conditions:

The above copyright notice and this permission notice shall be included in all copies or substantial portions of the Software.

THE SOFTWARE IS PROVIDED "AS IS", WITHOUT WARRANTY OF ANY KIND, EXPRESS OR IMPLIED, INCLUDING BUT NOT LIMITED TO THE WARRANTIES OF MERCHANTABILITY, FITNESS FOR A PARTICULAR PURPOSE AND NONINFRINGEMENT. IN NO EVENT SHALL THE AUTHORS OR COPYRIGHT HOLDERS BE LIABLE FOR ANY CLAIM, DAMAGES OR OTHER LIABILITY, WHETHER IN AN ACTION OF CONTRACT, TORT OR OTHERWISE, ARISING FROM, OUT OF OR IN CONNECTION WITH THE SOFTWARE OR THE USE OR OTHER DEALINGS IN THE SOFTWARE.

### A.1.2.3 NumPy License

From: <http://www.numpy.org/license.html>

Copyright © 2005-2018, NumPy Developers. All rights reserved.

Redistribution and use in source and binary forms, with or without modification, are permitted provided that the following conditions are met:

Redistributions of source code must retain the above copyright notice, this list of conditions and the following disclaimer.

Redistributions in binary form must reproduce the above copyright notice, this list of conditions and the following disclaimer in the documentation and/or other materials provided with the distribution.

Neither the name of the NumPy Developers nor the names of any contributors may be used to endorse or promote products derived from this software without specific prior written permission.

THIS SOFTWARE IS PROVIDED BY THE COPYRIGHT HOLDERS AND CONTRIBUTORS “AS IS” AND ANY EXPRESS OR IMPLIED WARRANTIES, INCLUDING, BUT NOT LIMITED TO, THE IMPLIED WARRANTIES OF MERCHANTABILITY AND FITNESS FOR A PARTICULAR PURPOSE ARE DISCLAIMED. IN NO EVENT SHALL THE COPYRIGHT OWNER OR CONTRIBUTORS BE LIABLE FOR ANY DIRECT, INDIRECT, INCIDENTAL, SPECIAL, EXEMPLARY, OR CONSEQUENTIAL DAMAGES (INCLUDING, BUT NOT LIMITED TO, PROCUREMENT OF SUBSTITUTE GOODS OR SERVICES; LOSS OF USE, DATA, OR PROFITS; OR BUSINESS INTERRUPTION) HOWEVER CAUSED AND ON ANY THEORY OF LIABILITY, WHETHER IN CONTRACT, STRICT LIABILITY, OR TORT (INCLUDING NEGLIGENCE OR OTHERWISE) ARISING IN ANY WAY OUT OF THE USE OF THIS SOFTWARE, EVEN IF ADVISED OF THE POSSIBILITY OF SUCH DAMAGE.

### A.1.2.4 ScyPy License

From: <https://www.scipy.org/scipylib/license.html>

Copyright © 2001, 2002 Enthought, Inc.

All rights reserved.

Copyright © 2003-2013 SciPy Developers.

All rights reserved.

Redistribution and use in source and binary forms, with or without modification, are permitted provided that the following conditions are met:

Redistributions of source code must retain the above copyright notice, this list of conditions and the following disclaimer.

Redistributions in binary form must reproduce the above copyright notice, this list of conditions and the following disclaimer in the documentation and/or other materials provided with the distribution.

Neither the name of Enthought nor the names of the SciPy Developers may be used to endorse or promote products derived from this software without specific prior written permission.

THIS SOFTWARE IS PROVIDED BY THE COPYRIGHT HOLDERS AND CONTRIBUTORS "AS IS" AND ANY EXPRESS OR IMPLIED WARRANTIES, INCLUDING, BUT NOT LIMITED TO, THE IMPLIED WARRANTIES OF MERCHANTABILITY AND FITNESS FOR A PARTICULAR PURPOSE ARE DISCLAIMED. IN NO EVENT SHALL THE REGENTS OR CONTRIBUTORS BE LIABLE FOR ANY DIRECT, INDIRECT, INCIDENTAL, SPECIAL, EXEMPLARY, OR CONSEQUENTIAL DAMAGES (INCLUDING, BUT NOT LIMITED TO, PROCUREMENT OF SUBSTITUTE GOODS OR SERVICES; LOSS OF USE, DATA, OR PROFITS; OR BUSINESS INTERRUPTION) HOWEVER CAUSED AND ON ANY THEORY OF LIABILITY, WHETHER IN CONTRACT, STRICT LIABILITY, OR TORT (INCLUDING NEGLIGENCE OR OTHERWISE) ARISING IN ANY WAY OUT OF THE USE OF THIS SOFTWARE, EVEN IF ADVISED OF THE POSSIBILITY OF SUCH DAMAGE.

### A.1.2.5Pandas License

From: <http://pandas.pydata.org/pandas-docs/stable/overview.html#license>

#### BSD 3-Clause License

Copyright (c) 2008-2012, AQR Capital Management, LLC, Lambda Foundry, Inc. and PyData Development Team.  
All rights reserved.

Redistribution and use in source and binary forms, with or without modification, are permitted provided that the following conditions are met:

Redistributions of source code must retain the above copyright notice, this list of conditions and the following disclaimer.

Redistributions in binary form must reproduce the above copyright notice, this list of conditions and the following disclaimer in the documentation and/or other materials provided with the distribution.

Neither the name of the copyright holder nor the names of its contributors may be used to endorse or promote products derived from this software without specific prior written permission.

THIS SOFTWARE IS PROVIDED BY THE COPYRIGHT HOLDERS AND CONTRIBUTORS "AS IS" AND ANY EXPRESS OR IMPLIED WARRANTIES, INCLUDING, BUT NOT LIMITED TO, THE IMPLIED WARRANTIES OF MERCHANTABILITY AND FITNESS FOR A PARTICULAR PURPOSE ARE DISCLAIMED. IN NO EVENT SHALL THE COPYRIGHT HOLDER OR CONTRIBUTORS BE LIABLE FOR ANY DIRECT, INDIRECT, INCIDENTAL, SPECIAL, EXEMPLARY, OR CONSEQUENTIAL DAMAGES (INCLUDING, BUT NOT LIMITED TO, PROCUREMENT OF SUBSTITUTE GOODS OR SERVICES; LOSS OF USE, DATA, OR PROFITS; OR BUSINESS INTERRUPTION) HOWEVER CAUSED AND ON ANY THEORY OF LIABILITY, WHETHER IN CONTRACT, STRICT LIABILITY, OR TORT (INCLUDING NEGLIGENCE OR OTHERWISE) ARISING IN ANY WAY OUT OF THE USE OF THIS SOFTWARE, EVEN IF ADVISED OF THE POSSIBILITY OF SUCH DAMAGE.

## A.1.2.6 Python License

From: <https://docs.python.org/3/license.html#psf-license-agreement-for-python-release>

### PSF LICENSE AGREEMENT FOR PYTHON 3.7.1¶

1. This LICENSE AGREEMENT is between the Python Software Foundation ("PSF"), and the Individual or Organization ("Licensee") accessing and otherwise using Python 3.7.1 software in source or binary form and its associated documentation.
2. Subject to the terms and conditions of this License Agreement, PSF hereby grants Licensee a nonexclusive, royalty-free, world-wide license to reproduce, analyze, test, perform and/or display publicly, prepare derivative works, distribute, and otherwise use Python 3.7.1 alone or in any derivative version, provided, however, that PSF's License Agreement and PSF's notice of copyright, i.e., "Copyright © 2001-2018 Python Software Foundation; All Rights Reserved" are retained in Python 3.7.1 alone or in any derivative version prepared by Licensee.
3. In the event Licensee prepares a derivative work that is based on or incorporates Python 3.7.1 or any part thereof, and wants to make the derivative work available to others as provided herein, then Licensee hereby agrees to include in any such work a brief summary of the changes made to Python 3.7.1.
4. PSF is making Python 3.7.1 available to Licensee on an "AS IS" basis. PSF MAKES NO REPRESENTATIONS OR WARRANTIES, EXPRESS OR IMPLIED. BY WAY OF EXAMPLE, BUT NOT LIMITATION, PSF MAKES NO AND DISCLAIMS ANY REPRESENTATION OR WARRANTY OF MERCHANTABILITY OR FITNESS FOR ANY PARTICULAR PURPOSE OR THAT THE USE OF PYTHON 3.7.1 WILL NOT INFRINGE ANY THIRD PARTY RIGHTS. 5. PSF SHALL NOT BE LIABLE TO LICENSEE OR ANY OTHER USERS OF PYTHON 3.7.1 FOR ANY INCIDENTAL, SPECIAL, OR CONSEQUENTIAL DAMAGES OR LOSS AS A RESULT OF MODIFYING, DISTRIBUTING, OR OTHERWISE USING PYTHON 3.7.1, OR ANY DERIVATIVE THEREOF, EVEN IF ADVISED OF THE POSSIBILITY THEREOF.
6. This License Agreement will automatically terminate upon a material breach of its terms and conditions.
7. Nothing in this License Agreement shall be deemed to create any relationship of agency, partnership, or joint venture between PSF and Licensee. This License Agreement does not grant permission to use PSF trademarks or trade name in a trademark sense to endorse or promote products or services of Licensee, or any third party.
8. By copying, installing or otherwise using Python 3.7.1, Licensee agrees to be bound by the terms and conditions of this License Agreement.

### A.1.2.7 Spyder License

From: <https://pypi.org/project/spyder/>. Spyder was released under MIT License (MIT)

From <https://opensource.org/licenses/MIT>

Permission is hereby granted, free of charge, to any person obtaining a copy of this software and associated documentation files (the "Software"), to deal in the Software without restriction, including without limitation the rights to use, copy, modify, merge, publish, distribute, sublicense, and/or sell copies of the Software, and to permit persons to whom the Software is furnished to do so, subject to the following conditions:

The above copyright notice and this permission notice shall be included in all copies or substantial portions of the Software.

THE SOFTWARE IS PROVIDED "AS IS", WITHOUT WARRANTY OF ANY KIND, EXPRESS OR IMPLIED, INCLUDING BUT NOT LIMITED TO THE WARRANTIES OF MERCHANTABILITY, FITNESS FOR A PARTICULAR PURPOSE AND NONINFRINGEMENT. IN NO EVENT SHALL THE AUTHORS OR COPYRIGHT HOLDERS BE LIABLE FOR ANY CLAIM, DAMAGES OR OTHER LIABILITY, WHETHER IN AN ACTION OF CONTRACT, TORT OR OTHERWISE, ARISING FROM, OUT OF OR IN CONNECTION WITH THE SOFTWARE OR THE USE OR OTHER DEALINGS IN THE SOFTWARE.

## A.2 APDS Workflow

The script “Run1\_APDS\_2018.py” implements a workflow example to model the steam-chamber for two geostatistical realizations with APDS. Figure B.1 shows that the Project folder initially has 2 subfolders. The subfolder “0\_Data” contains the vertical and horizontal permeabilities (KV1.npy, KV2.npy, KH1.npy, KH2.npy), the porosity (PHI1.npy, PHI2.npy), the water saturation (SW1.npy, SW2.npy), the rock-types (TRT1.npy, TRT2.npy) and the null cells (NullCells.npy). The subfolder “1\_Well-Trajectory” contains the producer well trajectory. The input data are NumPy arrays in GSLIB format.

After executing the “Run1\_APDS\_2018” program, 4 new subfolders are generated. The subfolder “3\_Graph-Sinks” contains the outputs of the Graph generator module, that is, the Graphs (Graph\_1.npy, Graph\_2.npy) and the Sinks (Sinks\_1.npy, Sinks\_2.npy). The subfolder “4\_Steam-Chamber” contains the outputs of the Steam-chamber generator module, that is, the ordered sequence of cells to build the steam-chambers (Chamberorder\_1.npy, Chamberorder\_2.npy) with their ranking values (Chambertime\_1.npy, Chambertime\_2.npy). Finally, the subfolder “5\_VTK” contains the outputs of the Post-processing module, that is, the VTK files (SteamChamber\_1.vtk, SteamChamber\_2.vtk ) for visualizing the steam-chambers in a third-party software.

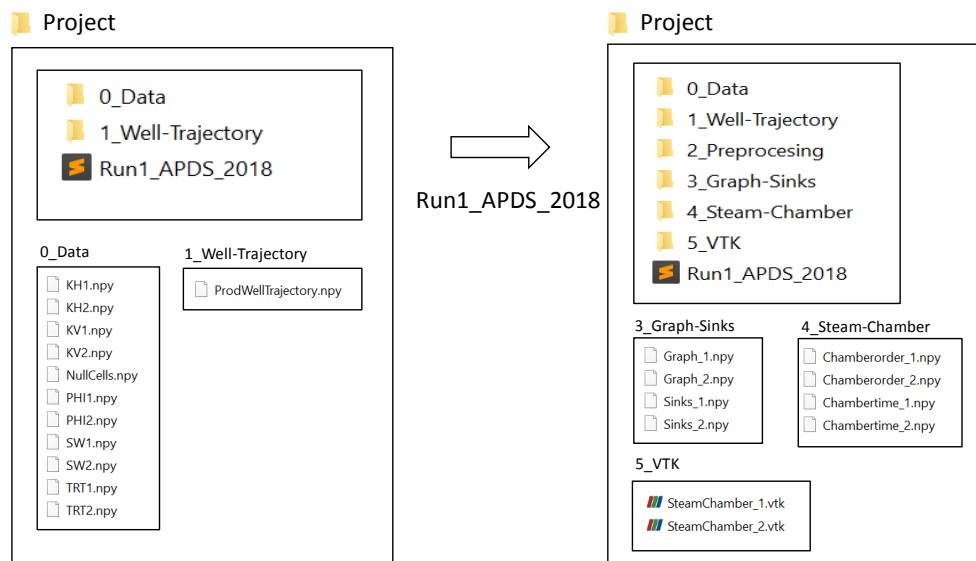


Figure A.1: Workflow to run APDS.

```

1 *****
2 **NAME: Run1_APDS_2018.py
3 **APPROXIMATE PHYSICS DISCRETE SIMULATOR (APDS)
4 ** WORKFLOW
5 *****
6 #####
7 ## Import Modules: pygeostat, pqdict, numpy, pandas
8 #####
9
10 import pygeostat as gs      # Read CCG terms of use
11 from pqdict import minpq    # Used by sagdgeom. MIT License.
12 import numpy as np         # Read License
13 import pandas as pd        # Read License
14 from math import cos, acos, atan, degrees, sin, radians
15 import os
16
17 #####
18 ## Licenses
19 #####
20 #####
21 ## MIT License for pqdict and Spyder
22 ## https://pqdict.readthedocs.io/en/latest/intro.html#license
23 ## https://pypi.org/project/spyder/
24 ## https://opensource.org/licenses/MIT
25 #####
26 THE SOFTWARE IS PROVIDED "AS IS", WITHOUT WARRANTY OF ANY KIND, EXPRESS OR IMPLIED,
27 INCLUDING BUT NOT LIMITED TO THE WARRANTIES OF MERCHANTABILITY, FITNESS FOR A
28 PARTICULAR PURPOSE AND NONINFRINGEMENT. IN NO EVENT SHALL THE AUTHORS OR COPYRIGHT
29 HOLDERS BE LIABLE FOR ANY CLAIM, DAMAGES OR OTHER LIABILITY, WHETHER IN AN ACTION OF
30 CONTRACT, TORT OR OTHERWISE, ARISING FROM, OUT OF OR IN CONNECTION WITH THE SOFTWARE
31 OR THE USE OR OTHER DEALINGS IN THE SOFTWARE.
32 #####
33 #####
34 ## CCG Terms of Use for pygeostat software
35 #####
36 THE SOFTWARE IS PROVIDED "AS IS", WITHOUT WARRANTY OF ANY KIND, EXPRESS OR IMPLIED,
37 INCLUDING BUT NOT LIMITED TO THE WARRANTIES OF MERCHANTABILITY, FITNESS FOR A
38 PARTICULAR PURPOSE AND NONINFRINGEMENT. IN NO EVENT SHALL THE AUTHORS OR COPYRIGHT
39 HOLDERS BE LIABLE FOR ANY CLAIM, DAMAGES OR OTHER LIABILITY, WHETHER IN AN ACTION OF

```

40 CONTRACT, TORT OR OTHERWISE, ARISING FROM, OUT OF OR IN CONNECTION WITH THE SOFTWARE  
41 OR THE USE OR OTHER DEALINGS IN THE SOFTWARE.

42 #####

43

44 #####

45 ## Python License

46 ## <https://docs.python.org/3/license.html#psf-license-agreement-for-python-release>

47 #####

48 PSF is making Python 3.7.1 available to Licensee on an "AS IS" basis. PSF MAKES NO REPRESENTATIONS OR  
49 WARRANTIES, EXPRESS OR IMPLIED. BY WAY OF EXAMPLE, BUT NOT LIMITATION, PSF MAKES NO  
50 AND DISCLAIMS ANY REPRESENTATION OR WARRANTY OF MERCHANTABILITY OR FITNESS FOR  
51 ANY PARTICULAR PURPOSE OR THAT THE USE OF PYTHON 3.7.1 WILL NOT INFRINGE ANY THIRD  
52 PARTY RIGHTS. 5. PSF SHALL NOT BE LIABLE TO LICENSEE OR ANY OTHER USERS OF PYTHON 3.7.1  
53 FOR ANY INCIDENTAL, SPECIAL, OR CONSEQUENTIAL DAMAGES OR LOSS AS A RESULT OF  
54 MODIFYING, DISTRIBUTING, OR OTHERWISE USING PYTHON 3.7.1, OR ANY DERIVATIVE THEREOF,  
55 EVEN IF ADVISED OF THE POSSIBILITY THEREOF.

56 #####

57

58 #####

59 ## numPy License

60 ## <http://www.numpy.org/license.html>

61 #####

62

63 THIS SOFTWARE IS PROVIDED BY THE COPYRIGHT HOLDERS AND CONTRIBUTORS "AS IS" AND ANY  
64 EXPRESS OR IMPLIED WARRANTIES, INCLUDING, BUT NOT LIMITED TO, THE IMPLIED WARRANTIES  
65 OF MERCHANTABILITY AND FITNESS FOR A PARTICULAR PURPOSE ARE DISCLAIMED. IN NO EVENT  
66 SHALL THE COPYRIGHT OWNER OR CONTRIBUTORS BE LIABLE FOR ANY DIRECT, INDIRECT,  
67 INCIDENTAL, SPECIAL, EXEMPLARY, OR CONSEQUENTIAL DAMAGES (INCLUDING, BUT NOT LIMITED  
68 TO, PROCUREMENT OF SUBSTITUTE GOODS OR SERVICES; LOSS OF USE, DATA, OR PROFITS; OR  
69 BUSINESS INTERRUPTION) HOWEVER CAUSED AND ON ANY THEORY OF LIABILITY, WHETHER IN  
70 CONTRACT, STRICT LIABILITY, OR TORT (INCLUDING NEGLIGENCE OR OTHERWISE) ARISING IN ANY  
71 WAY OUT OF THE USE OF THIS SOFTWARE, EVEN IF ADVISED OF THE POSSIBILITY OF SUCH DAMAGE.

72

73 #####

74 ## scyPy License

75 ## <https://www.scipy.org/scipylib/license.html>

76 #####

77 THIS SOFTWARE IS PROVIDED BY THE COPYRIGHT HOLDERS AND CONTRIBUTORS "AS IS" AND ANY  
78 EXPRESS OR IMPLIED WARRANTIES, INCLUDING, BUT NOT LIMITED TO, THE IMPLIED WARRANTIES  
79 OF MERCHANTABILITY AND FITNESS FOR A PARTICULAR PURPOSE ARE DISCLAIMED. IN NO EVENT  
80 SHALL THE REGENTS OR CONTRIBUTORS BE LIABLE FOR ANY DIRECT, INDIRECT, INCIDENTAL,  
81 SPECIAL, EXEMPLARY, OR CONSEQUENTIAL DAMAGES (INCLUDING, BUT NOT LIMITED TO,  
82 PROCUREMENT OF SUBSTITUTE GOODS OR SERVICES; LOSS OF USE, DATA, OR PROFITS; OR BUSINESS  
83 INTERRUPTION) HOWEVER CAUSED AND ON ANY THEORY OF LIABILITY, WHETHER IN CONTRACT,  
84 STRICT LIABILITY, OR TORT (INCLUDING NEGLIGENCE OR OTHERWISE) ARISING IN ANY WAY OUT  
85 OF THE USE OF THIS SOFTWARE, EVEN IF ADVISED OF THE POSSIBILITY OF SUCH DAMAGE.

86  
87 #####

88 ## Pandas License  
89 ## <http://pandas.pydata.org/pandas-docs/stable/overview.html#license>  
90 #####

91  
92 THIS SOFTWARE IS PROVIDED BY THE COPYRIGHT HOLDERS AND CONTRIBUTORS "AS IS" AND ANY  
93 EXPRESS OR IMPLIED WARRANTIES, INCLUDING, BUT NOT LIMITED TO, THE IMPLIED WARRANTIES  
94 OF MERCHANTABILITY AND FITNESS FOR A PARTICULAR PURPOSE ARE DISCLAIMED. IN NO EVENT  
95 SHALL THE COPYRIGHT HOLDER OR CONTRIBUTORS BE LIABLE FOR ANY DIRECT, INDIRECT,  
96 INCIDENTAL, SPECIAL, EXEMPLARY, OR CONSEQUENTIAL DAMAGES (INCLUDING, BUT NOT LIMITED  
97 TO, PROCUREMENT OF SUBSTITUTE GOODS OR SERVICES; LOSS OF USE, DATA, OR PROFITS; OR  
98 BUSINESS INTERRUPTION) HOWEVER CAUSED AND ON ANY THEORY OF LIABILITY, WHETHER IN  
99 CONTRACT, STRICT LIABILITY, OR TORT (INCLUDING NEGLIGENCE OR OTHERWISE) ARISING IN ANY  
100 WAY OUT OF THE USE OF THIS SOFTWARE, EVEN IF ADVISED OF THE POSSIBILITY OF SUCH DAMAGE.

101  
102 #####

103  
104 #####  
105 ## Folders with Outputs. Example of Workflow  
106 #####

107  
108 if not os.path.exists ('2\_Preprocessing'):  
109 os.makedirs ('2\_Preprocessing')  
110  
111 if not os.path.exists ('3\_Graph-Sinks'): # For Graphs and Sinks  
112 os.makedirs ('3\_Graph-Sinks')  
113  
114 if not os.path.exists ('4\_Steam-Chamber'):  
115 os.makedirs ('4\_Steam-Chamber') # For Chambertime and Chamberorder  
116  
117 if not os.path.exists ('5\_VTK'):  
118 os.makedirs ('5\_VTK') # For VTK files

```

118     os.makedirs ('5_VTK')
119
120     #####
121     ## Create Paths for Input and Output Data
122     #####
123
124     datapath = '0_Data/'
125     wellpath = '1_Well-Trajectory/'
126     procpath = '2_Preprocesing/'
127     graphpath = '3_Graph-Sinks/'
128     stchpath = '4_Steam-Chamber/'
129     vtkpath = '5_VTK/'
130
131
132     #####
133     ## Grid Definition
134     #####
135
136     grdstr=""40 1 25 - nx, xmn, xsiz
137           100 1 1 - ny , ymn , ysiz
138           50 1 1 - nz , zmn , zsiz ""
139
140     griddef = gs.GridDef (gridstr = gridstr)
141
142     nx = griddef.nx           # For convenience
143     ny = griddef.ny
144     nz = griddef.nz
145     xsiz = griddef.xsiz
146     ysiz = griddef.ysiz
147     zsiz = griddef.zsiz
148
149     #####
150     ## Constant, Conversion Factors
151     #####
152     m3ToStb = 6.28981      # Convert m3 to bbl
153     Resid_So = 0.25       # APDS input. Residual Oil Saturation
154     kvCutoff = 200        # kv Cut-off in md
155     BulkCellVol = xsiz*ysiz*zsiz*m3ToStb # Bulk cell volume in m3
156
157     #####
158     ## Load Well Trajectories
159     #####
160
161     well1= np.load (wellpath + 'ProdWellTrajectory.npy') # Producer Well
162     well2 = range(0,0)   # Range (0,0) if there is one well
163     source = load2wells(well1,well2)

```

```

164     injtracj = range (0,0) # Injector well trajectory
165
166     #####
167     ## Loop for 1 to N Geostatistical Realizations
168     #####
169
170     NReal = [1,2]      # List of realization indexes. This example has 2 realizations
171
172     for i in NReal:
173
174         #####
175         ## Load Input Data
176         #####
177
178         APDSRT = np.load (datapath + 'TRT%i.npy'%i)      # Rock Type
179         APDSPhi = np.load (datapath + 'PHI%i.npy'%i)     # Porosity
180         APDSKv = np.load (datapath + 'KV%i.npy'%i)      # KV
181         APDSKh = np.load (datapath + 'KH%i.npy'%i)      # KH
182         APDSSw = np.load (datapath + 'SW%i.npy'%i)      # SW
183         APDSNull = np.load (datapath + 'NullCells.npy') # 1 - 0
184
185         #####
186         ## Creating a Data-Frame
187         #####
188
189         df = pd.DataFrame ( {'Kv':APDSKv,
190                             'Kh':APDSKh,'RT':APDSRT,'Phi':APDSPhi,'Sw':APDSSw,'Null':APDSNull})
191
192         #####
193         ## Processing Rock-types ('RTGraph') to obtain a binary variable, (1) for net-rock and
194         ## (0) for non-net rock, to input the Graph Generator
195         ## The Hydrocarbon Cell Volume (HCV) is calculated
196         ## A dataframe is not necessary, but is convenient to work with Pandas
197         #####
198
199         df ['RTGraph'] = df ['RT']
200         df ['RTGraph'][df ['RTGraph'] == 5] = 0      # Rock Type 5 is shale. Code as 0
201         df ['RTGraph'][df ['RTGraph'] != 0] = 1     # Rock Types 2,3,4 != 0 are now 1
202         df ['RTGraph'][df ['Kv'] <= KvCutoff] = 0  # Apply Kv Cut-off
203         df ['RTGraph'][df ['Kv'] > KvCutoff] = 1   # Apply Kv Cut-off
204         df ['RTGraph'] = df ['RTGraph']* df ['Null'] # Apply Null Cells
205         df ['HCV'] = BulkCellVol*df['Phi']*((1-df ['Sw']) - Resid_So)
206         df ['HCV'][df ['HCV'] < 0] = 0             # If HCV is negative, then replace by zero
207
208
209     #####

```

```

210  ## Inputs to "Mygraph" program
211  #####
212
213      gslib = np.array (df['RTGraph'])          # mygraph program requires np.array
214      NCVapds = np.array (df['HCV'])
215      Kvapds = np.array (df['Kv'])
216      Khapds = np.array (df['Kh'])
217
218  #####
219  # Graph Generator Module
220  #####
221
222      Graph, sinks = mygraph (gslib, nx, ny, nz, Kvapds, Khapds, NCVapds)
223
224  #####
225  # Steam-Chamber Generator Module
226  #####
227
228      chambertime, chamberorder, parent_sink = saggeom (Graph, source, injtracj, sinks)
229  #####
230  ##  Save Graph, Sinks, Chambertime and Chamberorder
231  #####
232
233      np.save (graphpath + 'Sinks_%i'%(i), sinks)
234      np.save (graphpath + 'Graph_%i'%(i), Graph)
235      np.save (stchpath + 'Chambertime_%i'%(i), chambertime)
236      np.save (stchpath + 'Chamberorder_%i'%(i), chamberorder)
237
238  #####
239  ## Post-Processing Module
240  #####
241
242      grid= GridVTK (chamberorder, chambertime, nx, ny, nz)
243
244      VTKPlot (grdstr, grid, 'Time', vtkpath + 'SteamChamber_%i. vtk'%(i))
245
246  *****
247  ** End of Program
248  ** *****

```

```

1 *****
2 ** def load2wells (range1, range2):
3 *****
4 #####
5 ## Program Description
6 #####
7
8     Author: Enrique Gallardo
9     Date: June 2017
10    Use: Add two horizontal wells into a single list to generate the APDS's source. This
11    program is required by "Run1_APDS_2018.py"
12    Input:
13    range1: NumPy array with the indexes of the producer well trajectory
14    range2: NumPy array with the indexes of the producer well trajectory
15    Output:
16    source: python list with consolidated trajectories to steam-chamber module
17
18    #####
19
20    well1 = []
21    well2 = []
22
23    for iter in range1:
24        well1.append (iter)
25
26    for iter in range2:
27        well2.append (iter)
28
29    source=well1 + well2
30
31    return source
32
33 *****
34 ** End of Program
35 *****

```

### A.3 APDS Programs

APDS programs are presented by modules and in order of appearance.

#### A.3.1 Graph Generator Module Programs

```
1 *****
2 **def mygraph (gslib, nx, ny, nz, kv, kh, NetCelVol):
3 *****
4 #####
5 ## Program Description
6 #####
7
8     Author: Enrique Gallardo
9     Date: February 2018
10    Use: Identify unstimulated planes in a SAGD process
11    Input:
12    gslib: Binary (0-1) NumPy-array. 0 non-reservoir and 1 reservoir
13    nx, ny, nz: Cells in the grid in x, y, z directions, respectively
14    kv, kh: NumPy-array with vertical and horizontal permeabilities
15    NetCelVol: Numpy-array with net cell volumes
16    Output:
17    dict_unstplanes: Dictionary keyed with unst_idx and values is a
18    list with the unstimulated planes
19    set_unstplanes: Set with indexes of unstimulated cells
20    Output:
21    mygraph: Graph
22    set_sinks: Set with the sink cells
23
24 #####
25
26    import collections
27    keys_sand,_ = RockType_split(gslib)
28    SetOutSide = outside (nx, ny, nz)
29
30 #####
31 ## Mask Definitions
32 #####
33
34    bilevel_mask = [1,1,1,1,0,1,1,1,1,1,1,1,1,1,1,1,1]
35    lf_mask = [0,1,1,0,0,1,0,1,1,0,1,1,0,1,1,0,1,1]
36    ff_mask = [0,0,0,1,0,1,1,1,1,0,0,0,1,1,1,1,1,1]
37    rf_mask = [1,1,0,1,0,0,1,1,0,1,1,0,1,1,0,1,1,0]
```

```

38  bf_mask = [1,1,1,1,0,1,0,0,0,1,1,1,1,1,1,0,0,0]
39  flb_mask = [0,0,0,0,0,1,0,1,1,0,0,0,0,1,1,0,1,1]
40  frb_mask = [0,0,0,1,0,0,1,1,0,0,0,0,1,1,0,1,1,0]
41  brb_mask = [1,1,0,1,0,0,0,0,0,1,1,0,1,1,0,0,0,0]
42  blb_mask = [0,1,1,0,0,1,0,0,0,0,1,1,0,1,1,0,0,0]
43  tf_mask = [1,1,1,1,0,1,1,1,1,0,0,0,0,0,0,0,0,0]
44  tlf_mask = [0,1,1,0,0,1,0,1,1,0,0,0,0,0,0,0,0,0]
45  tff_mask = [0,0,0,1,0,1,1,1,1,0,0,0,0,0,0,0,0,0]
46  trf_mask = [1,1,0,1,0,0,1,1,0,0,0,0,0,0,0,0,0,0]
47  tbf_mask = [1,1,1,1,0,1,0,0,0,0,0,0,0,0,0,0,0,0]
48  fltc_mask = [0,0,0,0,0,1,0,1,1,0,0,0,0,0,0,0,0,0]
49  frtc_mask = [0,0,0,1,0,0,1,1,0,0,0,0,0,0,0,0,0,0]
50  brtc_mask = [1,1,0,1,0,0,0,0,0,0,0,0,0,0,0,0,0,0]
51  bltc_mask = [0,1,1,0,0,1,0,0,0,0,0,0,0,0,0,0,0,0]
52
53  #####
54  ## Location Indexes
55  #####
56
57  lfidx_all = [nx*iy for iy in range(ny*(nz))]
58  ffidx_all = [ix+(nx*ny*(iz)) for iz in range((nz)) for ix in range(nx)]
59  rfidx_all = [nx*(iy+1)-1 for iy in range(ny*(nz))]
60  bfidx_all = [(ix+(nx*ny*(iz)))+(nx*(ny-1)) for iz in range((nz)) for ix in range(nx)]
61  lf_idx = lfidx_all[:ny*(nz-1)]
62  ff_idx = ffidx_all[:nx*(nz-1)]
63  rf_idx = rfidx_all[:ny*(nz-1)]
64  bf_idx = bfidx_all[:nx*(nz-1)]
65  tlf_idx = lfidx_all[ny*(nz-1):]
66  tff_idx = ffidx_all[nx*(nz-1):]
67  trf_idx = rfidx_all[ny*(nz-1):]
68  tbf_idx = bfidx_all[nx*(nz-1):]
69  flb_idx = [nx*ny*(iz+1)-(nx*ny) for iz in range(nz-1)]
70  frb_idx = [nx*ny*(iz+1)-(nx*ny)+nx-1 for iz in range(nz-1)]
71  brb_idx = [nx*ny*(iz+1)-1 for iz in range(nz-1)]
72  blb_idx = [nx*ny*(iz+1)-nx for iz in range(nz-1)]
73  fltc_idx = [nx*ny*(nz)-(nx*ny)]
74  frtc_idx = [nx*ny*(nz)-(nx*ny)+nx-1]
75  brtc_idx = [nx*ny*(nz)-1]
76  bltc_idx = [nx*ny*(nz)-nx]
77  tf_idx = [(nx*ny*(nz-1))+ix for ix in range(nx*ny)]
78
79  #####
80  ## Apply Masks
81  #####
82
83  Mygraph = collections.defaultdict (dict) # Dictionaries

```

```

84 set_sinks = set()                # Set of sinks
85
86 for loc in keys_sand:
87
88     if loc not in SetOutSide:
89         neighbors, Hnbors = applymask (loc, bilevel_mask)
90
91     else:
92
93         if loc in lf_idx:
94             neighbors, Hnbors = applymask(loc, lf_mask)
95
96         if loc in ff_idx:
97             neighbors, Hnbors = applymask(loc, ff_mask)
98
99         if loc in rf_idx:
100            neighbors, Hnbors = applymask(loc, rf_mask)
101
102         if loc in bf_idx:
103             neighbors, Hnbors = applymask(loc, bf_mask)
104         if loc in flb_idx:
105             neighbors, Hnbors = applymask(loc, flb_mask)
106
107         if loc in frb_idx:
108             neighbors, Hnbors = applymask(loc, frb_mask)
109
110         if loc in brb_idx:
111             neighbors, Hnbors = applymask(loc, brb_mask)
112
113         if loc in blb_idx:
114             neighbors, Hnbors = applymask(loc, blb_mask)
115
116         if loc in tf_idx:
117             neighbors, Hnbors = applymask(loc, tf_mask)
118
119         if loc in tlf_idx:
120             neighbors, Hnbors = applymask(loc, tlf_mask)
121
122         if loc in tff_idx:
123             neighbors, Hnbors = applymask(loc, tff_mask)
124
125         if loc in trf_idx:
126             neighbors, Hnbors = applymask(loc, trf_mask)
127
128         if loc in tbf_idx:
129             neighbors, Hnbors = applymask(loc, tbf_mask)

```

```

130     if loc in fltc_idx:
131         neighbors, Hnbors = applymask(loc, fltc_mask)
132
133     if loc in frtc_idx:
134         neighbors, Hnbors = applymask(loc, frtc_mask)
135
136     if loc in brtc_idx:
137         neighbors, Hnbors = applymask(loc, brtc_mask)
138
139     if loc in bltc_idx:
140         neighbors, Hnbors = applymask(loc, bltc_mask)
141
142     #####
143     ## Sinks
144     #####
145
146     tsink = identifysink(Hnbors, gslib, loc)
147     set_sinks.add (tsink)
148
149     #####
150     ## Loop to Populate the Graph
151     #####
152
153     for neigh in neighbors:
154         if gslib[neigh]==0:
155             continue
156
157     #####
158     ## Permeabilities
159     #####
160
161     k_av = Harmonick (kv[loc],kv[neigh]) # Vertical permeability
162     k_ah = Harmonick (kh[loc],kh[neigh]) # Horizontal permeability
163
164     #####
165     ## Populating the Graph
166     ## Loc is first key; neigh is second key, and value is a tuple (kv, kh, CellVol)
167     #####
168
169     mygraph[loc][neigh]=[k_av, k_ah, NetCelVol[neigh]]
170
171     return mygraph, set_sinks
172
173     *****
174     ** End of Program
175     ** *****

```

```

1 *****
2 **def RockType_split (RT_array):
3 *****
4 #####
5 ## Program Description
6 #####
7
8     Author: Enrique Gallardo
9     Date: January 2018
10    Use: Split a NumPy binary array into non-reservoir (0) and reservoir cells (1)
11    Input:
12    RT_array: NumPy array coded shale (0) and sand (1)
13    Output:
14    keys_sand: List with 0-phyton indexes for sand (1)
15    keys_shale: List with 0-phyton indexes for shale (0)
16
17 #####
18
19     RT_array0 = np.where(RT_array == 0) # np.where generates iterators
20     RT_array1 = np.where(RT_array == 1)
21
22     keys_sand = RT_array1[0].tolist() # Iterator to list
23     keys_shale = RT_array0[0].tolist()
24
25     return keys_sand, keys_shale
26
27 *****
28 ** End of Program
29 ** *****

```

```

1 *****
2 **def outside (nx, ny, nz):
3 *****
4 #####
5 ## Program Description
6 #####
7
8     Author: Enrique Gallardo
9     Date: February 2018
10    Use: Subroutine identifies cells at the border of the grid
11    Input:
12    nx, ny, nz: Cells in the grid in x, y, z directions, respectively
13    Output:
14    Outside_idx: Set with 0-python indexes of cell at the grid border
15
16 #####
17
18    lfidx_all = [nx*iy for iy in range(ny*(nz))]
19    ffidx_all = [ix + (nx*ny*(iz)) for iz in range((nz)) for ix in range(nx)]
20    rfidx_all = [nx*(iy+1)-1 for iy in range(ny*(nz))]
21    bfidx_all = [(ix + (nx*ny*(iz))) + (nx*(ny-1)) for iz in range((nz)) for ix in range(nx)]
22    tf_idx = [(nx*ny*(nz-1)) + ix for ix in range(nx*ny)]
23    Outside_idx = lfidx_all + ffidx_all + rfidx_all + bfidx_all + tf_idx
24
25    return set (Outside_idx)
26
27 *****
28 ** End of Program
29 ** *****

```

```

1 *****
2 **def applymask (pyloc, mask):
3 *****
4 #####
5 ## Program Description
6 #####
7
8     Author: Enrique Gallardo
9     Date: June 2017
10    Note: Returns a list with Neighbors and Horizontal Neighbors of given cell and mask
11    Input:
12    Pyloc: Location in 0-python index, called pyloc
13    mask: Masks are defined inside the mygraph program
14    Output:
15    Neighbors: 0-python indexes of neighbors
16    Hnbors: 0-python indexes of horizontal neighbors
17
18    #####
19
20    from itertools import compress
21
22    loc=pyloc+1      # 0-python index is converted to 1-gslib index
23
24    #####
25    ## Neighbors
26    #####
27
28    locnbors = [loc-nx-1, loc-nx, loc-nx + 1, loc-1, loc, loc+1, loc+nx-1, loc+nx, loc+nx+1,
29               loc+(nx*ny)-nx-1,loc+(nx*ny)-nx,loc+(nx*ny)-nx+1,loc+(nx*ny)-1,loc+(nx*ny),
30               loc+(nx*ny)+1,loc+(nx*ny)+nx-1,loc+(nx*ny)+nx, loc+(nx*ny)+nx+1]
31
32    #####
33    ##Apply Mask
34    #####
35
36    neighbors = list(compress (locnbors, mask))
37    Hnbors = list(compress (locnbors, mask[:9]))
38    neighbors = [i-1 for i in neighbors] # Subtracting 1 to obtain 0-python indexes
39    Hnbors = [i-1 for i in Hnbors]     # Subtracting 1 to obtain 0-python indexes
40
41    return neighbors, Hnbors
42
43    *****
44    ** End of Program
45    ** *****

```

```

1 *****
2 **def identifysink (Hnbors, gslib, loc):
3 *****
4 #####
5 ## Program Description
6 #####
7
8     Author: Enrique Gallardo
9     Date: June 2017
10    Use: Mark a loc as a potential sink
11    Input:
12    Hnbors: Horizontal neighbors indexes
13    Gslib: Binary (0-1) NumPy-array. 0 for non-reservoir and 1 for reservoir.
14    loc: Location in 1-gslib index order
15    Output:
16    tsink: index of loc that is a potential sink
17
18    #####
19
20    binaryNbors = [gslib[i] for i in Hnbors ] # Mask
21
22    tsink = None # Initializing tsink
23
24    if any(I == 0 for i in binaryNbors):
25        tsink = loc
26
27    return tsink
28
29 *****
30 ** End of Program
31 *****

```

```

1 *****
2 * *def Harmonick (k1, k2):
3 *****
4 #####
5 ## Program Description
6 #####
7
8     Author: Enrique Gallardo
9     Date: June 2017
10    Use: Calculate harmonic average permeability
11    Input:
12    k1 and k2: Cell permeabilities in md
13    Output:
14    Harmonic average permeability in md
15
16 #####
17
18     harmk=1 / ((1/2) * ((1/k1) + (1/k2)))
19
20     return harmk
21
22 *****
23 ** End of Program
24 *****

```

### A.3.2 Steam-Chamber Module Programs

```
1 *****
2 **def sagdgeom (graph, source, injtracj, sinks):
3 *****
4 #####
5 ## Program Description
6 #####
7
8     Author: Enrique Gallardo
9     Date: February 2018
10    Use: This program generates the steam-chamber
11    Input:
12    graph: The Graph generated by the program mygraph
13    source: The well list generated by the program load2wells
14    injtracj: List with injector well trajectories
15    sinks: The sinks generated by the program mygraph
16    Output:
17    chamber: Dictionary. Key are the locations and value the chambertime
18    chamberorder: List with the order cells are added to steam-chamber
19    parent_sink: Parent sink of every cell
20
21 #####
22 ## Identify Unstimulated Planes
23 #####
24
25     prod_welllocson = np.asarray(source)
26     prod_welllocs1above = np.asarray(source) + (nx*ny*1)
27     prod_welllocs2above = np.asarray(source) + (nx*ny*2)
28     inj_welllocson = injtracj
29
30 #####
31 ## Concatenate all and get Unstimulated Indexes
32 #####
33
34     inj_welllocs =
35     np.concatenate([prod_welllocson,prod_welllocs1above,prod_welllocs2above,
36     inj_welllocson])
37     unst_idx = UnstimulatedidxsGraph(graph,inj_welllocs)
38
39 #####
40 ## Add to Unstimulated Indexes the Head and Toe of the Source Well
41 #####
42
43     head_idx = source[0]-1
44     toe_idx = source[-1]+1
```

```

45     unst_idx.append (head_idx)
46     unst_idx.append (toe_idx)
47
48     #####
49     ## Set of Unstimulated Planes
50     #####
51
52     _ , setunstplanes = Unstimulated_Planes (unst_idx, nx, ny, nz)
53
54     #####
55     ## Initializing Containers and Constants
56     #####
57
58     chamber = {}           # Dictionary. Keys are nodes. Values are model time
59     parent_sink = {}      # Dictionary. Keys are nodes. Values are parent sinks
60     pqedge = minpq()      # Priority queue
61     chamberorder = []     # List for chamberorder
62     sourcelist = []       # List for well trajectories
63     grav_fu = 32.174      # Gravity in field units [ft/sec2]
64     densityConvF = 16.01846 # Multiply lbm/ft3 * Conversion factor to get [kg/m3]
65     TransmConvF = 1.127   # Conversion factor to get field units
66     GravityConvF = 0.21584*1e-3 # Conversion factor to get field units
67     decexp = 1.003        # Deceleration Exponent. [1.003 is default. Dimensionless]
68
69     #####
70     # User Inputs.
71     #####
72
73     dens_bit = 1000       # Bitumen density [kg/m3] at steam temperature
74     m = 4.1               # Butler's temperature-viscosity exponent. Common range
75                           # is 3-5. See equation 3.5
76     visc = 7.31           # Kinematic viscosity at steam temperature [cp]
77     PermFactor=0.25       # Relative oil permeability [fraction]
78     maxtime = 3650        # Steam-chamber modeling time [days]
79     preheattime = 120     # Time to establish communication between producer
80                           # and injector well in days [120 days is default]
81
82     #####
83     ## Initialization from the Source List
84     #####
85
86     for i in source:
87
88         pqedge[i] = 0      # Initializing cells in source
89         parent_sink [i] = i # Initializing the parent sink
90         sinks.add (i)      # List of sinks is updated with well trajectory (source)

```

```

91     sourcelist.append (i) # Source as a list
92     set_sinks = sinks      # Sets are more efficient
93
94     #####
95     ## While Priority Queue is not empty, do this loop
96     #####
97
98     while pqedge:
99         node, cellTime = pqedge.popitem()
100        AbsTime = (cellTime**decexp)
101        chamber [node] = AbsTime
102        chamberorder.append (node)
103
104        if AbsTime > maxtime:          # Break loop if maxtime is reached
105            break
106        if node in set_sinks:
107            temp_parentsink = node
108        else:
109            temp_parentsink = parent_sink[node]
110
111        #####
112        ## Iterate the Neighbors
113        #####
114
115        for neighbor in graph[node]:
116
117            if neighbor in chamber:
118                continue
119
120            if (neighbor in pqedge) and (parent_sink[neighbor] == temp_parentsink):
121                continue
122
123        #####
124        ## Rules for Oil Viscosity
125        #####
126
127        if AbsTime < preheattime:      # Preheating time viscosity
128            visc= 3
129
130        if neighbor in setunstplanes:  # Viscosity for unstimulated planes
131            visc= 500
132
133        #####
134        ## Travel Cell Time Calculations
135        #####
136

```

```

137     s_angl,_ = s_ang3D (temp_parentsink, neighbor, nx, ny, nz, xsiz, ysiz, zsiz)
138     alpha=(90-s_angl)      # Alpha is the sink angle
139     Harm_k =
140     (((graph[node][neighbor][0])*sin(radians(alpha))**2) +
141     ((graph[node][neighbor][1])*cos(radians(alpha))**2)) / 1000
142
143     if alpha <= 10:
144         PotentGrad = 0.000001      # To avoid numerical instabilities
145     else:
146         PotentGrad = sin(radians(alpha))
147
148     Area_ft = AreaFlow (alpha, xsiz, ysiz, zsiz)
149     Qrate =
150     (TransmConvF*Area_ft*(Harm_k*PermFactor)*
151     (dens_bit/densityConvF)*GravityConvF*grav_fu*PotentGrad)/(visc*m)
152     new_rel_celltime = (graph[node][neighbor][2])/Qrate
153     new_abs_celltime = (new_rel_celltime) + (AbsTime)
154
155     #####
156     ## Update Priority Queue, Parent Sink
157     #####
158
159     if neighbor in pqedge:
160
161         if new_abs_celltime < pqedge[neighbor]:
162             pqedge[neighbor] = new_abs_celltime
163             parent_sink[neighbor] = temp_parentsink
164         else:
165             pqedge[neighbor] = new_abs_celltime
166             parent_sink[neighbor] = temp_parentsink
167
168     return chamber, chamberorder, parent_sink
169
170     *****
171     ** End of program
172     ** *****

```

```

1 *****
2 **def UnstimulatedidxsGraph (Graph, inj_welllocs):
3 *****
4 #####
5 ## Program Description
6 #####
7
8     Author: Enrique Gallardo
9     Date: February 2018
10    Use: Identify unstimulated cells in a SAGD process
11    Input:
12    Graph: Graph
13    inj_welllocs: Indexes of the injector well trajectory
14    Output:
15    unst_idx: List with indexes of unstimulated cells
16
17 #####
18
19    unst_idx=[]
20
21    for loc in inj_welllocs:
22        if not Graph[loc]:
23            unst_idx.append(loc)
24
25    return unst_idx
26
27 *****
28 ** End of Program
29 **
30 *****

```

```

1 *****
2 def Unstimulated_Planes (unst_idx, nx, ny, nz):
3 *****
4 #####
5 ## Program Description
6 #####
7
8     Author: Enrique Gallardo
9     Date: February 2018
10    Use: Identify unstimulated planes in a SAGD process
11    Input:
12    unst_idx: It is the output of the program UnstimulatedidxsGraph
13    nx, ny, nz: Cells in the grid in x, y, z directions, respectively.
14    Output:
15    dict_unstplanes: Dictionary keyed with unst_idx and values is a
16    list with the unstimulated planes
17    set_unstplanes: Set with indexes of unstimulated cells
18
19 #####
20
21    dict_unstplanes = {}      # Dictionary
22    set_unstplanes = set()   # Unstimulated plane set
23
24    for loc in unst_idx:
25        temp_idx = [loc + (nx*i) for i in range (ny*(nz))]
26        dict_unstplanes[loc] = temp_idx
27        set_unstplanes.update (temp_idx)
28
29    return dict_unstplanes, set_unstplanes
30
31 *****
32 ** End of Program
33 ** *****

```

```

1 *****
2 **def s_ang3D (loc1,loc2,nx,ny,nz,xsiz,ysiz,zsiz):
3 *****
4 #####
5 ## Program Description
6 #####
7
8     Author: Enrique Gallardo
9     Date: June 2017
10    Use: Calculate the angle between two cells.
11    Input:
12    loc1, loc2: Two locations using 0-python indexes
13    nx, ny, nz: Cells in the grid in x, y, z directions, respectively.
14    xsiz, ysiz, zsiz: Cell sizes in x, y, z directions, respectively.
15    Output:
16    s_ang: Angle between loc1 and loc2
17    dist: Distance between loc1 and loc 2 in meters
18
19 #####
20
21    vec = np. asarray (gslibindx(loc2,nx,ny,nz)) - np.asarray (gslibindx (loc1,nx,ny,nz))
22
23    dist= np.linalg.norm (vec*[xsiz, ysiz, zsiz])
24
25    if dist==0:          # To avoid an error message of dividing by zero
26        s_ang = None
27
28    else:
29
30        unitvec = (vec*[xsiz, ysiz, zsiz])/np.linalg.norm(vec*[xsiz, ysiz, zsiz])
31
32        s_ang = degrees (acos (unitvec [2]))
33
34    return s_ang, dist
35
36 *****
37 ** End of Program
38 ** *****

```

```

1 *****
2 **def gslibindx (loc, nx, ny, nz):
3 *****
4 #####
5 ## Program Description
6 #####
7
8     Author: Enrique Gallardo
9     Date: June 2017
10    Use: It gets a 0-index Python and return 1-gslib indexes. Needed by other subroutines
11    Input:
12    loc: Location index in 0-index Python order
13    nx, ny, nz: Cells in the grid in x, y, z directions, respectively
14    Output:
15    (ix, iy, iz): Tuple with gslib indexes ix, iy, iz, respectively
16
17 #####
18
19     iz = 1+int(loc/(nx*ny))
20     iy = 1+int((loc - (iz-1)*nx*ny)/nx)
21     ix = ((loc+1) - (iz-1)*(nx*ny)- ((iy-1)*nx))
22
23     return (ix, iy, iz)
24
25 *****
26 ** End of Program
27 ** *****

```

```

1 *****
2 **def AreaFlow (alpha, dx, dy, dz):
3 *****
4 #####
5 ## Program Description
6 #####
7
8     Author: Enrique Gallardo
9     Date: May 2018
10    Use: Transversal area
11    Input:
12    alpha: Complement of sink angle to 90°.
13    dx, dy, dz: Cell sizes in x, y, z directions, respectively. In meters.
14    Output/Return:
15    areaflow: Transversal area in ft2
16
17 #####
18
19    gamma=degrees(atan(dz/dy))
20
21    if alpha <= gamma:
22        areaflow=dz*cos(radians(alpha)) * dx*10.763
23    else:
24        areaflow=dy*sin(radians(alpha)) * dx*10.763
25
26    return areaflow
27
28 *****
29 ** End of Program
30 ** *****

```

### A.3.3 Post-processing Module Programs

```
1 *****
2 **def GridVTK (chamberorder, chambertime, nx, ny, nz):
3 *****
4 #####
5 ## Program Description
6 #####
7
8     Author: Enrique Gallardo
9     Date: May 2018
10    Use: Chambertime plotting function
11    Input:
12    chamberorder: NumPy array with chamberorder
13    chambertime: NumPy dictionary with chambertime
14    nx, ny, nz: Grid cells in x, y, z directions, respectively.
15    Output/Return:
16    Grid with chambertime in gslib format.
17
18 #####
19
20     grid = [0] *nx*ny*nz
21     length=int (len (chamberorder))
22
23     for k in chamberorder [: length]:
24         temporal = chambertime [k]
25         grid[k] = temporal
26
27     return grid
28
29 *****
30 ** End of Program
31 ** *****
```

```

1 *****
2 **def VTKPlot (grdstr, propertyarray, propertyname, outputname):
3 *****
4 #####
5 ## Program Description
6 #####
7
8     Author: Enrique Gallardo
9     Date: May 2018
10    Use: VTK plotting function. Compatible with latest pygeostat version
11    Input:
12    gridstr: grid-string for pygeostat
13    propertyarray: NumPy array with porosity, permeability, rock-type, etc.
14    propertyname: 'porosity', 'permeability', 'rock-type', etc.
15    outputname: 'porosity.vtk', 'permeability.vtk', 'rock-type.vtk', etc.
16    Output:
17    vtk file: To visualize the property in third-party software
18
19 #####
20
21    griddef = gs.GridDef (grdstr)
22    ColName=[propertyname]
23    dframe = pd.DataFrame (propertyarray, columns=ColName)
24    datfl = gs.DataFile (data=dframe, griddef=griddef)
25    datfl.writefile (outputname)
26
27 *****
28 ** End of Program
29 *****

```

## Appendix B

Insights about the relationship between FSD, SSD and the utility function were drawn from Equation 4.4. Appendix B derives this equation from the expected utility definition, as given in Levy (2016).

The expected utility of the payoff  $x$  with  $a \leq x \leq b$  is:

$$E[u(x)] \equiv \int_a^b f(x) u(x) dx \quad (\text{B-1})$$

The difference in expected utilities between two projects F and G can be written as:

$$\Delta \equiv E_F[u(x)] - E_G[u(x)] = \int_a^b f(x) u(x) dx - \int_a^b g(x) u(x) dx \quad (\text{B-2})$$

Aggregating terms on the right side:

$$\Delta \equiv \int_a^b [f(x) - g(x)] u(x) dx \quad (\text{B-3})$$

Knowing that the integral of  $f(x)$  is  $F(x)$ , that is,

$$F(x) = \int_a^x f(t) dx \quad (\text{B-4})$$

Equation B-3 is integrated by parts to obtain:

$$\Delta = [F(x) - G(x)]u(x) \Big|_a^b - \int_a^b [F(x) - G(x)] u'(x) dx \quad (\text{B-5})$$

The first term of the right-hand reduced to zero because for  $x = b$ ,  $F(b) - G(b) = 0$  and for  $x = a$ ,  $F(a) - G(a) = 0$ . Then,  $\Delta$  results in:

$$\Delta = E_F[u(x)] - E_G[u(x)] = \int_a^b [G(x) - F(x)] u'(x) dx \quad (\text{B-6})$$